2023

Environment, communication and decision for multiagent systems

Lu Zhao

ENVIRONMENT, COMMUNICATION AND DECISION FOR MULTIAGENT SYSTEMS

by

LU ZHAO

Presented to the Faculty of the Graduate School of
The University of Texas at Arlington in Partial Fulfillment
of the Requirements
for the Degree of

DOCTOR OF PHILOSOPHY

THE UNIVERSITY OF TEXAS AT ARLINGTON
August 2023

ACKNOWLEDGEMENTS

I would like to express my heartfelt gratitude to my supervisor Dr. Yan Wan for her guidance in my PhD program and her incredible impact on my life. When we first met in late 2018, I was contemplating the direction of my academic and professional life, but she saw potential in me and encouraged me to explore the field of electrical engineering. Her unwavering support, guidance, and belief in my abilities have been instrumental in shaping my journey. Her mentorship has not only expanded my knowledge and skills but has also instilled in me the confidence to believe in myself. Her constructive feedback and opportunities to collaborate with experts in the field have also been invaluable in my growth as a researcher. I am eternally grateful for the faith she placed in me and for her unwavering commitment to my academic achievement.

I would also like to thank my dissertation committee members, Dr. Frank L. Lewis, Dr. Hongsheng Lu, Dr. Ramtin Madani, and Dr. Ioannis D. Schizas, for their insightful comments and discussions to help me improve this work.

My sincere thanks also go to my fellow labmates and friends at UTA, Dr. Chenyuan He, Dr. Mushuang Liu, Dr. Yangyang Qian, Dr. Han Jiang, Jiajian Chang, Siyu Zhou and Binoy Mathai George, for their support and companionship during these years.

I deeply thank my parents for being my rock and for all that they have done for me. Their dedication as parents has not only shaped my academic journey but has also instilled in me the values of perseverance, determination, and resilience. I am proud to be their child, and I will continue to make them proud as I move forward in my career. Also, I would like to thank my lovely partner, Xinqi Wei, for participating in my life and bringing me a lot of happiness.

Finally, I would like to thank the support of my research under NSF Grants 1714519, 1724248, and 1839804, ARO Grant W911NF-20-1-0132, ONR Grant N00014-18-1-2221, and contracts from the Toyota Motor North America R&D, InfoTech Labs, Ford Motors, and Dell Technologies.

July 11, 2023

ABSTRACT

ENVIRONMENT, COMMUNICATION AND DECISION FOR MULTIAGENT SYSTEMS

Lu Zhao, Ph.D.

The University of Texas at Arlington, 2023

Supervising Professor: Yan Wan

Multiagent systems (MAS) are ubiquitous in modern systems and have found broad applications, such as in intelligent transportation systems (ITS). Environment, communication and decision are among the essential components of MAS. The realistic environment in which MAS operates is usually stochastic, and its modeling, identification and estimation are important to consider. The communication in MAS is also critical for decisions. For example, in ITS, to improve travel efficiency and reduce traffic accidents, scheduling schemes for Vehicle-to-Everything (V2X) communication need to be developed. MAS decisions also need to be robust to uncertainties. For example, in mixed-traffic autonomous driving, the decisions for autonomous vehicles need to take into consideration human drivers' uncertain behaviors to avoid crash and ensue safe driving. This dissertation contributes to the MAS research in the aforementioned three aspects: environment, communication and decision.

In the first thrust of the dissertation, we capture the stochastic spatiotemporal environment in which the MAS operates using a discrete-time stochastic model, namely the influence model (IM). The identifiability and estimation of IMs with

reduced computation for real MAS applications are thoroughly studied in this dissertation, considering, first, a specific network topology (i.e., the uniform completely connected homogeneous networks), second, general homogeneous and heterogeneous networks, and finally, partially observed IMs (POIMs). Compared with using the standard master Markov chain approach for estimation, our proposed approaches are much more computationally efficient. In addition, per the authors' knowledge, our work is the first in the literature that studies the identifiability of heterogeneous IMs and heterogeneous POIMs.

In the second thrust of the dissertation, we study sub-6 GHz assisted mmWave scheduling and design a distributed V2X communication scheduling scheme with multiples head nodes for long highway traffic. The long highway is divided into contiguous and non-overlapping sections, and a head node within each section collects mmWave link requests, runs the scheduler and coordinates with each other to achieve conflict-free schedules. A decomposition-based approximate solution is developed to address the intra-section computational scalability. Two coordination schemes are designed to address the inter-section communication scalability, and to achieve an overall conflict-free transmission schedule with low control overhead.

In the third thrust, we propose a stochastic hierarchical game (SHG) to support safe and efficient autonomous driving decision under uncertain intentions in mixed-traffic scenarios. First, a random mobility model (RMM) is developed to capture the uncertain intentions of MAS, including the random switching behavior. Then, an efficient sampling-based uncertainty evaluation technique, named the multivariate probabilistic collocation method integrated with an orthogonal fractional factorial design (MPCM-OFFD) is leveraged to solve the SHG with reduced computation by using a limited number of sample scenarios while guaranteeing the safety.

TABLE OF CONTENTS

[1] © 2020 IEEE. Reprinted, with permission, from [L. Zhao, C. He and Y. Wan, "Reduced-Order Estimation of the Uniform Completely Connected Homogeneous Influence Model (UCC-HIM)," in *IEEE Control Systems Letters*, vol. 5, no. 6, pp. 2186-2191, Dec. 2021].

LIST OF ILLUSTRATIONS

LIST OF TABLES

CHAPTER 1

INTRODUCTION

1.1 Background and Motivation

A multiagent system (MAS) is a system composed of multiple interacting agents. In contrast to single-agent systems, the MASs are more flexible, robust, and efficient in solving complex and challenging tasks [1]. Therefore, the MASs have found broad applications, such as in transportation systems, power grids, social networks and pandemic spread [2–5]. Environment, communication and decision are among the essential components of MAS [6–8].

The realistic environment in which MAS operates is usually stochastic, and its modeling, identification and estimation are important to consider [9–11]. The influence model (IM) has been used in the literature to capture the stochastic spatiotemporal environment of MAS [12, 13]. The IM describes the evolution of networked Markov chains using local-level update rules modulated by abstracted network-level influences. IM is tractable in analysis with its reduced-order representation, but its identifiability and estimation remain challenging due to the tight coupling of network- and local- level interactions. In the literature, the identifiability analysis is limited to homogeneous IMs, and the identifiability condition leveraging the standard master Markov chain approach is not straightforward to check and computationally expensive [14]. Furthermore, there is no study in the literature on the identifiability of heterogeneous IMs despite the broad applications. Such a gap also exists for the identifiability of the partially-observed IMs (POIMs) [14]. Unlike identifiability, the estimation of IMs and POIMs has been investigated in some studies using methods

such as the maximum likelihood estimation (MLE) and expectation maximization (EM) [14–17]. However, significant limitations exist, such as the sensitivity to initial conditions [18], applicability to only two-state local Markov chains [19], and high computational cost [20, 21]. Therefore, we are motivated to study the identifiability and estimation of general IMs and POIMs with reduced computation.

Communication plays an important role in the safety and efficiency of MAS [22–24]. In intelligent transportation systems (ITS), collective perception and vehicle platooning all benefit from Vehicle-to-Everything (V2X) communication [25, 26]. Sub-6 GHz V2X-assisted mmWave communication has been proposed to support extensive data exchange in ITS applications, where the sub-6 GHz channel works as the control panel and the mmWave channel as the data panel [27]. MmWave transmission scheduling arranges mmWave links for transmission to avoid the waste of bandwidth resources due to collision in channel sharing [28]. We developed a centralized mmWave scheduling scheme with several scheduling algorithms which consider realistic V2X data features to achieve an optimized channel utilization [29, 30]. However, it is not applicable for long highway traffic with respect to the communication and computing scalability. First, control information exchange beyond the sub-6 GHz communication range requires multi-hop packet forwarding and incurs large control signalling overhead [31–33]. The computational complexity of solving the NP-complete scheduling optimization problem can also be high if there is heavy communication load for the long highway [30, 34–36]. Thus, we are motivated to develop a distributed scheduling scheme to address both communication and computational scalability issues for long highway traffic.

Decision-making under uncertainty is also an important subject for MAS. In autonomous driving, autonomous vehicles need to navigate safely and efficiently in complex traffic scenarios. One challenge in decision resides in the inherent uncertain

driver behaviors. There are some studies in the literature that model uncertain intentions of traffic participants [37–39], however the limitations lie in the inaccurate probabilities of rare traffic scenarios learned with finite data (e.g., abrupt intention changes) and inaccurate confidence bounds for making safe decisions [40]. Game theoretic-based approaches provide a systematic mathematical framework to model interactions among multiple traffic participants and to solve for optimal payoffs in non-cooperative traffic environments [41–43]. A Bayesian game that considers uncertain driver behavior was developed in [44]. However, it is not scalable with the number of game players. We are motivated to develop a novel stochastic game framework that more realistically captures uncertain driver behaviors and efficiently achieves safe decisions.

1.2 Overview of this Dissertation

This dissertation first investigates the stochastic spatiotemporal environment of MAS and studies the identifiability and estimation of IMs with reduced computation. Next we study the communication and decision issues of MAS in the context of ITS. With regard to communication in ITS, we study the sub-6 GHz V2X-assisted mmWave communication scheduling problem for long highway traffic. With regard to decision in ITS, we leverage the game theoretic-based approach to facilitate safe and efficient decisions under complex stochastic traffic environment. The results are documented in 9 papers [29, 30, 45–51]. The following five chapters include the main results.

In Chapter 2, we study the reduced-order estimation of IMs. For the uniform completely connected homogeneous IM (UCC-HIM), a canonical class of IM, we prove that it is identifiable. Then we construct a reduced-order Markov chain to facilitate the estimation study. The dimension of this reduced-order Markov chain is far less

than the master Markov chain and we find the one-to-one mapping between these two Markov chains. By using the proposed reduced-order Markov chain, an efficient parameter estimation algorithm is developed. Compared with the master Markov chain approach, the same accuracy is achieved but with significant reduction of computational load. Simulation studies verify efficiency of our proposed parameter estimation algorithm and demonstrate its practical value in real applications. The results are documented in paper [52] published in IEEE Control Systems Letters and presented in 2021 American Control Conference.

In Chapter 3, we take a structural approach to study the identifiability and estimation of both the homogeneous IMs and the heterogeneous IMs with reduced computation. To facilitate the identifiability analysis, we introduce the joint-margin matrix which connects the first-order and highest-order representations of IMs. Based on the joint-margin matrix, we find that the local Markov chain transition matrices are always identifiable and their ranks determine the identifiability of the network influence matrix. The if-and-only-if identifiability condition identified in this chapter for the homogeneous IMs is much simpler to check compared to that in [14]. For heterogeneous IMs, the if-and-only-if identifiability condition identified is the first in the literature and shows that the individual local Markov chain transition matrix determines the identifiability of the corresponding row of the network influence matrix. Based on the identifiability analysis, we develop the joint-margin probability based estimation (JMPE) methods for both the homogeneous IMs and heterogeneous IMs. The effectiveness of the proposed methods is validated through simulation studies. Compared to the maximum likelihood estimation and the linear algebra based estimation approaches, we find that the JMPE method retains accuracy with significantly reduced computation. The results are documented in paper [46] submitted to IEEE Transactions on Systems, Man and Cybernetics: Systems.

In Chapter 4, we provide new results on the estimation and identifiability of homogeneous and heterogeneous partially observed IMs (POIMs). Through exploring the joint-margin matrix introduced in Chapter 3, we develop a POIM estimation algorithm, named the expectation maximization-based JMPE (EM-JMPE), which includes two steps, estimating the joint-margin matrix from observations and obtaining POIM parameters from the joint-margin matrix. We also provide new identifiability conditions for POIMs by introducing the reduced-size joint-margin matrix, whose relationship with the fully-observed joint-margin matrix is presented. In the homogeneous case, we show that the new necessary condition is tighter or at least the same as that in [14]. The necessary condition for the heterogeneous case is the first in the literature. Simulation studies demonstrate the use of the results and validate their effectiveness. The results are documented in paper [47] published in IEEE Control Systems Letters and presented in 2022 Conference on Decision and Control.

In Chapter 5, we study the sub-6 GHz V2X-assisted mmWave link scheduling for long highway traffic. A distributed scheduling scheme is proposed. The long highway is divided into contiguous and non-overlapping sections. For each section, a head node collects mmWave link requests and determines a conflict-free transmission schedule through coordinating with other head nodes. We address both the computational challenge for individual head node to solve the scheduling problem in a section, and the communication challenge for multiple head nodes to resolve cross-section conflicts. To address the intra-section computational challenge, we develop a decomposition-based approximate solution, which leverages the spectral analysis of conflict table to decompose the scheduling problem in a section with minimal dependencies among sub-problems. Remaining dependencies are addressed through a permutation and enumeration procedure. To address the inter-section communication challenge, two coordination schemes are designed to avoid heavy control overhead for

an overall conflict-free transmission schedule. The rule-based scheme uses predefined rules to eliminate conflicted links. The section-parity-based scheme groups head nodes based on the parity of their section IDs, and head nodes from two groups conduct scheduling with modified constraints in order. Both schemes are simple to implement. Simulation studies using MATLAB validate the effectiveness of the proposed distributed scheduling scheme. The results are documented in paper [48] to submit to IEEE Transactions on Intelligent Transportation Systems.

In Chapter 6, we propose a novel stochastic hierarchical game (SHG) for autonomous driving, where the uncertain intentions of drivers are captured. The proposed SHG uses the random mobility model (RMM) to capture uncertain driver intentions of random switching behavior, and uses the multivariate probabilistic collocation method integrated with an orthogonal fractional factorial design (MPCM-OFFD) to solve the SHG efficiently. Comparative simulation studies have been conducted to validate the effectiveness of the proposed SHG. Comparing the performances of the SHG to those of the hierarchical game that does not consider uncertain intentions, the safety of the ego is achieved with reduced repeated play frequency, realistic braking maneuver, and timely response to abrupt intention changes in emergencies. The results are documented in paper [49] to submit to IEEE Intelligent Transportation Systems Magazine.

CHAPTER 2

REDUCED-ORDER ESTIMATION OF THE UNIFORM COMPLETELY CONNECTED HOMOGENEOUS INFLUENCE MODEL (UCC-HIM)[1]

2.1 Introduction

The influence model (IM) is a discrete-time stochastic model that captures spatiotemporal network dynamics [53, 54]. It constitutes a reduced-order representation of networked Markov chains through abstracting network-level interactions and local-level update rules. IM has been used in diverse stochastic network applications, such as power networks, social networks, virus spreads, and weather evolution [16, 55–57].

In order to use IM in stochastic network applications, one critical step is to estimate underlying model parameters from observation data. Identifiability deals with the uniqueness of IM estimates. In [58], the identifiability conditions for homogeneous IM were recently provided. Through exploiting the mapping structure between IM and its equivalent master Markov chain, the identifiability analysis led to a linear algebra-based estimator. The paper also developed a baseline maximum likelihood estimator (MLE) for comparison. Several other MLE based estimators have been developed in the literature [15, 16]. Of our interest, [17] developed an IM estimation algorithm based on its corresponding first-order representation, i.e., the influence matrix. All of these existing estimation algorithms have limitations of some sorts in their performance. The computation of the linear algebra-based approach grows exponen-

[1] © 2020 IEEE. Reprinted, with permission, from [L. Zhao, C. He and Y. Wan, "Reduced-Order Estimation of the Uniform Completely Connected Homogeneous Influence Model (UCC-HIM)," in *IEEE Control Systems Letters*, vol. 5, no. 6, pp. 2186-2191, Dec. 2021].

tially with the increase of network size. The performance of the MLE is sensitive to initial guesses, and local optima are difficult to avoid. Furthermore, obtaining the influence matrix from data is complex and prone to errors due to the coupling effect of network- and local- level interactions. To overcome these challenges, we here develop an IM estimation algorithm that is both accurate and computationally effective, including for large networks.

In this chapter, we take a structural approach to study reduced-computation IM estimation methods for IM. Network topology plays an important role in network dynamics, and topology-based approaches have been widely used in studies such as network identification, state estimation, network design and control [59–61]. As a first step, we here focus on a canonical class of IM, named the uniform completely connected homogeneous influence model (UCC-HIM). In UCC-HIM, all sites are fully connected with common mutual influence and local status update rules. Stochastic networks of such a topology capture agent interactions in close proximity and has been used in studies in a wide range of applications, including e.g., banking systems, the emergence of social norms, wireless sensor networks and protein interaction networks [62–65].

For this UCC-HIM, we develop an efficient estimation algorithm that exploits its symmetric topological property. Compared to the MLE and linear algebra-based estimators developed for general IMs, the proposed algorithm significantly reduces the computational complexity while maintains accuracy.

The rest of the chapter is structured as follows. The fundamentals of the IM and the UCC-HIM problem formulation are introduced in Section 2.2. In Section 2.3, a reduced-order Markov chain is introduced to facilitate the analysis for UCC-HIM based on its special network topology. Then an efficient parameter estimation algorithm is developed through exploiting structures of the reduced-order Markov

chain. In Section 2.4, two simulation studies are conducted to verify effectiveness of the proposed estimation algorithm. Section 2.5 concludes the chapter.

2.2 Preliminaries of the Influence Model

2.2.1 The influence Model (IM)

An IM is composed of N interacting sites. Each site i has M_i possible statuses, where $i \in \{1, 2, \cdots, N\}$. A scalar $s_i[k] \in \{1, 2, \cdots, M_i\}$ indexes the status of site i at time k. $S_i[k]$, a row vector of length M_i, also denotes site i's status at time k, where all entries are filled with '0's except a '1' at the location corresponding to the status index $s_i[k]$. For example, $S_i[k] = [1\ 0\ \cdots\ 0]$ when $s_i[k] = 1$.

At each time step, site i updates its status based on the network influence matrix $D \in \mathbb{R}^{N\times N}$ and local Markov chain transition matrix $A_{ji} \in \mathbb{R}^{M_j \times M_i}$, where $j \in \{1, 2, \cdots, N\}$. D and A_{ji} are row stochastic matrices. The 4-step update rule is summarized as follows.

1. Choose site j as site i's determining site with probability $d_{i,j}$, where $d_{i,j}$ is the element of D denoting the probability that i is influenced by j.
2. Calculate $p_{ij}[k+1] \in \mathbb{R}^{1\times M_i}$, the probability of site i's next status, based on the current status of site j as $p_{ij}[k+1] = S_j[k]A_{ji}$, where each element $a_{m,n}$ of A_{ji} is the conditional probability for site i's next status to be n given that site j's current status is m.
3. Determine $P_i[k+1] \in \mathbb{R}^{1\times M_i}$, the probability mass function of site i's next status by considering the influence of all sites on site i as
$$P_i[k+1] = \sum_{j=1}^{N} d_{i,j} p_{ij}[k+1] = \sum_{j=1}^{N} d_{i,j} S_j[k] A_{ji}. \tag{2.1}$$
4. $S_i[k+1]$ is then obtained by realizing $P_i[k+1]$, i.e., sampling random numbers according to the distribution $P_i[k+1]$.

Cascading $S_i[k]$ and $P_i[k+1]$ into row vectors $S^H[k]$ and $P^H[k+1]$ of length $\sum_{i=1}^{N} M_i$, we have

$$S^H[k] = \begin{bmatrix} S_1[k] & S_2[k] & \dots & S_N[k] \end{bmatrix}, \tag{2.2}$$

$$P^H[k+1] = \begin{bmatrix} P_1[k+1] & P_2[k+1] & \dots & P_N[k+1] \end{bmatrix}. \tag{2.3}$$

Then the above 4-step update rule leads to the IM dynamics succinctly captured by the two following iterative equations,

$$P^H[k+1] = S^H[k]H, \tag{2.4}$$

$$S^H[k+1] = MultiRealize(P^H[k+1]), \tag{2.5}$$

where $S^H[k+1]$ is obtained by realizing each $P_i[k+1]$ respectively, and $H \in \mathbb{R}^{\sum_{i=1}^{N} M_i \times \sum_{i=1}^{N} M_i}$ is the influence matrix defined as:

$$H \triangleq \begin{bmatrix} d_{1,1}A_{11} & \dots & d_{N,1}A_{1N} \\ \vdots & \vdots & \vdots \\ d_{1,N}A_{N1} & \dots & d_{N,N}A_{NN} \end{bmatrix}. \tag{2.6}$$

If all sites have the same number of statuses, M, and $A_{ji} = A$ for all i and j, the IM is referred to as the homogeneous influence model (HIM), with the state vector $S^H[k]$ of length MN. The dimension of state grows linearly with network size. A state matrix $S^G[k] \in \mathbb{R}^{N \times M}$ is further introduced to capture the HIM state in its matrix form

$$S^G[k] = \begin{bmatrix} S_1[k]' & S_2[k]' & \dots & S_N[k]' \end{bmatrix}'. \tag{2.7}$$

The corresponding influence matrix in (2.6) is then simplified to $H \triangleq D' \otimes A$, where $\otimes$ is the Kronecker product, and the superscript $'$ denotes the transpose operation.

In this chapter, we focus on the HIM with a canonical network topology, referred to as the uniform completely connected homogeneous influence model (UCC-HIM). In

UCC-HIM, all sites are fully connected with the same mutual influence, i.e., $d_{i,j} = \frac{1}{N}$ $\forall\ i, j \in \{1, 2, \cdots, N\}$. An example of UCC-HIM is shown in Figure 2.1. The UCC-HIM has practical values, e.g., it captures the voting behaviors in leaderless social networks and other types of network interactions in close proximity.

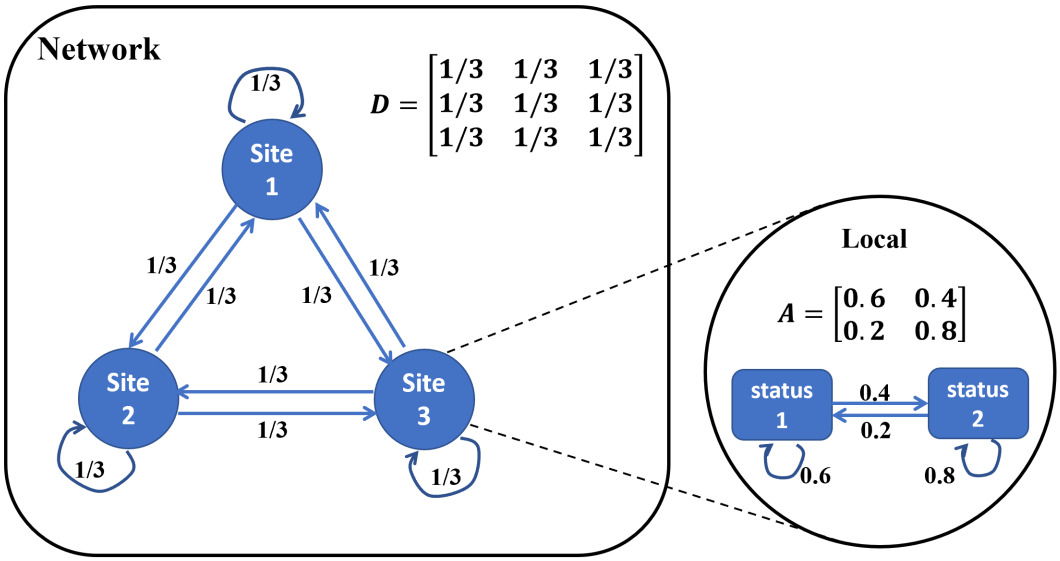

Figure 2.1: An example of UCC-HIM of 3 sites and 2 statuses at each site.

2.2.2 The Master Markov Chain Representation of IM

The dynamics of IM can also be captured by its equivalent master Markov chain [53]. As the name suggests, the master Markov chain representation uses the Markov properties of IM and constructs a big Markov chain with states as the combination of all site statuses. There are a total of M^N states in the master Markov chain representation. A scalar $s^g[k] \in \{1, 2, \cdots, M^N\}$ is adopted to index the states based on the statuses of all sites, i.e., $s_i[k]\ \forall\ i \in \{1, 2, \cdots, N\}$ as

$$s^g[k] = \sum_{i=1}^{N} (s_i[k] - 1) M^{N-i} + 1. \tag{2.8}$$

The event matrix $B \in \mathbb{R}^{M^N \times MN}$ captures all states of the master Markov chain [53]. The qth row of B is the state vector S^H corresponding to $s^g = q$. For example, for the UCC-HIM network in Figure 2.1 with 3 sites and 2 statuses for each site, i.e., $N = 3$ and $M = 2$, there are 8 states in the Markov chain in total. The state $s^g = 4$ corresponds to $s_1 = 1$, $s_2 = 2$ and $s_3 = 2$, and hence $S_1 = [1\ 0]$, $S_2 = [0\ 1]$, $S_3 = [0\ 1]$, to form $S^H = [1\ 0\ 0\ 1\ 0\ 1]$ in the 4th row of B,

$$B = \begin{bmatrix} 1 & 0 & 1 & 0 & 1 & 0 \\ 1 & 0 & 1 & 0 & 0 & 1 \\ 1 & 0 & 0 & 1 & 1 & 0 \\ 1 & 0 & 0 & 1 & 0 & 1 \\ 0 & 1 & 1 & 0 & 1 & 0 \\ 0 & 1 & 1 & 0 & 0 & 1 \\ 0 & 1 & 0 & 1 & 1 & 0 \\ 0 & 1 & 0 & 1 & 0 & 1 \end{bmatrix}.$$

The master Markov chain is characterized by its state transition matrix $G \in \mathbb{R}^{M^N \times M^N}$, which gives the conditional probability of its next state $s^g[k+1]$ given its current state $s^g[k]$. Let $S_p^G[k]$ and $S_q^G[k+1]$ denote the state matrices corresponding to $s^g[k] = p$ and $s^g[k+1] = q$, respectively. The elements of G can be obtained in a succinct form as:

$$g_{p,q} = P(s^g[k+1] = q | s^g[k] = p) = \prod_{n=1}^{N} \prod_{m=1}^{M} z_{n,m}, \tag{2.9}$$

where $z_{n,m}$ is the nth row and mth column element of matrix $Z_{pq} \in \mathbb{R}^{N \times M}$.

$$Z_{pq} = \left(D S_p^G[k] A\right)^{\circ S_q^G[k+1]}. \tag{2.10}$$

The superscript $\circ$ denotes the element-wise exponential operator. In particular, for two matrices X and Y with the same dimension, the mth row and nth column element

of the outcome of $X^{\circ Y}$, $(X^{\circ Y})_{m,n}$, is calculated as ${X_{m,n}}^{Y_{m,n}}$. Let $P^G[k+1] = DS_P^G[k]A$, the ith row of $P^G[k+1]$ indicates $P_i[k+1]$ with $i \in \{1, \cdots, N\}$ according to (2.1). Z_{pq} is constructed to obtain the probabilities of all sites at the local statuses captured in $S_q^G[k+1]$. $g_{p,q}$ is obtained by multiplying these probabilities since the statuses of all sites evolve independently. More details can be found in [58].

The comparison between the influence model dynamics (2.4) and its Master Markov chain representation (2.9) clearly shows the effectiveness of the influence model. The HIM of MN states captures the dynamics of its equivalent master Markov chain of M^N states.

2.2.3 Problem Formulation

Despite the tractability of the influence model due to its reduced-order formulation, model estimation cannot easily be achieved in an effective way. The master Markov chain G has been used as a step for the estimation of the IM [58]. However, as expected, the computation involved in the master Markov chain-based estimation approach increases exponentially with the network size. The large computational cost of G limits its practical use, especially for large networks.

In this chapter, we take a structural approach to study a class of IM, namely, the UCC-HIM, and provide an efficient parameter estimation algorithm. The problem is formulated as follows.

Problem: Consider a UCC-HIM of N sites with M statuses for each site. Given L independent observation sequences $O = \{O_1, O_2, \cdots, O_L\}$ with $O_i = \big[S^H[1]_i, S^H[2]_i, \cdots, S^H[K]_i\big]$, where the initial network state $S^H[1]_i$ can be arbitrary, estimate the underlying local transition matrix A with $L, K \to \infty$.

2.3 Parameter Estimation for the Uniform Completely Connected Homogeneous Influence Model (UCC-HIM)

In this section, we develop an efficient parameter estimation algorithm for the UCC-HIM. We first study the identifiability. Then we construct a reduced-order Markov chain through exploiting the symmetric network topology of the UCC-HIM. The mapping relationship between the reduced-order Markov chain and the master Markov chain is illustrated next. The analysis of the reduced-order Markov chain leads to an efficient and accurate estimation algorithm.

2.3.1 The Identifiability of The UCC-HIM

Lemma 1. *[58] The influence model is identifiable from the observation sequences O with $L, K \to \infty$, if and only if the underlying parameters A and D can be uniquely determined from the master Markov chain G.*

Lemma 2. *[58] A can be uniquely determined from G as*

$$a_{m,n} = \sqrt[N]{g_{\sum_{i=1}^{N}(m-1)M^{N-i}+1,\sum_{j=1}^{N}(n-1)M^{N-j}+1}}, \tag{2.11}$$

where $a_{m,n}$ is the mth row and nth column entry of A and $\sum_{i=1}^{N}(m-1)M^{N-i}+1$ is the master Markov chain's state with all sites in the same local status m.

Based on the above lemmas, we prove the identifiability of the UCC-HIM in Theorem 1.

Theorem 1. *Any UCC-HIM is identifiable.*

Proof. For a UCC-HIM of N sites, D is determined and takes the form of $d_{i,j} = \frac{1}{N}$ $\forall\ i, j \in \{1, 2, \cdots, N\}$. Because A can be determined uniquely from G according to Lemma 2, the theorem is proved naturally according to Lemma 1. □

2.3.2 The Reduced-order Markov Chain R

From (2.11), we see that the transition matrix of the master Markov chain G is needed to obtain A. The dimension of G is M^N, making the estimation computation grow exponentially with network size. To efficiently estimate A, we introduce a reduced-order Markov chain R by first showing its states and then the transition matrix.

The reduced-order Markov chain records the number of sites in each status. We adopt a length-M vector $S^R[k] = [r_1 \ \cdots \ r_m \ \cdots \ r_M]$ to denote the state of the reduced-order Markov chain R at time k, where r_m is the number of sites whose local statuses are m. Hence $0 \leq r_m \leq N$ and $\sum_{m=1}^{M} r_m = N$. In other words, $S^R[k] = \sum_{i=1}^{N} S_i[k]$. By counting all the possible $S^R[k]$, the reduced-order Markov chain R has r states, where

$$r = \left(\!\!\binom{M}{N}\!\!\right) = \binom{M+N-1}{N} = \frac{(M+N-1)!}{(M-1)!N!}. \tag{2.12}$$

The notation $((\cdot))$ and $(\cdot)$ denote the multiset and combination operations, respectively. r is the number of ways to assign M statuses to the N sites, with repetitions allowed and ordering disregarded. See [66], p.71 for the details of this multiset operation. To index the r states $S^R[k]$, we introduce a scalar $s^r[k] \in \{1, 2, \cdots, r\}$. Given $S^R[k]$, $s^r[k]$ is calculated as

$$s^r[k] = \sum\nolimits_{i=1}^{M-1} \sum\nolimits_{j=0}^{N-1-\sum_{m=1}^{i} r_m} \binom{M-i+j-1}{j} + 1. \tag{2.13}$$

Note that in the summation, if a term's upper bound is less than the lower bound, the term is zero [67].

For the example of $N = 3$ and $M = 2$ in Figure 2.1, the states of R, $S^R[k]$, are [3 0], [2 1], [1 2] and [0 3]. $r = \frac{(2+3-1)!}{(2-1)!3!} = 4$ in this case. The state $S^R[k] = [1\ 2]$ is indexed with $s^r[k] = 3$.

The transition matrix $R \in \mathbb{R}^{r\times r}$ of the reduced-order Markov chain indicates the conditional probability mass functions (PMFs) of its next state given its current state. Let $S_p^R[k]$ and $S_q^R[k+1]$ denote the state vectors corresponding to $s^r[k] = p$ and $s^r[k+1] = q$, respectively. R can be obtained according to the following theorem.

Theorem 2. *For a UCC-HIM with the network influence matrix D and local transition matrix A, each element of the reduced-order Markov chain R is calculated as*

$$R_{p,q} = P(s^r[k+1] = q | s^r[k] = p) = C_q \prod_{m=1}^{M} \left(X_{pq} \boldsymbol{e}_m\right), \tag{2.14}$$

where $1 \le p, q \le r$, C_q is the qth entry of length r column vector C, X_{pq} is a length M row vector, and $\boldsymbol{e}_m$ is a length M column vector of zeros, except a single '1' at its mth entry.

$$C_q = \frac{N!}{\prod_{m=1}^{M} \left(S_q^R[k+1]\boldsymbol{e}_m\right)!}, \tag{2.15}$$

$$X_{pq} = \left(\frac{1}{N} S_p^R[k] A\right)^{\circ S_q^R[k+1]}. \tag{2.16}$$

Proof. To obtain the conditional probability of $s^r[k+1] = q$ given $s^r[k] = p$, we start with the conditional probability of individual sites' next statuses given $s^r[k] = p$. Let $P_{i|p}[k+1]$ denote the conditional PMF of site i's next status given $s^r[k] = p$ and $S_p^R[k]\mathbf{e}_m$ indicates the mth entry of $S_p^R[k]$. According to the influence model's 4-step update rule in Section 2.2.1, at time k, site i chooses a site in status m as its determining site with probability $\frac{1}{N}$, where $m \in \{1, \cdots, M\}$. Then, the probability of its next status in n based on the status of the determining site can be calculated as $\frac{1}{N} a_{m,n}$. With $S_p^R[k]\mathbf{e}_m$ sites in status m and $m \in \{1, \cdots, M\}$, the probability of site

i's next status in n, $P(s_i[k+1]=n|s^r[k]=p)$, can be calculated as $\sum_{m=1}^{M}\frac{S_p^R[k]\mathbf{e}_m}{N}a_{m,n}$. Hence we have

$$\begin{aligned} P_{i|p}[k+1] &= \begin{bmatrix} P(s_i[k+1]=1|s^r[k]=p) \\ P(s_i[k+1]=2|s^r[k]=p) \\ \vdots \\ P(s_i[k+1]=M|s^r[k]=p) \end{bmatrix}' \\ &= \begin{bmatrix} \sum_{m=1}^{M}\frac{S_p^R[k]\mathbf{e}_m}{N}a_{m,1} \\ \sum_{m=1}^{M}\frac{S_p^R[k]\mathbf{e}_m}{N}a_{m,2} \\ \vdots \\ \sum_{m=1}^{M}\frac{S_p^R[k]\mathbf{e}_m}{N}a_{m,M} \end{bmatrix}' = \frac{1}{N}S_p^R[k]A. \end{aligned} \tag{2.17}$$

Because of the symmetric network topology of the UCC-HIM, i.e., all the elements in D are identical, each site i shares the same conditional PMF of their next status given $s^r[k]=p$, which is $P_{i|p}[k+1]$.

Because the statuses of all sites evolve independently, $R_{p,q}$ can be obtained as follows. First, choose $S_q^R[k+1]\mathbf{e}_1$ sites from N sites and assign them local status 1 with probability $P(s_i[k+1]=1|s^r[k]=p)^{\left(S_q^R[k+1]\mathbf{e}_1\right)}$. Next, choose $S_q^R[k+1]\mathbf{e}_2$ sites from $N-S_q^R[k+1]\mathbf{e}_1$ sites and assign them local status 2 with probability $P(s_i[k+1]=2|s^r[k]=p)^{\left(S_q^R[k+1]\mathbf{e}_2\right)}$. This process continues, and eventually, choose $S_q^R[k+1]\mathbf{e}_M$ sites from the rest sites and assign them local status M with probability $P(s_i[k+1]=M|s^r[k]=p)^{\left(S_q^R[k+1]\mathbf{e}_M\right)}$. Hence we have

$$\begin{aligned} &R_{p,q}=P(s^r[k+1]=q|s^r[k]=p) \\ &=\binom{N}{S_q^R[k+1]\mathbf{e}_1}(P_{i|p}[k+1]\mathbf{e}_1)^{\left(S_q^R[k+1]\mathbf{e}_1\right)} \\ &\binom{N-S_q^R[k+1]\mathbf{e}_1}{S_q^R[k+1]\mathbf{e}_2}(P_{i|p}[k+1]\mathbf{e}_2)^{\left(S_q^R[k+1]\mathbf{e}_2\right)}\ \dots \\ &\binom{N-\sum_{l=1}^{M-1}\left(S_q^R[k+1]\mathbf{e}_l\right)}{S_q^R[k+1]\mathbf{e}_M}(P_{i|p}[k+1]\mathbf{e}_M)^{\left(S_q^R[k+1]\mathbf{e}_M\right)} \end{aligned} \tag{2.18}$$

$$
\begin{aligned}
&= \prod_{m=1}^{M} \binom{N - \sum_{l=1}^{m-1} \left(S_q^R[k+1]\mathbf{e}_l\right)}{S_q^R[k+1]\mathbf{e}_m} (P_{i|p}[k+1]\mathbf{e}_m)^{\left(S_q^R[k+1]\mathbf{e}_m\right)} \\
&= \frac{N!}{\prod_{m=1}^{M}(S_q^R[k+1]\mathbf{e}_m)!} \prod_{m=1}^{M} \left(\left(\frac{1}{N} S_p^R[k] A \right)^{\circ S_q^R[k+1]} \right) \mathbf{e}_m \\
&= C_q \prod_{m=1}^{M} (X_{pq}\mathbf{e}_m).
\end{aligned}
$$

The penultimate equality is established based on the fact that $\sum_{l=1}^{M} S_q^R[k+1]\mathbf{e}_l = N$ and $(N-N)! = 0! = 1$. □

2.3.3 The mapping relationship between R and G

In this section, we show the mapping relationship between R and its corresponding master Markov chain G. We start with constructing the state-transfer vector T which captures the relationship between the states of R and G, and then show that R and G have a one-to-one mapping relationship.

Lemma 3. *The M^N states in the master Markov chain G and the r states in the reduced-order Markov chain R have a many-to-one mapping, captured by the state-transfer vector $T \in \mathbb{R}^{M^N \times 1}$ whose row index is s^g while each entry indicates the corresponding s^r. T can be obtained by calculating the scalar index of each row in B_u using* (2.13) *where*

$$B_u = B(\mathbf{1}_N \otimes I_M). \tag{2.19}$$

$\mathbf{1}_N$ is an all-one column vector of length N, and I_M is an M-dimensional identity matrix.

$$B = [B_1, \cdots, B_i, \cdots, B_N], \tag{2.20}$$

$$B_i = \mathbf{1}_{M^{i-1}} \otimes I_M \otimes \mathbf{1}_{M^{N-i}}. \tag{2.21}$$

Proof. Each row of the event matrix B indicates one of the M^N states of the master Markov chain G. B_u is constructed as in (2.19) to store the number of sites at each

local status for all the rows in B, i.e., each row of B_u indicates one of the r states $S^R[k]$ of the reduced-order Markov chain R with repetition. Then the entries of T, $s^r[k]$, can be obtained using (2.13) given each row of B_u, $S^R[k]$. □

Note that the number of repetitions of $S^R[k]$ in B_u is captured by the length r column vector C in Theorem 2, named as the state-count vector herein.

For example, in the $N = 3$ and $M = 2$ network shown in Figure 2.1,

$$B_u = \begin{bmatrix} 3 & 2 & 2 & 1 & 2 & 1 & 1 & 0 \\ 0 & 1 & 1 & 2 & 1 & 2 & 2 & 3 \end{bmatrix}',$$

$$C = \begin{bmatrix} 1 & 3 & 3 & 1 \end{bmatrix}',$$

and

$$T = \begin{bmatrix} 1 & 2 & 2 & 3 & 2 & 3 & 3 & 4 \end{bmatrix}'.$$

$s^g[k] = 2$, 3, and 5 all correspond to $s^r[k] = 2$.

Theorem 3. *For a UCC-HIM with the network influence matrix D and local transition matrix A, G and R have a one-to-one mapping as:*

$$R = WGV, \tag{2.22}$$

$$G = VRU, \tag{2.23}$$

where $V \in \mathbb{R}^{M^N \times r}$ is constructed based on the state-transfer vector T as

$$V_{k,l} = \begin{cases} 1 & if\ l = T_k \\ 0 & otherwise \end{cases} \qquad 1 \le k \le M^N, 1 \le l \le r. \tag{2.24}$$

$W \in \mathbb{R}^{r \times M^N}$ is obtained by transposing V and then leaving only the left first '1' in each row and setting the rest '1's to '0'. $U \in \mathbb{R}^{r \times M^N}$ is constructed based on V and the state-count vector C by $U_{l,k} = \frac{V_{k,l}}{C_l}$.

Proof. We show the proof by explaining the construction of the auxiliary matrices V, W and U.

Because all elements of the network influence matrix D are identical, we find that in the state-transfer vector T, the indices of the identical elements indicate the column indexes and row indexes with identical state transition probabilities in G. To obtain R based on G, V is constructed to add up G's columns according to T. W is constructed to delete the repeated rows of G according to T. Equation (2.22) is thus proven.

Reversely, the state transition probability in G can also be uniquely determined by R because of the symmetric network structure. To obtain G from R, V is constructed to duplicate R's rows according to T, and U is constructed to expand the information in R's columns according to T and the state-count vector C. To reconstruct the columns of G, we only need to divide the columns in R with corresponding states by their numbers of repetitions in G which are recorded in C. Therefore, we have (2.23). □

According to Theorem 3, R is a reduced-order representation of G for the UCC-HIM, obtained by discarding and merging redundant information in G. Because G is uniquely determined from the observation sequences, it also implies that R is unique.

The dimension of the reduced Markov chain R is $r = \frac{(M+N-1)!}{(M-1)!N!}$, which is far less than the dimension of master Markov chain G, M^N. Figure 2.2 shows a comparison between the dimensions of the master Markov chain G and the reduced-order Markov chain R. With the increase of network size N and the number of statuses M, the dimension of G increases dramatically, while the dimension growth of R is very slow, indicating the significant dimension and computational cost reduction using R.

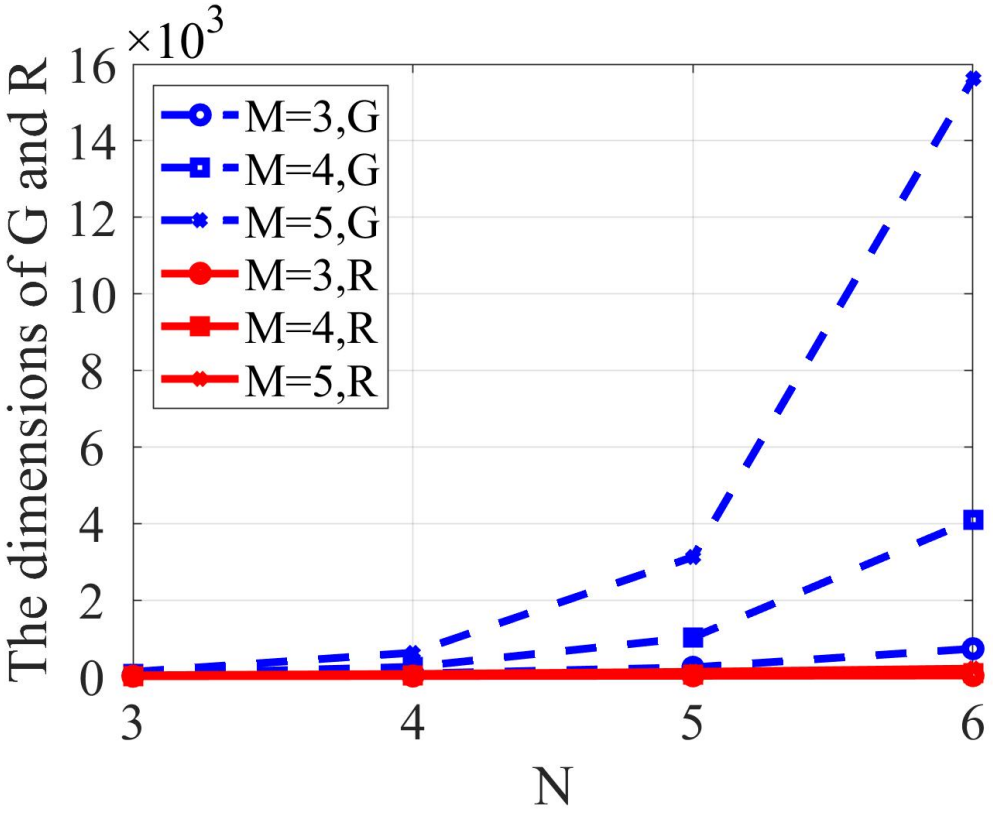

Figure 2.2: The dimensions of G and R with different N and M

2.3.4 The Estimation Algorithm for A based on R

In this subsection, we develop an efficient estimation algorithm for A from observation sequences of the UCC-HIM.

First, we show that the reduced-order Markov chain R can be uniquely constructed from observation sequences by counting the corresponding state transition frequencies based on the law of large numbers [68]. Because G can be uniquely determined from the observation sequences, and G and R have a one-to-one mapping, R can also be uniquely determined. This result is summarized in the following lemma.

Lemma 4. *Given the observation sequences of a UCC-HIM, O, with $L, K \to \infty$, the reduced-order Markov chain R can be uniquely constructed.*

The next theorem shows the estimation for A based on the reduced-order Markov chain R.

Theorem 4. *Given the reduced-order Markov chain R of the UCC-HIM, the elements of A can be uniquely determined as*

$$a_{m,n} = \sqrt[N]{R_{r+1-\sum_{k=0}^{M-m}\binom{N+k-1}{k},r+1-\sum_{k=0}^{M-n}\binom{N+k-1}{k}}}. \tag{2.25}$$

Proof. According to (2.13), $r+1-\sum_{k=0}^{M-m}\binom{N+k-1}{k}$ denotes the state of the reduced-order Markov chain R where all sites are in local status m, i.e., $S^R[k] = [0 \cdots N \cdots 0]$, with all positions filled with '0's except an 'N' at the mth position. According to (2.14), (2.16) and (2.15), we have

$$\begin{aligned} &R_{r+1-\sum_{k=0}^{M-m}\binom{N+k-1}{k},r+1-\sum_{k=0}^{M-n}\binom{N+k-1}{k}} \\ &= 1\ a^0_{m,1}\cdots a^N_{m,n}\cdots a^0_{m,M} = a^N_{m,n}. \end{aligned} \tag{2.26}$$

Therefore, (2.25) is derived. □

Note that the estimation of A from R has the same accuracy as the estimation from G according to (2.11) and (2.25).

2.4 Simulation Studies

To demonstrate the results developed in Section 2.3, two simulation studies are conducted. Example 1 verifies the practicability and efficiency of the estimation algorithm. Example 2 is a real-world application that models the decision making process in a social network using the UCC-HIM.

2.4.1 Example 1: Estimation of A in the UCC-HIM

To verify efficiency of the proposed estimation algorithm, we compare the performance of our algorithm with the estimation algorithm using the master Markov

chain approach. We consider a UCC-HIM with 5 sites and 3 statuses for each sites. The network influence matrix D has element $d_{i,j} = \frac{1}{5}$, $\forall i, j \in \{1, \cdots, 5\}$. The local transition matrix A is given as

$$A = \begin{bmatrix} 0.36 & 0.32 & 0.32 \\ 0.33 & 0.40 & 0.27 \\ 0.35 & 0.25 & 0.40 \end{bmatrix}.$$

An observation sequence of length $400,000$ is generated. Then G and R are computed by finding the state transition frequencies respectively. According to Theorem 4, the estimated local transition matrix $\hat{A}$ through R is

$$\hat{A} = \begin{bmatrix} 0.3347 & 0.3395 & 0.3258 \\ 0.3083 & 0.4106 & 0.2812 \\ 0.3132 & 0.2538 & 0.4330 \end{bmatrix},$$

which is identical to the estimation through G. The mean squared errors (MSE) for $\hat{A}$ is 4.6860×10^{-4}, showing the accuracy of the estimation. The execution time of our reduced-order algorithm based on R is about half of that based on G, indicating the improved efficiency.

2.4.2 Example 2: Support or Oppose?

In social network models, agents interact with each other and update their opinions based on rules that capture the influences from other agents [69]. When no individual takes the role of opinion leaders and all individuals exert the same influences to the whole team, the opinion propagation can be captured as the UCC-HIM.

In a leaderless social network, discussion and voting are two common steps in a decision-making process. In this example, a group of 5 people meet to discuss whether

to act on a problem. There are two statuses for each person, support or oppose. Their opinions may change during the discussion due to the influences they receive from others. The mutual influences in the group are identical. The ones who oppose have a greater impact than those who support. After thorough discussions, people vote for the final decision. We can model this process using a UCC-HIM. For example, $d_{i,j} = \frac{1}{5}\ \forall i, j \in \{1, \ldots, 5\}$ and $A = \begin{bmatrix} 0.7 & 0.3 \\ 0.2 & 0.8 \end{bmatrix}$ due to the tendency to oppose.

According to Theorem 2, the reduced-order Markov chain R has 6 states and can be computed as

$$R = \begin{bmatrix} 0.1681 & 0.3602 & 0.3087 & 0.1323 & 0.0283 & 0.0024 \\ 0.0778 & 0.2592 & 0.3456 & 0.2304 & 0.0768 & 0.0102 \\ 0.0313 & 0.1562 & 0.3125 & 0.3125 & 0.1562 & 0.0313 \\ 0.0102 & 0.0768 & 0.2304 & 0.3456 & 0.2592 & 0.0078 \\ 0.0024 & 0.0283 & 0.1323 & 0.3087 & 0.3602 & 0.1681 \\ 0.0003 & 0.0064 & 0.0512 & 0.2048 & 0.4096 & 0.3277 \end{bmatrix}.$$

The state s^r ranges from 1 to 6, with $s^r - 1$ denoting the number of people who oppose. Using the reduced Markov chain R, we can effectively predict the final voting result. The steady-state distribution of R is determined by the left eigenvector of R associated with the eigenvalue '1', which is [0.0217 0.0978 0.2162 0.2976 0.2565 0.1102]. Hence, the probability of 3 people opposing is the largest (0.2976). The probability that more than 2 people oppose is 0.6643, indicating that more than half of the people are more likely to oppose this action eventually. According to the majority rule, the final decision is more probable to be 'oppose'. If using the master Markov chain to obtain the steady-state results, the eigen-analysis of a 32×32 Markov chain is required, which incurs more computation.

2.5 Conclusion

In this chapter, we study the reduced-order estimation of IM. For UCC-HIM, a canonical class of IM, we prove that it is identifiable. Then we construct a reduced-order Markov chain R to facilitate the estimation study. The dimension of R is far less than the master Markov chain G. We find the one-to-one mapping between R and G. By using R, an efficient parameter estimation algorithm for A is developed. Compared with the master Markov chain approach, the same accuracy is achieved but with significant reduction of computational load. Simulation studies verify efficiency of our proposed parameter estimation algorithm and demonstrate its practical value in real applications.

CHAPTER 3

STRUCTURAL ANALYSIS OF THE STOCHASTIC INFLUENCE MODEL FOR IDENTIFIABILITY AND REDUCED-ORDER ESTIMATION

Nomenclature

N	The number of sites in an influence model.
M_n	The number of local statuses for site n.
$S_n[k]$	Local status vector of site n at time k.
$s_n[k]$	Local status index of site n at time k.
D	Network influence matrix.
A_{ln}	Transition matrix of the local Markov chain between site l and site n.
$d_{n,l}$	Probability that site l has influence on site n.
$P_n[k]$	Probability mass function (PMF) of site n's statuses at time k.
$S_V[k]$	State vector of the influence model at time k.
$P_V[k]$	State probability vector of the influence model at time k.
H	Influence matrix of the influence model.
M	The number of local statuses for each site in a homogeneous or heterogeneous influence model.
A	Transition matrix of the local Markov chain in a homogeneous influence model.
$a_{m,q}$	The mth row and qth column entry of A.
A_n	Transition matrix of the local Markov chain for site n in a heterogeneous influence model.
$a_{n_{m,q}}$	The ith row and jth column entry of A_n.

B The event matrix.

B_n The nth block of B.

$s[k]$ State index of the Master Markov chain representation of the influence model at time k.

G Transition matrix of the Master Markov chain representation of the influence model.

$S_M[k]$ State matrix of the homogeneous or heterogeneous influence model at time k.

$P_M[k]$ State probability matrix of the homogeneous or heterogeneous influence model at time k.

$g_{i,j}$ The ith row and jth column entry of G.

$S[k]$ State vector of the Master Markov chain representation of the influence model at time k.

$P[k]$ Probability mass function (PMF) of the master Markov chain representation of the influence model at time k.

F The number of independent observation sequences.

Y Independent observation sequences.

$Y^{(f)}$ The fth independent observation sequence.

T The length of independent observation sequences.

θ Parameters of the influence model. $\theta = (D, A_{ln})$ for a general influence model, $\theta = (D, A)$ for a homogeneous influence model and $\theta = (D, A_n)$ with $n \in \{1, \cdots, N\}$ for a heterogeneous influence model.

J The joint-margin matrix of the influence model.

J_n The nth block of J.

$J_{n_{i,m}}$ The ith row and mth column entry of J_n.

$\mathcal{A}_m$ The mth local Markov information matrix in a homogeneous influence model.

$\mathcal{A}_{n_m}$ The mth local Markov information matrix of site n in a heterogeneous influence model.

3.1 Introduction

The influence model (IM) is a reduced-order stochastic network model that captures the spatiotemporal dynamics in a network of interactive Markov chains [53, 54]. In IMs, the evolution of networked Markov chains depends on the local-level status update rules under abstracted network-level influences. This representation allows the tractability of IM for both individual and collective behaviors. IMs can be classified into homogeneous IMs and heterogeneous IMs based on whether the local-level status update rules are identical or not. With the features such as reduced order representation and tractable analysis, IMs have been applied in many network applications, including power networks [3, 13, 55, 70], social networks [4, 16, 71–73], transportation systems [2,74,75], virus spread and pandemics [56,76,77], and weather evolution [12, 14, 78].

The identifiability and estimation of IMs are critical for their use in real applications. Despite the tractability of IM analysis with its reduced-order representation, the identifiability and estimation of IM remain challenging due to the tight coupling of network- and local- level interactions. In the literature, the identifiability analysis is only limited to the homogeneous IMs, e.g., [14] and [45]. Our prior work [14] is the first that provides the identifiability conditions for homogeneous IMs, through exploring the corresponding master Markov chain representation. However, the if-and-only-if condition provided there is not straightforward to check and involves significant computation. The identifiability condition in [45] applies to IMs of a specific topology.

Heterogeneous IMs are more flexible to capture various interactions among system components, but have been rarely studied in the literature. The analysis of heterogeneous IMs is much more challenging compared with the homogeneous counterpart, because a variety of local-level status update rules can be involved, which makes the coupling effects of network- and local- level interaction more complex. Furthermore, to the best of our knowledge, there is no study on the identifiability of heterogeneous IMs despite the broad applications.

Unlike identifiability, the estimation of IMs has been studied in the literature, however significant limitations exist with regard to performance of the existing parameter estimation methods. The maximum likelihood estimation (MLE) has been commonly used in IM parameter estimation studies [14–16]. The expectation maximization (EM) algorithm has also been used to estimate the parameters of IM in the existence of latent states [17] or unobservable sites [14]. The MLE and EM methods are sensitive to initial conditions and may converge to local optima [18]. In addition, high computational cost is inevitable [20, 21]. Paper [19] developed a convex quadratic programming for IMs with two local statuses. In our prior study, a linear algebra based estimator (LAE) was proposed based on the corresponding master Markov chain of the homogeneous IM [14]. The LAE approach is very effective for small-size networks but also consumes high computation cost for large-size networks. To address the computational issue, paper [45] studied a canonical topology of the IMs called the uniformly completely connected homogeneous IM (UCC-HIM), and developed a reduced-order estimation by recognizing its special symmetric network structure. However, the reduced-order method therein only applies to IMs of a specific topology. In summary, the estimation methods in the literature are either directed to specific topologies of IMs or have high computational load.

In this chapter, we are thus motivated to study the identifiability and estimation of general IMs with reduced computation. We do this by taking an structural analysis approach that establishes a novel connection between the high-order and low-order representations of the IM. In particular, instead of resorting back to the master Markov chain representation which incurs significant computation [14], we explore the connection between the IM's first-order influence matrix and highest-order master Markov chain representations. Based upon the structural relationship, we introduce the joint-margin matrix to facilitate the identifiability analysis and provide easy-to-check if-and-only-if identifiability conditions for both homogeneous IMs and a broad class of the heterogeneous IMs, referred to as the heterogeneous IMs without ambiguity. By exploiting the identifiability properties of IM, we further develop the joint-margin probability based estimation methods for both homogeneous and heterogeneous IMs. This new analytical approach to IM identification and estimation results in significantly reduced computational cost while maintaining the estimation accuracy. This is the first reduced-order estimation study for general IMs, and thus provides the promise for the use of IMs in real applications with limited computation complexity. The main contributions of this chapter are summarized as follows.

- A new framework for the identifiability and estimation analysis of IM is proposed by exploring the connection between the first-order and highest-order representations of IMs. Compared to [14] where only the highest-order representation of IMs was analyzed, this framework takes the form that combines the marginal and joint probabilities, which simplifies the formulation while maintaining sufficient information for identifiability and estimation analysis.
- If-and-only-if identifiability conditions for homogeneous IMs are given. Compared to [14], the succinct forms of identifiability conditions are much simpler to check with reduced computation.

- If-and-only-if identifiability conditions for heterogeneous IMs are for the first time provided in the literature to the best of our knowledge.
- Computationally effective parameter estimation methods for both homogeneous and heterogeneous IMs are provided based on the structural identifiability analysis.

The rest of the chapter is structured as follows. In Section 3.2, the preliminaries of IM are given and the identifiability and estimation problems are formulated. The connection between the first-order and highest-order representations of IMs is explored in Section 3.3. The identifiability analysis of the homogeneous and heterogeneous IM is provided in Section 3.4, followed by the parameter estimation algorithms in Section 3.5. Simulation studies are illustrated in Section 3.6. Section 3.7 draws the conclusions for this chapter.

3.2 Preliminaries and Problem Formulation

3.2.1 The influence model (IM)

Consider an IM of N sites, each of which has M_n local statuses for $n \in \{1, 2, \cdots, N\}$. Let the length-$M_n$ row vector, $S_n[k]$ and scalar $s_n[k]$ denote the local status of site n at time k in its vector and scalar forms, respectively. Here $S_n[k]$ has a single '1' as its $s_n[k]$-th entry and '0's everywhere else. The IM is described by the network influence matrix $D \in \mathbb{R}^{N\times N}$ and the local Markov chain transition matrix $A_{ln} \in \mathbb{R}^{M_l \times M_n}$, where D and A_{ln} are row stochastic matrices [53, 54]. Illustration of the A_{ln} and D matrices and the update rules are described below.

1. Site n's next status is determined by site l according to the probability $d_{n,l}$, i.e., site l has a probability of $d_{n,l}$ to become site n's determining site, where $d_{n,l}$ is the nth row and lth column element of D.

2. The conditional probability mass function (PMF) of site n's next status given its determining site l's current status $P_{n|l}[k+1] \in \mathbb{R}^{1\times M_n}$ is $S_l[k]A_{ln}$, where the mth row and qth column element of A_{ln} indicates the conditional probability for site n's next status to be q given site l's current status m, i.e., $P(s_n[k+1]=q|s_l[k]=m)$.
3. The PMF of site n's next status, $P_n[k+1] \in \mathbb{R}^{1\times M_n}$ is determined by all sites' current statuses according to

$$P_n[k+1] = \sum_{l=1}^{N} d_{n,l} P_{n|l}[k+1] = \sum_{l=1}^{N} d_{n,l} S_l[k] A_{ln}. \tag{3.1}$$

4. Site n's next status is obtained through sampling according to the corresponding PMF $P_n[k+1]$, i.e., $S_n[k+1] = Realize(P_n[k+1])$.

Placing the status vectors and the corresponding PMFs in row vectors $S_V[k] \in \mathbb{R}^{1\times\sum_{n=1}^{N} M_n}$ and $P_V[k] \in \mathbb{R}^{1\times\sum_{n=1}^{N} M_n}$,

$$S_V[k] = \begin{bmatrix} S_1[k] & S_2[k] & \cdots & S_N[k] \end{bmatrix}, \tag{3.2}$$

$$P_V[k] = \begin{bmatrix} P_1[k] & P_2[k] & \cdots & P_N[k] \end{bmatrix}, \tag{3.3}$$

we obtain the overall dynamics

$$P_V[k+1] = S_V[k]H, \tag{3.4}$$

$$S_V[k+1] = MultiRealize\left(P_V[k+1]\right), \tag{3.5}$$

where $H \in \mathbb{R}^{\sum_{n=1}^{N} M_n \times \sum_{n=1}^{N} M_n}$ is the influence matrix defined as [53]

$$H \triangleq \begin{bmatrix} d_{1,1}A_{11} & \dots & d_{N,1}A_{1N} \\ \vdots & \vdots & \vdots \\ d_{1,N}A_{N1} & \dots & d_{N,N}A_{NN} \end{bmatrix}, \tag{3.6}$$

and 'MultiRealize' indicates that $S_V[k+1]$ is obtained by realizing each PMF $P_n[k+1]$ in $P_V[k+1]$.

The influence matrix H is referred as the first-order representation of IM, because it captures the dynamics of individual sites' statuses as in (3.4). The dynamics of the joint statuses of multiple sites cannot be directly obtained from H. In order to capture joint statuses, higher-order representations of IM are required [53].

In this chapter, we study the widely applicable homogeneous IM and a broad class of heterogeneous IMs. The number of statuses in each site is the same, i.e., $M_n = M$ for $\forall n \in \{1, 2, \cdots, N\}$. The local Markov chain transition matrices are the same for the homogeneous case and can be different for the heterogeneous case. The mathematical descriptions of these two classes of IM being considered in this chapter are given as follows.

1. Homogeneous IM: all sites have the same local Markov chain transition matrix, i.e., $A_{ln} = A$ for $\forall\ n, l \in \{1, 2, \cdots, N\}$. $a_{m,q}$ with $m, q \in \{1, 2, \cdots, M\}$ denotes the mth row and qth column entry of A. The corresponding influence matrix is [53]

$$H = D' \otimes A, \tag{3.7}$$

   where $\otimes$ denotes the Kronecker product. See Fig. 3.1 for an example.

2. Heterogeneous IM: each site n can have its own local Markov chain transition matrix A_n, i.e., $A_{ln} = A_n$ for $\forall\ n, l \in \{1, 2, \cdots, N\}$. $a_{n_{m,q}}$ with $m, q \in \{1, 2, \cdots, M\}$ denotes the mth row and qth column entry of A_n. The corresponding influence matrix is

$$H = \begin{bmatrix} D'C_1 \otimes A_1 & D'C_2 \otimes A_2 & \cdots & D'C_N \otimes A_N \end{bmatrix}, \tag{3.8}$$

   where C_n denotes the column vector with '1' as its nth entry and '0' everywhere else. An example is given in Fig. 3.2.

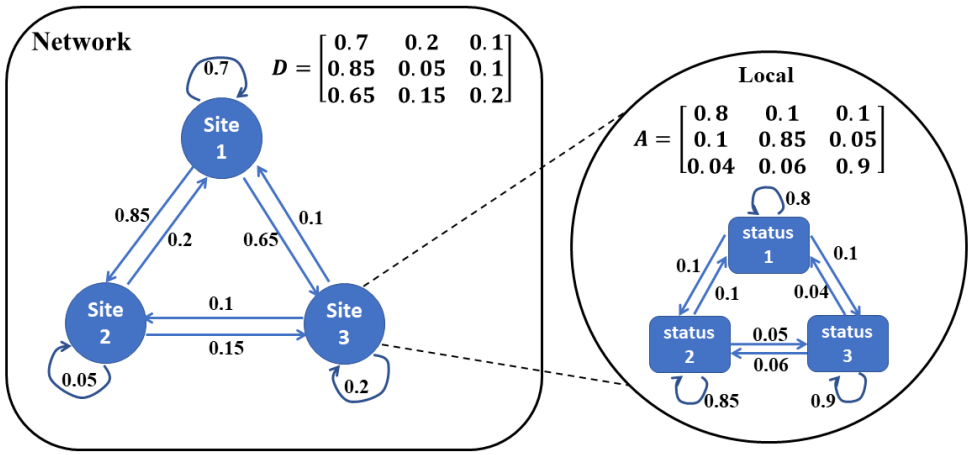

Figure 3.1: An example of homogeneous IM of 3 sites and 3 statuses at each site.

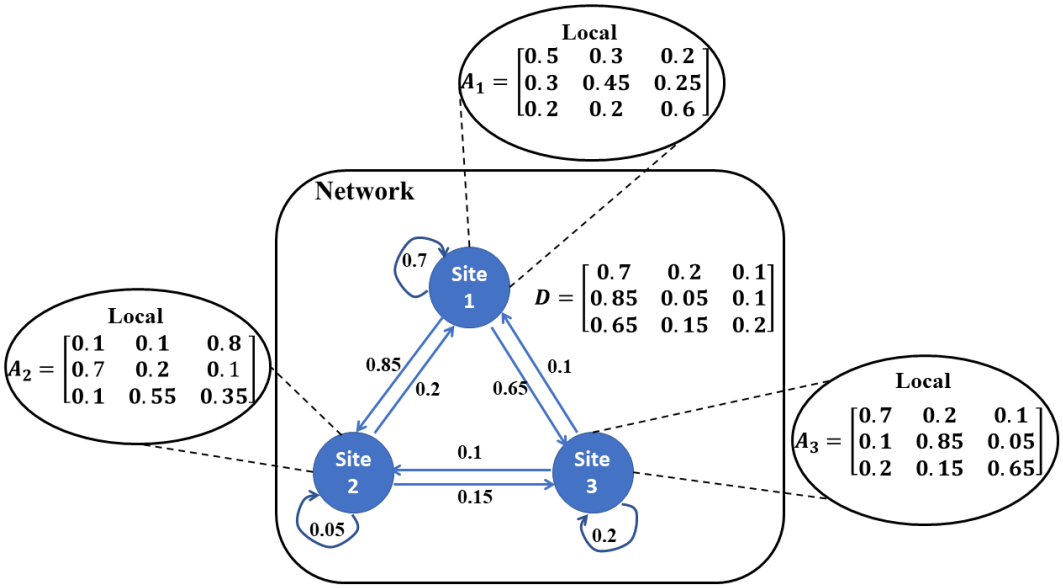

Figure 3.2: An example of heterogeneous IM of 3 sites and 3 statuses at each site.

3.2.2 Illustrative Social Network Examples of the IM

The above homogeneous and heterogeneous IM models can capture influence dynamics in broad network applications. Because human opinions are easily influ-

enced by people around them [79–81], here we take opinion propagation in social networks as an example to illustrate the models [45].

We use the homogeneous IM of $N = 3$ and $M = 3$ in Fig. 3.1 as an example for illustration. The 3 sites represent 3 persons, and the 3 statuses '1', '2' and '3' represent that each person can have 3 votes on a certain event, i.e., 'in favour', 'against' and 'abstention'.

The mutual influences of individuals' opinions are described by the network influence matrix D. For instance, $d_{1,1}$, $d_{2,1}$ and $d_{3,1}$ are largest elements within each row to capture that person '1' has more authority to influence the decisions of the network. In other words, all three persons are most likely to choose person '1' as the determining person to decide their next votes according to the first update rule.

The local Markov chain transition matrix A illustrates the conditional probabilities of how individuals change their opinions based on the determining person's current opinion. For instance, all 3 persons tend to follow the determining person's opinions since the local Markov chain transition matrix A is row diagonally dominant according to the second update rule.

Given the current opinion of 3 persons as '2', '1' and '1', i.e., $S_1[k] = [0\ 1\ 0]$, $S_2[k] = [1\ 0\ 0]$ and $S_3[k] = [1\ 0\ 0]$, the PMF for person '2's opinion at next time step can be obtained by calculating $P_2[k+1] = \sum_{l=1}^{3} d_{2,l} S_l[k] A = [0.205\ 0.7375\ 0.0575]$.

In a more general setting, individuals may use the determining person's opinions in different ways due to different personal experiences. This can be captured by introducing nonidentical local Markov chain transition matrices, and hence to formulate the heterogeneous IM. In the example in Fig. 3.2, person '3' tends to follow the determining person's opinion while person '2' does not. Given the determining person '1's current status as '2', i.e., $S_1[k] = [0\ 1\ 0]$, the conditional PMFs of all 3 persons' next statuses can be obtained by calculating $P_{n|1}[k+1] = S_1[k] A_n$ according to the second

update rule and thus we have $P_{1|1}[k+1] = [0.3\ 0.45\ 0.25]$, $P_{2|1}[k+1] = [0.7\ 0.2\ 0.1]$ and $P_{3|1}[k+1] = [0.1\ 0.85\ 0.05]$.

3.2.3 The event matrix B and master Markov chain G

To gain more insights into the collective behavior of network sites, we describe in this subsection the event matrix B, and the master Markov chain G which is the highest-order representation of IM that captures the dynamics of the joint statuses of all sites [53].

For both homogeneous and heterogeneous IM, there are M^N possible combinations of all sites' local statuses in the influence process, i.e., M^N possible $S_V[k]$. The event matrix $B \in \mathbb{R}^{M^N \times MN}$ lists all M^N possible $S_V[k]$ as its rows and can be constructed as

$$B = \begin{bmatrix} B_1 & B_2 & \cdots & B_N \end{bmatrix}, \tag{3.9}$$

where $B_n \in \mathbb{R}^{M^N \times M}$ is the nth block of B.

$$B_n = \mathbf{1}_{M^{n-1}} \otimes I_M \otimes \mathbf{1}_{M^{N-n}}, \tag{3.10}$$

where $\mathbf{1}_{M^{n-1}}$ denotes the all-ones column vector of length M^{n-1} and I_M is the M-dimensional identity matrix. For example, a network with 3 sites and 2 statuses for each site, i.e., $N = 3$ and $M = 2$, has an event matrix

$$B = \begin{bmatrix} 1 & 0 & 1 & 0 & 1 & 0 \\ 1 & 0 & 1 & 0 & 0 & 1 \\ 1 & 0 & 0 & 1 & 1 & 0 \\ 1 & 0 & 0 & 1 & 0 & 1 \\ 0 & 1 & 1 & 0 & 1 & 0 \\ 0 & 1 & 1 & 0 & 0 & 1 \\ 0 & 1 & 0 & 1 & 1 & 0 \\ 0 & 1 & 0 & 1 & 0 & 1 \end{bmatrix}.$$

The master Markov chain representation of IM captures the collective behavior of all sites in the network. There are M^N states in the master Markov chain and each state is indexed by the row number of B. Let a scalar $s[k]$ denote the state index of the master Markov chain at time k, and $s[k]$ can be obtained by the local status of each site $s_n[k]$ as [14]

$$s[k] = \sum_{n=1}^{N} (s_n[k] - 1) M^{N-n} + 1. \tag{3.11}$$

The state transition matrix $G \in \mathbb{R}^{M^N \times M^N}$ of the master Markov chain captures the conditional probability of its next state $s[k+1]$ given its current state $s[k]$. To construct G, the state vector $S_V[k]$ and the probability vector $P_V[k]$ are rewritten into the corresponding matrix forms $S_M[k] \in \mathbb{R}^{N \times M}$ and $P_M[k] \in \mathbb{R}^{N \times M}$, i.e.,

$$S_M[k] = \begin{bmatrix} S_1[k]' & S_2[k]' & \dots & S_N[k]' \end{bmatrix}', \tag{3.12}$$

$$P_M[k] = \begin{bmatrix} P_1[k]' & P_2[k]' & \dots & P_N[k]' \end{bmatrix}', \tag{3.13}$$

where the superscript $'$ denotes the transpose operation. Let $S_M[k]_i$ and $S_M[k+1]_j$ denote the state matrices corresponding to $s[k] = i$ and $s[k+1] = j$, respectively. The elements of G can be obtained as

$$g_{i,j} = P(s[k+1] = j | s[k] = i) = \prod_{n=1}^{N} \prod_{m=1}^{M} p_{n,m}, \tag{3.14}$$

where $p_{n,m}$ is the nth row and mth column element of matrix $P_{i \to j} \in \mathbb{R}^{N \times M}$ [45].

$$P_{i \to j} = P_M[k+1]^{\circ S_M[k+1]_j}, \tag{3.15}$$

where the superscript $\circ$ denotes the element-wise exponential operator of two matrices with same dimension [45]. Specifically, for two matrices X and Z, the nth row and mth column element of $X^{\circ Z}$ can be obtained by $X_{n,m}$ raised to the power of $Z_{n,m}$. According to (3.1), for the homogeneous IM,

$$P_M[k+1] = DS_M[k]_i A. \tag{3.16}$$

For the heterogeneous IM,

$$P_M[k+1] = \begin{bmatrix} R_1 DS_M[k]_i A_1 \\ \vdots \\ R_n DS_M[k]_i A_n \\ \vdots \\ R_N DS_M[k]_i A_N \end{bmatrix}, \tag{3.17}$$

where R_n denotes the row vector with '1' as its nth entry and '0' everywhere else. Thus, the dynamics of IM captured by the master Markov chain is given as

$$P[k+1] = S[k]G, \tag{3.18}$$

$$S[k+1] = Realize\left(P[k+1]\right), \tag{3.19}$$

where $S[k] \in \mathbb{R}^{1\times M^N}$ has '1' as its $s[k]$-th entry and '0' everywhere else. $S[k]$ and $P[k] \in \mathbb{R}^{1\times M^N}$ denote the state vector and PMF of the master Markov chain, respectively.

The following lemma states the relationship between the first-order and highest-order representations of IM.

Lemma 5. *[53] Given an IM, the influence matrix H and the corresponding master Markov chain transition matrix G have the relationship as*

$$BH = GB. \tag{3.20}$$

3.2.4 Identifiability of the homogeneous IMs

The identifiability of an IM describes whether the underlying parameters of the IM can be determined uniquely given sufficient observations. The identifiability conditions of IM is important because it determines whether the estimated model is unique and affects subsequent analysis and design that rely on the inherent structure of the IM.

Given F independent observation sequences as $Y = \{Y^{(1)}, Y^{(2)}, \cdots, Y^{(F)}\}$ where $Y^{(f)} = \left[S_V^{(f)}[1], S_V^{(f)}[2], \cdots, S_V^{(f)}[T]\right]$ with $f \in \{1, 2, \cdots, F\}$ and T is the length of the observation sequence, the identifiability of the underlying homogeneous IM is defined as follows.

Definition 1 [14]: The homogeneous IM is identifiable if and only if the optimal solution to the following likelihood function is unique given Y with $F, T \to \infty$,

$$\hat{\theta} = \arg\max_{\theta} P(Y|\theta), \tag{3.21}$$

where $\theta = (D, A)$.

The identifiability of the homogeneous IM was first investigated in [14] by examining the master Markov chain representation of IM. The main results are summarized in the following lemma.

Lemma 6. *[14] Given the master Markov transition matrix G of the homogeneous IM, the local Markov chain transition matrix A can be uniquely obtained as*

$$a_{m,q} = \sqrt[N]{g_{\frac{(m-1)(M^N-1)}{M-1}+1,\frac{(q-1)(M^N-1)}{M-1}+1}}, \tag{3.22}$$

where $\frac{(m-1)(M^N-1)}{M-1}+1$ is the state index of the master Markov chain with all sites in local status m, i.e., $S_n = [0 \ \cdots \ 1 \ \cdots \ 0]$ with '1' as its mth entry and '0' everywhere else for $\forall\ n \in \{1, 2, \cdots, N\}$. The network influence matrix D can be uniquely determined if and only if $Null(O) \subseteq Null(V)$ by

$$G_c = OE, \tag{3.23}$$

$$D_c = VE, \tag{3.24}$$

where G_c and D_c denote the column-vectorized version of G and D, respectively, $O \in \mathbb{R}^{M^{2N}\times N^N}$ is the local Markov information-centric matrix composed of specific combinations of elements in A, $E \in \mathbb{R}^{N^N\times 1}$ is constructed by specific combinations of elements in D, and $V \in \mathbb{R}^{N^2\times N^N}$ is the network influence permutation matrix composed of '1's and '0's constructed based merely on D.

Lemma 6 provides a necessary and sufficient identifiability condition for the homogeneous IM. However, it is not very easy to check as it relies on constructing the matrices $G \in \mathbb{R}^{M^N\times M^N}$, $O \in \mathbb{R}^{M^{2N}\times N^N}$ and $V \in \mathbb{R}^{N^2\times N^N}$. With the growth of network size, the dimensions of the matrices G, O and V increase rapidly, and hence high computational cost is needed to check the condition.

3.2.5 Problem Formulation

As summarized above, for homogeneous IMs, the existing identifiability check and parameter estimation methods consume high computation cost. In addition, there exists no study on the identifiability and estimation of heterogeneous IMs per our knowledge. We are thus motivated to study in this chapter the identifiability and estimation of general IMs with reduced computation. This is conducted through a new structural analysis that establishes the connection between the IMs' first-order and highest-order representations. The problems investigated in this chapter are formulated as follows.

Problem 1: Given Y with $F, T \to \infty$, determine the identifiability of the underlying homogeneous IM, i.e., whether the corresponding parameters $\theta = (D, A)$ can be uniquely determined from sufficient observations.

Problem 2: Given Y with $F, T \to \infty$, estimate the parameters $\theta = (D, A)$ of the underlying homogeneous IM.

Instead of resorting to the master Markov chain G and examining the matrices O and V which consume significant computation, we aim to find an easy-to-check identifiability condition and a computationally efficient parameter estimation algorithm for the homogeneous IM. Next, we study for the first time the identifiability and estimation problems for heterogeneous IMs.

Definition 2: The heterogeneous IM is identifiable if and only if the optimal solution to the following likelihood function is unique given Y with $F, T \to \infty$,

$$\hat{\theta} = \arg\max_{\theta} P(Y|\theta), \tag{3.25}$$

where $\theta = (D, A_n)$ for $\forall\ n \in \{1, 2, \cdots, N\}$.

Problem 3: Given Y with $F, T \to \infty$, determine the identifiability of the underlying heterogeneous IM, i.e., whether the corresponding parameters $\theta = (D, A_n)$ for $\forall\ n \in \{1, 2, \cdots, N\}$ can be uniquely determined from sufficient observations.

Problem 4: Given Y with $F, T \to \infty$, estimate the parameters $\theta = (D, A_n)$ for $\forall\ n \in \{1, 2, \cdots, N\}$ of the underlying heterogeneous IM.

Note that given adequate observations, i.e., $F,\ T \to \infty$, the identifiability condition and estimation algorithm of IMs are not affected by the stability of IMs.

3.3 The joint-margin matrix for the IM

In this section, to study the identifiability and estimation of IMs with reduced computation, we first construct the joint-margin matrix J which bridges the first-order and highest-order representations of a general IM. We then present the specific forms of J in homogeneous and heterogeneous IMs for subsequent identifiability and estimation studies.

3.3.1 The joint-margin matrix J in the IM

In this subsection, we first show the construction of the joint-margin matrix and then illustrate its relationship with the master Markov chain G and the influence matrix H.

The joint-margin matrix $J \in \mathbb{R}^{M^N \times MN}$ indicates the conditional PMFs of individual sites' next statuses given the current master Markov chain state. J consists of N blocks as

$$J = \begin{bmatrix} J_1 & J_2 & \cdots & J_N \end{bmatrix}, \tag{3.26}$$

where $J_n \in \mathbb{R}^{M^N \times M}$ for $n \in \{1, 2, \cdots, N\}$ is the nth block of J. The ith row and mth column element of J_n indicates the conditional probability of site n's next status as

$m \in \{1, 2, \cdots, M\}$ given the current master Markov chain state $i \in \{1, 2, \cdots, M^N\}$, i.e.,

$$J_{n_{i,m}} = P(s_n[k+1] = m | s[k] = i). \tag{3.27}$$

J_n is a row stochastic matrix.

In the following lemma, we show the relationships among the joint-margin matrix J, the influence matrix H, the master Markov chain G and the event matrix B.

Lemma 7.

$$J = GB = BH \tag{3.28}$$

Proof. First, we show $J = GB$. The ith row of the master Markov transition matrix G indicates the conditional PMF of its next state $s[k+1]$ given its current state $s[k] = i$. To obtain the conditional PMF of site n's next status $s_n[k+1] = m$ given $s[k] = i$ as in (3.27), we need to sum up all the probabilities of M^{N-1} states of G that have the corresponding local status of site n at next time step in G.

Let $\mathcal{S}_{n_m}$ denote the set of G's state indices which have site n's status as m. $\mathcal{S}_{n_m}$ is of size M^{N-1}. Note that the mth column of the nth block of the event matrix B, B_n, indicates the G's states indices which contain site n's status as m. Now we have

$$\begin{aligned} J_{n_{i,m}} &= P\left(s_n[k+1] = m | s[k] = i\right) \\ &= \sum_{j \in \mathcal{S}_{n_m}} P\left(s[k+1] = j | s[k] = i\right) = R_i G B_n C_m \end{aligned}. \tag{3.29}$$

R_iG indicates the ith row of G with $s[k] = i$, and B_nC_m locates G's states $s[k+1] = j$ corresponding to $s_n[k+1] = m$. Hence, we have

$$\begin{aligned} J_n &= \begin{bmatrix} R_1 \\ R_2 \\ \vdots \\ R_{M^N} \end{bmatrix} GB_n \begin{bmatrix} C_1 & C_2 & \cdots & C_M \end{bmatrix} \\ &= I_{M^N} GB_n I_M = GB_n, \end{aligned} \tag{3.30}$$

$$\begin{aligned} J &= \begin{bmatrix} J_1 & J_2 & \cdots & J_N \end{bmatrix} \\ &= \begin{bmatrix} GB_1 & GB_2 & \cdots & GB_N \end{bmatrix} = GB. \end{aligned} \tag{3.31}$$

(3.28) is obtained according to (3.20). □

Lemma 7 shows how to obtain J from G. Next, we show in the other direction how G can be obtained from J. Note that B is generally not a square matrix and hence does not necessarily have an inverse matrix. Lemmas 7 and 8 together show the one-to-one mapping between J and G.

Lemma 8. *The (i,j)th entry of the Master markov chain*

$$\begin{aligned} g_{i,j} &= P(s[k+1] = j | s[k] = i) \\ &= \prod_{n=1}^{N} P(s_n[k+1] = m_n | s[k] = i) = \prod_{n=1}^{N} J_{n_{i,m_n}} \end{aligned} \tag{3.32}$$

where $s_n[k+1] = m_n \in \{1, 2, \cdots, M\}$ is the status of individual site corresponding to $s[k+1] = j$ for $\forall\ n \in \{1, 2, \cdots, N\}$.

Proof. Equation (3.32) holds due to the fact that all sites evolve independently. □

3.3.2 The joint-margin matrix J in the homogeneous IM

In this subsection, we further show how the joint-margin matrix J is represented by the parameters $\theta = (D, A)$ in the homogeneous IM.

To represent J_n for $n \in \{1, 2, \cdots, N\}$ by its columns, we introduce the notation $\mathcal{A}_m \in \mathbb{R}^{M^N \times N}$ with $m \in \{1, 2, \cdots, M\}$, the mth local Markov information matrix. $\mathcal{A}_m$ is constructed using the mth column of A as

$$\mathcal{A}_m = \begin{bmatrix} a_{1,m} & a_{1,m} & \cdots & a_{1,m} \\ \vdots & \vdots & \vdots & \vdots \\ a_{q_1,m} & a_{q_2,m} & \cdots & a_{q_N,m} \\ \vdots & \vdots & \vdots & \vdots \\ a_{M,m} & a_{M,m} & \cdots & a_{M,m} \end{bmatrix}, \tag{3.33}$$

where q_n indicates the local status of site n. The row indices of all elements within each row of the matrix $\mathcal{A}_m$, $(q_1, q_2, \cdots, q_N)$ correspond to one of the M^N possible states of the master Markov chain. For example, given $N = 3$ and $M = 2$, $\mathcal{A}_2$ is constructed using the 2th column of A as

$$\mathcal{A}_2 = \begin{bmatrix} a_{1,2} & a_{1,2} & a_{1,2} \\ a_{1,2} & a_{1,2} & a_{2,2} \\ a_{1,2} & a_{2,2} & a_{1,2} \\ a_{1,2} & a_{2,2} & a_{2,2} \\ a_{2,2} & a_{1,2} & a_{1,2} \\ a_{2,2} & a_{1,2} & a_{2,2} \\ a_{2,2} & a_{2,2} & a_{1,2} \\ a_{2,2} & a_{2,2} & a_{2,2} \end{bmatrix}.$$

Based on the influence matrix H in (3.7), the event matrix B in (3.9) and (3.10) and $J = BH$ in (3.28), we represent J_n for $n \in \{1, 2, \cdots, N\}$ by its columns as

$$J_n = \begin{bmatrix} \mathcal{A}_1 D' C_n & \mathcal{A}_2 D' C_n & \ldots & \mathcal{A}_M D' C_n \end{bmatrix}. \tag{3.34}$$

$D'C_n$ indicates the nth column of matrix D', i.e., the transpose of nth row of matrix D.

The mapping from $\theta = (D, A)$ to the joint-margin matrix J is denoted by the function $\eta_J : \theta \to J$ and the corresponding inverse mapping is denoted by the inverse function $\eta_\theta^{-1} : J \to \theta$.

3.3.3 The joint-margin matrix J in the heterogeneous IM

We also show how the joint-margin matrix J is represented by the parameters $\theta = (D, A_n)$ for $\forall\ n \in \{1, 2, \cdots, N\}$ in the heterogeneous IM.

Similarly to the homogeneous IM, we first introduce $\mathcal{A}_{n_m} \in \mathbb{R}^{M^N \times N}$ with $m \in \{1, 2, \cdots, M\}$, the mth local Markov information matrix of site n for $\forall\ n \in \{1, 2, \cdots, N\}$ in the heterogeneous IM. $\mathcal{A}_{n_m}$ is constructed using the mth column of matrix A_n as

$$\mathcal{A}_{n_m} = \begin{bmatrix} a_{n_{1,m}} & a_{n_{1,m}} & \cdots & a_{n_{1,m}} \\ \vdots & \vdots & \vdots & \vdots \\ a_{n_{q_1,m}} & a_{n_{q_2,m}} & \cdots & a_{n_{q_N,m}} \\ \vdots & \vdots & \vdots & \vdots \\ a_{n_{M,m}} & a_{n_{M,m}} & \cdots & a_{n_{M,m}} \end{bmatrix}, \tag{3.35}$$

where q_n indicates the local status of site n, and the row index of the elements in each row of the matrix $\mathcal{A}_{n_m}$, $(q_1, q_2, \cdots, q_N)$ indicates one of the possible states of

the master Markov chain. For example, given $N = 3$ and $M = 2$, $\mathcal{A}_{3_2}$ is constructed using the 2th column of A_3 as

$$\mathcal{A}_{3_2} = \begin{bmatrix} a_{3_{1,2}} & a_{3_{1,2}} & a_{3_{1,2}} \\ a_{3_{1,2}} & a_{3_{1,2}} & a_{3_{2,2}} \\ a_{3_{1,2}} & a_{3_{2,2}} & a_{3_{1,2}} \\ a_{3_{1,2}} & a_{3_{2,2}} & a_{3_{2,2}} \\ a_{3_{2,2}} & a_{3_{1,2}} & a_{3_{1,2}} \\ a_{3_{2,2}} & a_{3_{1,2}} & a_{3_{2,2}} \\ a_{3_{2,2}} & a_{3_{2,2}} & a_{3_{1,2}} \\ a_{3_{2,2}} & a_{3_{2,2}} & a_{3_{2,2}} \end{bmatrix}.$$

Based on the influence matrix H in (3.8), the event matrix B in (3.9) and (3.10) and $J = BH$ in (3.28), we represent the columns of J_n for $\forall\ n \in \{1, 2, \cdots, N\}$ in a heterogeneous IM as

$$J_n = \begin{bmatrix} \mathcal{A}_{n_1} D' C_n & \mathcal{A}_{n_2} D' C_n & \cdots & \mathcal{A}_{n_M} D' C_n \end{bmatrix}. \tag{3.36}$$

The mapping from $\theta = (D, A_n)$ for $\forall\ n \in \{1, 2, \cdots, N\}$ to the joint-margin matrix J is denoted by the function $\xi_J : \theta \to J$ and the corresponding inverse mapping is denoted by the inverse function $\xi_\theta^{-1} : J \to \theta$.

3.4 Identifiability Analysis of the IM

In this section, we present the main results on the sufficient and necessary conditions for the identifiability of both the homogeneous IM and the heterogeneous IM through the corresponding joint-margin matrix J.

3.4.1 Sufficient and Necessary Conditions for the Identifiability of the Homogeneous IM

We first show in the following lemma that the identifiability of the homogeneous IM is equivalent to the uniqueness of the solution to the inverse function $\eta_\theta^{-1} : J \to \theta$.

Lemma 9. *Given the independent observation sequences Y with $F, T \to \infty$, the underlying homogeneous IM is identifiable if and only if the solution to $\eta_\theta^{-1}(J)$ is unique where $\theta = (D, A)$.*

Proof. G can be uniquely determined from the observation sequences Y [14]. In addition, as the event matrix B is fixed once M and N are given, J can be uniquely determined from Y based on Lemma 7. Furthermore, as J and G have an one-to-one mapping according to Lemmas 7 and 8, the state transition information contained in G and J is equivalent. Therefore, we come to the conclusion that the homogeneous IM is identifiable if and only if the solution to $\eta_\theta^{-1}(J)$ is unique. □

Lemma 9 transforms the identifibility analysis of the homogeneous IM into the uniqueness of the solution to $\eta_\theta^{-1}(J)$. Note that according to (3.27), J can be determined directly from the observation sequences Y with $F, T \to \infty$ by counting the corresponding frequencies based on the law of large numbers [68]. Lemma 9 suggests that the the identifiability analysis using J instead of G saves computation, as $G \in \mathbb{R}^{M^N \times M^N}$ and $J \in \mathbb{R}^{M^N \times MN}$. We next provide the uniqueness analysis of A and D in the following two theorems, respectively.

Theorem 5. *Given the joint-margin matrix J of a homogeneous IM with the network influence matrix D and local Markov chain transition matrix A, $\eta_A^{-1} : J \to A$ has the unique solution*

$$a_{m,q} = J_{n_{\frac{(m-1)(M^N-1)}{M-1}+1,q}}, \tag{3.37}$$

where $m, q \in \{1, 2, \cdots, M\}$ for any $n \in \{1, 2, \cdots, N\}$.

Proof. $\frac{(m-1)\left(M^N-1\right)}{M-1}+1$ is the state index of the master Markov chain with all sites in local status m. According to (3.33) and (3.34), for any $n \in \{1,2,\cdots,N\}$, we have

$$\begin{aligned} & J_{n\,\frac{(m-1)\left(M^N-1\right)}{M-1}+1,q} \\ & = P\left(s_n[k+1]=q|s[k]=\frac{(m-1)\left(M^N-1\right)}{M-1}+1\right) \\ & = \sum_{l=1}^{N} d_{n,l}a_{m,q} = a_{m,q}. \end{aligned} \tag{3.38}$$

The last equation holds because the network influence matrix D is a stochastic matrix, i.e., $\sum_{l=1}^{N} d_{n,l}=1$. □

Theorem 6. *Given the joint-margin matrix J of a homogeneous IM with the network influence matrix D and local Markov chain transition matrix A, $\eta_D^{-1}: J \to D$ has the unique solution if and only if $rank(A) > 1$.*

Proof. First, we prove that $rank(A) > 1$ is a sufficient condition for the uniqueness of the solution to $\eta_D^{-1}: J \to D$.

If $rank(A) > 1$, at least one column of A has two or more nonidentical entries, because A is a stochastic matrix. Let a_1 and a_2 denote the two nonidentical entries in the mth column of matrix A with $m \in \{1,2,\cdots,M\}$. There always exists a Nth order minor of matrix $\mathcal{A}_m$ that is nonzero, because

$$\begin{vmatrix} a_1 & a_2 & \cdots & a_2 \\ a_2 & a_1 & \cdots & a_2 \\ \vdots & \vdots & \ddots & \vdots \\ a_2 & a_2 & \cdots & a_1 \end{vmatrix} = (a_1-a_2)^{N-1}\left(a_1+(N-1)a_2\right) \neq 0 \tag{3.39}$$

if $a_1 \neq a_2$ and $N > 1$. This indicates that $rank(\mathcal{A}_m) = N$, i.e., $\mathcal{A}_m$ is full column rank. According to (3.34), with J_nC_m indicating the mth column of J_n, the solution to $\mathcal{A}_m D' C_n = J_n C_m$ is unique, i.e., the nth row of D can be uniquely determined. By

solving all N equations $\mathcal{A}_m D' C_n = J_n C_m$ for $\forall\ n \in \{1, 2, \cdots, N\}$, D can be uniquely determined. Hence we come to the conclusion that if $rank(A) > 1$, the solution to $\eta_D^{-1}(J)$ is unique.

Next, we prove that $rank(A) > 1$ is a necessary condition for the uniqueness of the solution to $\eta_D^{-1} : J \to D$. Because A is a stochastic matrix, all rows of A are identical when $rank(A) = 1$. The elements within each column of A are identical. In this case, all elements in $\mathcal{A}_m$ are identical and hence $rank(\mathcal{A}_m) = 1$ for $\forall\ m \in \{1, 2, \cdots, M\}$, which implies that we cannot find an $\mathcal{A}_m$ so that the solutions to $\mathcal{A}_m D' C_n = J_n C_m$ for $\forall\ n \in \{1, 2, \cdots, N\}$ are unique. This leads to the conclusion that if $rank(A) = 1$, the solution to $\eta_D^{-1}(J)$ is not unique.

Combining the above analysis, we conclude that the network influence matrix D can be uniquely determined if and only if $rank(A) > 1$. □

Theorem 6 also also implies the approach to calculate the network influence matrix D through the joint margin matrix J, as shown in the following corollary.

Corollary 1. *When $rank(A) > 1$, the network influence matrix D can be determined uniquely by solving the following equation*

$$\mathcal{A}_m D' = JW, \tag{3.40}$$

where $\mathcal{A}_m$ is constructed as in (3.33) *by the mth column of A which has at least two nonidentical entries. $W \in \mathbb{R}^{MN \times N}$ is constructed as*

$$W_{x,n} = \begin{cases} 1 & if\ x = (n-1)M + m \\ 0 & otherwise \end{cases} \tag{3.41}$$

where $1 \le x \le MN,\ 1 \le n \le N$.

Proof. The nth row of D can be obtained by solving $\mathcal{A}_m D' C_n = J_n C_m$ for $n \in \{1, 2, \cdots, N\}$ according to Theorem 6. To combine all N equations in a matrix form,

we use the auxiliary matrix W to place the mth column of J_n for $\forall\, n \in \{1, 2, \cdots, N\}$ in a matrix, i.e., the mth, $(m+M)$th, $(m+2M)$th, $\cdots$, $(m+(N-1)M)$th columns of the joint-margin matrix J. Equation (3.40) is thus proven.

□

Theorems 5 and 6 lead to the sufficient and necessary condition for the identifiability of the homogeneous IM.

Theorem 7. *Given the joint-margin matrix J of a homogeneous IM with the network influence matrix D and local Markov chain transition matrix A, a homogeneous influence model is identifiable if and only if $rank(A) > 1$.*

Proof. A can be uniquely obtained from the joint-margin matrix J according to Theorem 5, and D can be determined uniquely if and only if $rank(A) > 1$ according to Theorem 6. Based on Lemma 9, this theorem is proved. □

Remark 1. *Theorem 7 finds a computationally efficient and easy-to-check sufficient and necessary condition for the identifiability of the homogeneous IM. Note that the condition developed in [14] is in a more complicated form. As shown in Lemma 6, the condition there requires to obtain $G \in \mathbb{R}^{M^N \times M^N}$ from observation data and then to construct the matrices $O \in \mathbb{R}^{M^{2N} \times N^N}$ and $V \in \mathbb{R}^{N^2 \times N^N}$ of very large dimensions. In contrast, here only the matrix $J \in \mathbb{R}^{M^N \times MN}$ is needed to construct A and to check its rank. We also note that the condition $rank(A) > 1$ was provided in [14] as a necessary condition. In this chapter, we prove that it is a stronger necessary and sufficient condition.*

3.4.2 Sufficient and Necessary Conditions for the Identifiability of the Heterogeneous IM

In this subsection, we further analyze the sufficient and necessary condition for the identifiability of the heterogeneous IM through the corresponding joint-margin matrix J. Similar to Lemma 9, we show in the following lemma that the identifiability of heterogeneous IM is equivalent to the uniqueness of the solution to the inverse function $\xi_\theta^{-1} : J \to \theta$.

Lemma 10. *Given the independent observation sequences Y with $F, T \to \infty$, the underlying heterogeneous IM is identifiable if and only if the solution to $\xi_\theta^{-1}(J)$ is unique where $\theta = (D, A_n)$ for $\forall\ n \in \{1, 2, \cdots, N\}$.*

Proof. The proof is similar to that of Lemma 9 and omitted here. □

Base on Lemma 10, we show the uniqueness of A_n and D of the heterogeneous IM for $\forall\ n \in \{1, 2, \cdots, N\}$ in the following two theorems, respectively.

Theorem 8. *Given the joint-margin matrix J of a heterogeneous IM with the network influence matrix D and local Markov chain transition matrices A_n with $n \in \{1, 2, \cdots, N\}$, $\xi_{A_n}^{-1} : J \to A_n$ has the unique solution*

$$a_{n_{m,q}} = J_{n_{\frac{(m-1)\left(M^N-1\right)}{M-1}+1,q}} \tag{3.42}$$

where $m, q \in \{1, 2, \cdots, M\}$ for $\forall\ n \in \{1, 2, \cdots, N\}$.

Proof. Similar to the proof of Theorem 5, in the heterogeneous IM, according to (3.35) and (3.36), we have for $\forall\ n \in \{1, 2, \cdots, N\}$,

$$\begin{aligned} & J_{n_{\frac{(m-1)\left(M^N-1\right)}{M-1}+1,q}} \\ &= P\left(s_n[k+1] = q | s[k] = \frac{(m-1)\left(M^N-1\right)}{M-1} + 1\right) \\ &= \sum_{l=1}^{N} d_{n,l} a_{n_{m,q}} = a_{n_{m,q}}. \end{aligned} \tag{3.43}$$

The last equation holds due to the fact that D is a stochastic matrix, i.e., $\sum_{l=1}^{N} d_{n,l} = 1$. □

Theorem 9. *Given the joint-margin matrix J of a heterogeneous IM with the network influence matrix D and local Markov chain transition matrices A_n with $n \in \{1, 2, \cdots, N\}$, $\xi_D^{-1} : J \to D$ has the unique solution if and only if $rank(A_n) > 1$ for $\forall\ n \in \{1, 2, \cdots, N\}$.*

Proof. First we show that $rank(A_n) > 1$ for $\forall\ n \in \{1, 2, \cdots, N\}$ is a sufficient condition for the uniqueness of the solution to $\xi_D^{-1} : J \to D$.

The proof is similar to that of Theorem 6. For any site n, if $rank(A_n) > 1$, we can always find a column in A_n indexed by $m \in \{1, 2, \cdots, M\}$ with at least two nonidentical entries to construct $\mathcal{A}_{n_m}$ so that the solution to $\mathcal{A}_{n_m} D' C_n = J_n C_m$ is unique. In other words, if $rank(A_n) > 1$, the nth row of matrix D can be determined uniquely. Considering all rows of D, we come to the conclusion that if $rank(A_n) > 1$ for $\forall\ n \in \{1, 2, \cdots, N\}$, the solution to $\xi_D^{-1}(J)$ is unique.

Then we prove that $rank(A_n) > 1$ for $\forall\ n \in \{1, 2, \ldots, N\}$ is also a necessary condition for the uniqueness of the solution to $\xi_D^{-1} : J \to D$.

Similar to the proof of Theorem 6, for any site n, if $rank(A_n) = 1$, we cannot find a column in A_n indexed by $m \in \{1, 2, \cdots, M\}$ with at least two nonidentical entries to construct $\mathcal{A}_{n_m}$ so that the solution to $\mathcal{A}_{n_m} D' C_n = J_n C_m$ is unique. In other words, if $rank(A_n) = 1$, the nth row of matrix D cannot be determined uniquely. To account for all rows of D, we come to the conclusion that if $rank(A_n) = 1$ for $\exists\ n \in \{1, 2, \cdots, N\}$, the solution to $\xi_D^{-1}(J)$ is not unique.

Combining the conclusions above, we conclude that the network influence matrix D can be determined uniquely if and only if $rank(A_n) > 1$ for $\forall\ n \in \{1, 2, \cdots, N\}$. □

Theorem 9 also indicates the approach to calculate the network influence matrix D in the heterogeneous IM, as shown in the following corollary.

Corollary 2. *If* $rank(A_n) > 1$ *for* $\forall\ n \in \{1, 2, \cdots, N\}$*, the network influence matrix* D *can be determined uniquely by solving the following* N *equations*

$$\mathcal{A}_{n_m} D' C_n = J_n C_m, \tag{3.44}$$

where $n \in \{1, 2, \cdots, N\}$*.* $\mathcal{A}_{n_m}$ *is constructed as in* (3.35) *by the* m*th column of* A_n *which has at least two nonidentical entries.*

Proof. See proof of Theorem 9. □

Theorems 8 and 9 lead to the sufficient and necessary condition for the identifiability of the heterogeneous IM. This is the first time the identifiability of the heterogeneous IM is investigated in the literature.

Theorem 10. *Given the joint-margin matrix* J *of a heterogeneous IM with the network influence matrix* D *and local Markov chain transition matrices* A_n *with* $n \in \{1, 2, \cdots, N\}$*, a heterogeneous IM is identifiable if and only if* $rank(A_n) > 1$ *for* $\forall\ n \in \{1, 2, \cdots, N\}$*.*

Proof. According to Theorems 8 and 9, A_n for $\forall\ n \in \{1, 2, \cdots, N\}$ can be obtained uniquely from J, and D can be determined uniquely if and only if $rank(A_n) > 1$ for $\forall\ n \in \{1, 2, \cdots, N\}$. Based on Lemma 10, the theorem is proven. □

3.5 Estimation Algorithms of the IM

The joint-margin matrix J introduced in Section 3.3 plays an important role in the identifiability analysis of both homogeneous and heterogeneous IM in Section 3.4. Building upon the joint-margin matrix J, we develop in this section the joint-

margin probability based estimation (JMPE) approaches for the parameters of both the homogeneous and heterogeneous IM.

First, we describe the joint-margin probability based estimation (JMPE) technique to determine $\theta = (D, A)$ in the homogeneous IM. As shown in Algorithm 1, the joint-margin matrix J is obtained from the observation sequences by calculating the corresponding frequencies. Next, the local Markov chain transition matrix A is determined by specific elements of J according to Theorem 5. Then, based on Theorem 6, whether the network influence matrix D can be uniquely obtained from J is checked. If D is identifiable, D is found according to Corollary 1. Note that A can determined by J_n for any $n \in \{1, 2, \cdots, N\}$ and J_1 is used in the Algorithm 1.

Algorithm 1 Joint-Margin Probability Based Estimation for Homogeneous IM

Input:

Observation sequences Y.

Output:

Matrices A and D.

Calculate state transition frequencies according to (3.27) from the observation sequences Y, and then construct J_n for $n \in \{1, 2, \cdots, N\}$. J is obtained according to (3.26).

Compute the local Markov chain transition matrix A from J_1 according to (3.37).

if $rank(A) > 1$ **then**

    Find the mth column of A that has at least two nonidentical entries and then construct $\mathcal{A}_m$ as (3.33).

    Construct W according to (3.41).

    Apply the least squares regression to (3.40) to obtain the network influence matrix D.

else

    The influence model is not identifiable.

end if

Remark 2. *The computation for parameter estimation involves estimating the local Markov transition matrix A and the influence matrix D. A is estimated by* (3.22) *in LAE [14], which requires calculating an Nth root. However, JMPE uses* (3.37)*, which only requires finding specific elements of J. The estimation of D in LAE [14] needs to solve M^{2N} equations for N^N unknowns according to* (3.23)*. In contrast, JMPE requires to solve $M^N N$ equations for N^2 unknowns according to* (3.40)*. Thus, JMPE*

is more efficient than LAE in [14], and this computational reduction becomes more significant with the increase of network size N.

A JMPE technique is also developed to determine $\theta = (D, A_n)$ for $\forall\ n \in \{1, 2, \cdots, N\}$ in the heterogeneous IM as shown in Algorithm 2. The procedure is similar to the homogeneous case except that the joint-margin matrix J instead of its one block is needed to determine the local Markov chain transition matrices A_n. Note that the column indices m in each A_n for $n \in \{1, 2, \cdots, N\}$ used to construct the local Markov information matrices $\mathcal{A}_{n_m}$ may be different. In this case, the N equations used to obtain the matrix D are not organized in the matrix form and are solved individually instead.

Note that JMPE is a stable estimator (i.e., robust against variations in the observations [82]) given adequate observations, i.e., Y with $F,\ T \to \infty$. This is because that obtaining J from Y is stable based on the law of large numbers [68] and obtaining estimated parameters from J is also stable as it only involves simple linear algebra.

Algorithm 2 Joint-Margin Probability Based Estimation for Heterogeneous IM

Input:

Observation sequences Y.

Output:

Matrices A_n and D for $\forall\ n \in \{1, 2, \ldots, N\}$.

Calculate state transition frequencies according to (3.27) from the observation sequences Y, and then construct J_n for $\forall\ n \in \{1, 2, \cdots, N\}$.

Compute the local Markov chain transition matrix A_n from J_n for $\forall\ n \in \{1, 2, \cdots, N\}$ according to (3.42).

for $n = 1 : N$ **do**

  if $rank(A_n) > 1$ **then**

    Find the mth column of A_n which has at least two nonidentical entries and then construct $\mathcal{A}_{n_m}$ according to (3.35).

    Apply the least squares regression to (3.44) to obtain the nth row of the network influence matrix D.

  else

    The influence model is not identifiable.

  end if

end for

3.6 Simulation studies

In this section, we present some numerical results to validate the theorems and corollaries in Section 3.4 and illustrate the effectiveness and efficiency of the estimation algorithms developed in Section 3.5. An example of opinion propagation

in a social network is also provided to show the applicability of heterogeneous IMs. We use MATLAB on a Dell XPS 13 laptop for simulations.

3.6.1 Case 1: An Identifiable Homogeneous IM

Consider a homogeneous IM of 3 sites with 3 local statuses for each site. The underlying parameter $\theta = (D, A)$ is given as follows, based on which an observation sequence of length $40,000$ is generated.

$$A = \begin{bmatrix} 0.50 & 0.30 & 0.20 \\ 0.30 & 0.45 & 0.25 \\ 0.20 & 0.20 & 0.60 \end{bmatrix}, \; D = \begin{bmatrix} 0.70 & 0.20 & 0.10 \\ 0.10 & 0.85 & 0.05 \\ 0.20 & 0.15 & 0.65 \end{bmatrix}.$$

According to Theorem 7, the homogeneous IM is identifiable because $rank(A) > 1$. The JMPE approach in Algorithm 1 is applied to estimate $\theta = (D, A)$ from the generated observation sequence. The results are given as follows,

$$\hat{A}_{JMPE} = \begin{bmatrix} 0.5159 & 0.2868 & 0.1973 \\ 0.2881 & 0.4481 & 0.2637 \\ 0.2012 & 0.2116 & 0.5873 \end{bmatrix},$$

$$\hat{D}_{JMPE} = \begin{bmatrix} 0.6839 & 0.2032 & 0.1145 \\ 0.1025 & 0.8495 & 0.0497 \\ 0.2057 & 0.1766 & 0.6147 \end{bmatrix},$$

where the subscript denotes the estimation algorithm used.

In addition, the commonly-used maximum likelihood estimation (MLE) and the linear algebra based estimation (LAE) [14] are applied to the same observation sequence for comparative performance analysis. The results are shown as follows,

$$\hat{A}_{MLE} = \begin{bmatrix} 0.5008 & 0.3009 & 0.1983 \\ 0.3014 & 0.4507 & 0.2479 \\ 0.1977 & 0.2024 & 0.6000 \end{bmatrix},$$

$$\hat{D}_{MLE} = \begin{bmatrix} 0.6844 & 0.2130 & 0.1026 \\ 0.1020 & 0.8292 & 0.0688 \\ 0.2078 & 0.1479 & 0.6443 \end{bmatrix},$$

$$\hat{A}_{LAE} = \begin{bmatrix} 0.5035 & 0.3090 & 0.1875 \\ 0.3003 & 0.4664 & 0.2333 \\ 0.2112 & 0.2180 & 0.5708 \end{bmatrix},$$

$$\hat{D}_{LAE} = \begin{bmatrix} 0.6742 & 0.2108 & 0.1150 \\ 0.1024 & 0.8103 & 0.0873 \\ 0.2038 & 0.1437 & 0.6525 \end{bmatrix}.$$

The mean squared error (MSE) and execution time (ET) are used as two metrics for algorithm performance comparison, as shown in Table 3.1. The ET of MLE is the largest among three methods despite its smallest MSE. Compared to MLE, the computational cost of JMPE is significantly reduced with the MSE increased slightly. Compared to LAE, JMPE has similar accuracy but with lower computational cost.

Table 3.1: The performance comparison of three estimation algorithms for the homogeneous IM

Method	MSE	ET (second)
JMPE	1.9660×10^{-4}	0.3800
MLE	7.3839×10^{-5}	209.0850
LAE	3.4135×10^{-4}	0.5100

3.6.2 Case 2: A Non-identifiable Homogeneous IM

Consider a homogeneous IM of 3 sites with 3 local statuses for each site. The underlying parameter $\theta = (D, A)$ is given as follows, based on which 100 observation sequences of length $40,000$ are generated.

$$A = \begin{bmatrix} 0.60 & 0.25 & 0.15 \\ 0.60 & 0.25 & 0.15 \\ 0.60 & 0.25 & 0.15 \end{bmatrix}, \; D = \begin{bmatrix} 0.70 & 0.20 & 0.10 \\ 0.10 & 0.85 & 0.05 \\ 0.20 & 0.15 & 0.65 \end{bmatrix}.$$

According to Theorem 7, the homogeneous IM is not identifiable because $rank(A) = 1$. Applying the MLE method to each generated observation sequence, we can uniquely determine A, but the estimations of D vary each time, indicating that D is non-identifiable. The average MSE is 0.0996 in the range of $(0.0082, 0.2026)$.

3.6.3 Case 3: An Identifiable Heterogeneous IM

Consider a heterogeneous IM of 3 sites with 3 local statuses for each site. The underlying parameters $\theta = (D, A_n)$ with $n \in \{1, 2, 3\}$ are given as follows, based on which an observation sequence of length $40,000$ is generated.

$$A_1 = \begin{bmatrix} 0.70 & 0.20 & 0.10 \\ 0.10 & 0.85 & 0.05 \\ 0.20 & 0.15 & 0.65 \end{bmatrix}, \; A_2 = \begin{bmatrix} 0.10 & 0.10 & 0.80 \\ 0.50 & 0.20 & 0.30 \\ 0.10 & 0.55 & 0.35 \end{bmatrix},$$

$$A_3 = \begin{bmatrix} 0.50 & 0.30 & 0.20 \\ 0.30 & 0.45 & 0.25 \\ 0.20 & 0.20 & 0.60 \end{bmatrix}, \; D = \begin{bmatrix} 0.10 & 0.10 & 0.80 \\ 0.50 & 0.20 & 0.30 \\ 0.05 & 0.60 & 0.35 \end{bmatrix}.$$

Because $rank(A_n) > 1$ for $\forall\ n \in \{1, 2, 3\}$, the heterogeneous IM is identifiable according to Theorem 10. Applying the JMPE method in Algorithm 2, we obtain the following results with MSE of 8.3420×10^{-5}.

$$\hat{A}_{1\ JMPE} = \begin{bmatrix} 0.6861 & 0.2141 & 0.0998 \\ 0.0966 & 0.8481 & 0.0554 \\ 0.2018 & 0.1630 & 0.3652 \end{bmatrix},$$

$$\hat{A}_{2\ JMPE} = \begin{bmatrix} 0.0964 & 0.0953 & 0.8083 \\ 0.5150 & 0.2088 & 0.2762 \\ 0.0922 & 0.5532 & 0.3546 \end{bmatrix},$$

$$\hat{A}_{3\ JMPE} = \begin{bmatrix} 0.5011 & 0.2937 & 0.2052 \\ 0.2912 & 0.4394 & 0.2695 \\ 0.2036 & 0.2000 & 0.5964 \end{bmatrix},$$

$$\hat{D}_{JMPE} = \begin{bmatrix} 0.1045 & 0.0954 & 0.8008 \\ 0.4987 & 0.1942 & 0.3084 \\ 0.0395 & 0.6000 & 0.3637 \end{bmatrix}.$$

MLE is also applied to the same observation sequence for comparison. The results are shown as follows with MSE of 2.8079×10^{-5}, a little smaller than that by JMPE. However, the ET of MLE is 201.7741 seconds, significantly larger than JMPE (0.3314 seconds).

$$\hat{A}_{1\ MLE} = \begin{bmatrix} 0.6982 & 0.2042 & 0.0976 \\ 0.0978 & 0.8505 & 0.0517 \\ 0.2063 & 0.1506 & 0.6431 \end{bmatrix},$$

$$\hat{A}_{2\ MLE} = \begin{bmatrix} 0.1001 & 0.0916 & 0.8083 \\ 0.5065 & 0.2005 & 0.2930 \\ 0.0905 & 0.5570 & 0.3525 \end{bmatrix},$$

$$\hat{A}_{3\ MLE} = \begin{bmatrix} 0.5010 & 0.3004 & 0.1986 \\ 0.3018 & 0.4512 & 0.2471 \\ 0.1969 & 0.2008 & 0.6023 \end{bmatrix},$$

$$\hat{D}_{MLE} = \begin{bmatrix} 0.0948 & 0.1000 & 0.8052 \\ 0.4919 & 0.2013 & 0.3068 \\ 0.0494 & 0.5877 & 0.3628 \end{bmatrix}.$$

3.6.4 Case 4: A Non-identifiable Heterogeneous IM

Consider a heterogeneous IM with 2 sites with 2 local status for each site. The underlying parameter $\theta = (D, A_n)$ with $n \in \{1, 2\}$ is given as follows. 100 observation sequences with length $4,000$ are generated.

$$A_1 = \begin{bmatrix} 0.70 & 0.30 \\ 0.35 & 0.65 \end{bmatrix},\ A_2 = \begin{bmatrix} 0.55 & 0.45 \\ 0.55 & 0.45 \end{bmatrix},\ D = \begin{bmatrix} 0.40 & 0.60 \\ 0.50 & 0.50 \end{bmatrix}.$$

According to Theorem 10, the heterogeneous IM is not identifiable because $rank(A_2) = 1$. Applying the MLE method to each generated observation sequence, we find that A_n for $n \in \{1, 2\}$ can be determined uniquely, however the estimations of D vary in each run. More preciously, the 2nd row of D cannot be determined uniquely, indicating that D is not identifiable.

3.6.5 Case 5: Support or Oppose?

In Case 5, we show the implementation of heterogeneous IMs in capturing the opinion propagation of a social network.

Consider a group of 7 individuals, each of whom can have one of the two opposite opinions towards a certain event, e.g., 'support' and 'oppose', which are captured as local statuses '1' and '2'. Each individual can be influenced differently by those around them (captured by matrix D) and can determine his/her own opinion differently given neighbors' opinions (captured by matrices A_n). 7 individuals have diverse behaviors, reflected by the parameters of the heterogeneous IM as follows. Person '1' is very persistent in his own idea and good at persuading others, indicated by $d_{1,1} = 0.95$ and $d_{i,1} = 0.4$ for $i \in \{2, \cdots, 7\}$. Persons '2' and '3' follow the same way to determine their own opinions, indicated by $A_2 = A_3$, while persons '4', '5' and '6' have their similar ways, indicated by $A_4 = A_5 = A_6$. Person '7' plays devil's advocate, reflected by A_7 with all '1's as its anti-diagonal elements. The initial opinion of all but person '1' is 'oppose'. The underlying parameters of the heterogeneous IM with $N = 7$ and $M = 2$ are summarized as follows.

$$D = \begin{bmatrix} 0.95 & 0 & 0.05 & 0 & 0 & 0 & 0 \\ 0.4 & 0.1 & 0.1 & 0.1 & 0.1 & 0.1 & 0.1 \\ 0.4 & 0.1 & 0.1 & 0.1 & 0.1 & 0.1 & 0.1 \\ 0.4 & 0.1 & 0.1 & 0.1 & 0.1 & 0.1 & 0.1 \\ 0.4 & 0.1 & 0.1 & 0.1 & 0.1 & 0.1 & 0.1 \\ 0.4 & 0.1 & 0.1 & 0.1 & 0.1 & 0.1 & 0.1 \\ 0.4 & 0.1 & 0.1 & 0.1 & 0.1 & 0.1 & 0.1 \end{bmatrix},$$

$$A_1 = \begin{bmatrix} 1 & 0 \\ 0 & 1 \end{bmatrix}, A_7 = \begin{bmatrix} 0 & 1 \\ 1 & 0 \end{bmatrix}.$$

$$A_2 = A_3 = \begin{bmatrix} 1 & 0 \\ 0.2 & 0.8 \end{bmatrix}, A_4 = A_5 = A_6 = \begin{bmatrix} 1 & 0 \\ 0.5 & 0.5 \end{bmatrix}.$$

According to Theorem 10, the underlying heterogeneous IM is identifiable. Applying the JMPE and MLE to observation sequences, the MSE of the estimated parameters are 5.2642×10^{-6} and 0.0902 for JMPE and MLE respectively, showing that a higher accuracy is achieved with our developed approach. Meanwhile, the efficiency has also been improved with ET as 187.8477 seconds and 311.4101 seconds for JMPE and MLE, respectively.

The estimated parameters of the underlying heterogeneous IM can be used to predict the final voting result after thorough discussions. The influence matrix H can be reconstructed from $\hat{\theta} = (\hat{D}, \hat{A}_n)$ based on (3.8). The steady-state status probability for each individual can be determined by the left eigenvector of H associated with its eigenvalue '1', which is

$$\begin{bmatrix} 0.8295 & 0.1705 \\ 0.8283 & 0.1717 \\ 0.8288 & 0.1712 \\ 0.8941 & 0.1059 \\ 0.8960 & 0.1040 \\ 0.8920 & 0.1080 \\ 0.2126 & 0.7874 \end{bmatrix},$$

where the ith row indicates the steady-state status probability of person i for $i \in \{1, 2, \cdots, 7\}$. The final voting result is more probable to be 'support' based on the majority rule because 6 out of 7 individuals are more likely to support the event. We also observe that individuals with a similar way to determine their own opinions have similar steady-state status probability distributions, e.g., persons '4', '5' and '6'. Finally, note that if using a master Markov chain, the number of states to track the dynamics will be $2^7 = 128$ and the analysis using a transition matrix $G \in \mathbb{R}^{128 \times 128}$

will incur significant computational cost, compared to $H \in \mathbb{R}^{14\times 14}$ using the influence model.

3.7 Conclusion

In this chapter, we took a structural approach to study the identifiability and estimation of both the homogeneous IMs and the heterogeneous IMs with reduced computation. To facilitate the identifiability analysis, we introduced the joint-margin matrix J which connects the first-order and highest-order representations of IMs. Based on J, we find that the local Markov chain transition matrices are always identifiable and their ranks determine the identifiability of the network influence matrix D. The if-and-only-if identifiability condition identified in this chapter for the homogeneous IMs is much simpler to check compared to that in [14]. For heterogeneous IMs, the if-and-only-if identifiability condition identified is the first in the literature and shows that the individual local Markov chain transition matrix determines the identifiability of the corresponding row of D. Based on the identifiability analysis, we developed the joint-margin probability based estimation (JMPE) methods for both the homogeneous IMs and heterogeneous IMs. The effectiveness of the proposed methods is validated through simulation studies. Compared to the maximum likelihood estimation and the linear algebra based estimation approaches, we find that the JMPE method retains accuracy with significantly reduced computation.

CHAPTER 4

IDENTIFIABILITY AND ESTIMATION OF PARTIALLY-OBSERVED INFLUENCE MODELS[1]

4.1 Introduction

The influence model (IM) is a discrete-time stochastic model that captures the spatiotemporal dynamics of networked Markov chains [53]. IMs utilize a convex combination of local-level update rules modulated by network-level influences for the evolution of local Markov chains. This reduced-order representation allows the tractability of IMs and has found usages in diverse stochastic network applications, such as power networks, transportation systems, social networks, pandemics and weather evolution [2, 12, 70, 71, 77]. Partially-observed IM (POIM) is an IM in which the statuses for some sites are unobserved. POIMs are often seen in practical applications for reasons such as limited sensing coverage capabilities and deliberate concealment [83, 84].

There exist some studies in the literature on the estimation of POIM model parameters from observation data. Through connecting POIMs with hidden Markov models (HMMs), expectation maximization (EM)-based estimation approaches have been developed [14, 17, 85]. Computational costs for these methods are large, and surge with the increase of network size. In addition, existing estimation studies are all developed for POIMs with identical local update rules, namely the homoge-

[1] © 2022 IEEE. Reprinted, with permission, from [L. Zhao and Y. Wan, "Identifiability and Estimation of Partially Observed Influence Models," in *IEEE Control Systems Letters*, vol. 6, pp. 3385-3390, 2022].

neous POIMs. POIMs with nonidentical local update rules, namely the heterogeneous POIMs, are more flexible to capture network dynamics. The estimation of heterogeneous POIMs becomes more challenging, because that the variety of local update rules leads to more complex coupling of interactions among sites. There exists no study in the literature on the estimation of heterogeneous POIMs per our knowledge. In this chapter, we study the estimation of both homogeneous and heterogeneous POIMs with reduced computation. We explore the joint-margin matrix, the concept of which was first introduced in [46]. The matrix connects the highest-order and first-order representations of IMs, and was shown to play a significant role in the identifiability and estimation of fully-observed IMs. We here develop a new estimation algorithm by integrating EM and joint-margin probability based estimation (JMPE), called EM-JMPE.

POIM identifiability refers to the property that the estimation of POIM model parameters is unique. Unlike estimation, the identifiability of POIMs has been rarely studied in the literature despite its importance in practical applications. Reference [14] is the first in the literature that studied the identifiability of homogeneous POIMs, which provided a necessary condition for a subset of parameters to be identifiable. There exists no study in the literature on the identifiability of heterogeneous POIMs per our knowledge. In this chapter, we study the identifiability of both homogeneous and heterogeneous POIMs by introducing a reduced-size joint-margin matrix. The matrix is constructed to account for incomplete state information from POIM observation data. The approach provides a tighter or at least the same necessary condition as that in [14] for a subset of parameters of homogeneous POIMs, and also provides the first necessary condition in the literature for heterogeneous POIMs.

4.2 Preliminaries and Problem Formulation

4.2.1 IM and POIM

IM is a network of Markov chains (see Fig. 4.1 for an example). It is characterized by a 4-tuple $(N, M_n, D, A_{l,n})$ where N is the number of sites, M_n is the number of local statuses for site n, $D \in \mathbb{R}^{N\times N}$ is the network influence matrix and $A_{l,n} \in \mathbb{R}^{M_l \times M_n}$ is the local Markov transition matrix between sites l and n, where $n, l \in \{1, 2, \cdots, N\}$.

An IM evolves as follows. Each site n randomly chooses a neighboring site l as its influencing site with probability $d_{n,l}$, and updates its status according to l's status and the transition matrix $A_{l,n}$. $d_{n,l}$ is the nth row and lth column element of D. $A_{l,n}$ has the mth row and qth column element $a_{l,n_{m,q}} = P(s_n[k+1] = q | s_l[k] = m)$, the conditional probability to capture the influence of site l's status m on site n's status q. Let $S_n[k] \in \mathbb{R}^{1\times M_n}$ with single '1' as its $s_n[k]$th entry and '0' everywhere else to denote the local status of site n at time instant k, and $P_n[k] \in \mathbb{R}^{1\times M_n}$ to denote the probability mass function (PMF). The dynamics of site n can be captured as

$$P_n[k+1] = \sum_{l=1}^{N} d_{n,l} S_l[k] A_{l,n}, \;\; S_n[k+1] = Realize(P_n[k+1]), \tag{4.1}$$

where $Realize()$ denotes the random sampling operation for the corresponding PMF.

To facilitate the analysis, the overall network state at k, $S[k] \in \mathbb{R}^{1\times \sum_{n=1}^{N} M_n}$ and the corresponding probability, $P[k] \in \mathbb{R}^{1\times \sum_{n=1}^{N} M_n}$ can be represented by stacking all individual status vectors and PMFs as row vectors, respectively, i.e., $S[k] = [S_1[k]\ S_2[k]\ \cdots\ S_N[k]]$ and $P[k] = [P_1[k]\ P_2[k]\ \cdots\ P_N[k]]$. We also use a scalar $s[k] \in \{1, 2, \cdots, \prod_{n=1}^{N} M_n\}$ to index $S[k]$. The overall network dynamics can be simplified as

$$P[k+1] = S[k]H, \quad S[k+1] = MultiRealize(P[k+1]), \tag{4.2}$$

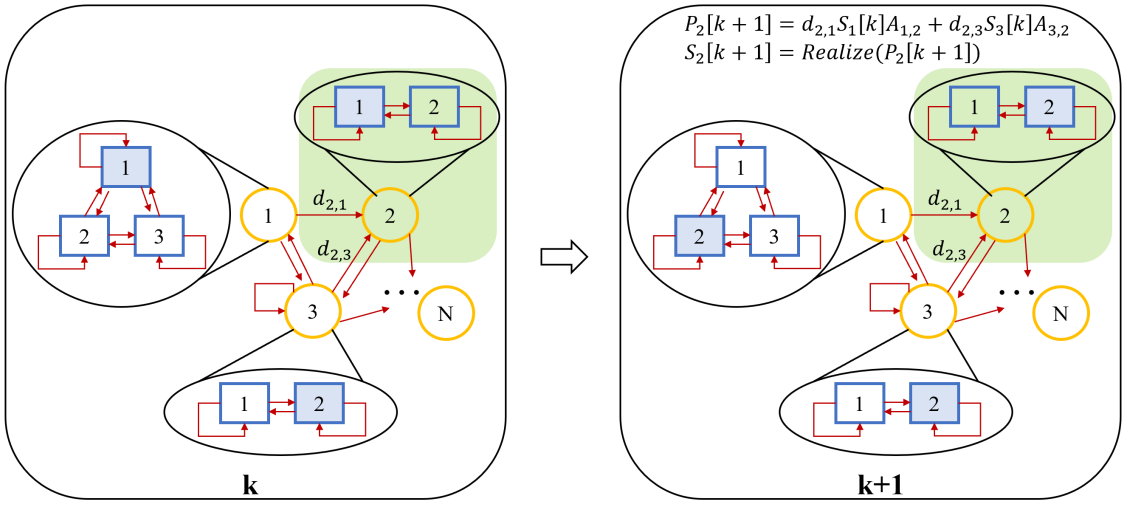

Figure 4.1: An N-site IM example. Each circle represents a site. A square represents the status, and a blue one denotes the current status at a particular time. Take site 2 (marked with green) as an example. If choosing site 1 as its influencing site (with probability $d_{2,1}$), it updates its status from 1 to 2 based on the status of site 1, $S_1[k]$, and $A_{1,2} = \begin{bmatrix} 0 & 0 & 0 \\ 1 & 1 & 1 \end{bmatrix}'$ with $'$ denoting the transpose.

where the influence matrix $H \in \mathbb{R}^{\sum_{n=1}^{N} M_n \times \sum_{n=1}^{N} M_n}$ is defined as

$$H \triangleq \begin{bmatrix} d_{1,1}A_{1,1} & \dots & d_{N,1}A_{1,N} \\ \vdots & \vdots & \vdots \\ d_{1,N}A_{N,1} & \dots & d_{N,N}A_{N,N} \end{bmatrix}. \tag{4.3}$$

$MultiRealize()$ denotes the random sampling operations for each PMF in $P[k+1]$.

In this chapter, homogeneous IMs refer to the IMs where all sites have the same number of local statuses and identical local Markov transition matrices, i.e., $M_n = M$ and $A_{l,n} = A\ \forall n, l \in \{1, 2, \cdots, N\}$. Heterogeneous IMs refer to the IMs where the local Markov transition matrices can be different, $A_{l,n} = A_n\ \forall n, l \in \{1, 2, \cdots, N\}$, but all sites have the same number of local statuses, $M_n = M$.

POIM is an IM where the statuses of some sites are unobserved. Let $\mathcal{N}$ and $\bar{\mathcal{N}}$ denote the set of observed and unobserved sites, respectively. The observed and

unobserved sites are labelled as $\mathcal{N} = \{1, 2, \cdots, |\mathcal{N}|\}$ and $\bar{\mathcal{N}} = \{|\mathcal{N}| + 1, |\mathcal{N}| + 2, \cdots, N\}$, where $|.|$ denotes the size. Similarly to the construction of $S[k]$, we use $S_P[k] \in \mathbb{R}^{1\times M|\mathcal{N}|}$ to denote the network state for observed sites at k, and $S_U[k] \in \mathbb{R}^{1\times M|\bar{\mathcal{N}}|}$ for unobserved sites. The scalar $s_P[k]$ is to index $S_P[k]$, and $s_U[k]$ is to index $S_U[k]$.

4.2.2 The joint-margin matrix

The joint-margin matrix $J \in \mathbb{R}^{M^N\times MN}$ connects the joint probability of network states and marginal probability of local statuses in IMs [46]. J is composed of N blocks as $J = [J_1\ J_2\ \cdots\ J_N]$, where the nth block of J, $J_n \in \mathbb{R}^{M^N\times M}$, is a row stochastic matrix, in which the ith row and mth column element $J_{n_{i,m}}$ is the conditional probability of site n's next status as m given the current network state i, i.e., $P(s_n[k+1] = m|s[k] = i)$.

In homogeneous IMs, J_n can be expressed using the parameters $\gamma = (D, A)$ as

$$J_n = \left[\begin{array}{cccc} \mathcal{A}_1 D' C_n & \mathcal{A}_2 D' C_n & \cdots & \mathcal{A}_M D' C_n \end{array}\right], \tag{4.4}$$

where C_n is the column vector with appropriate length of all zeros except '1' in its nth entry. $\mathcal{A}_m \in \mathbb{R}^{M^N\times N}$ is the mth local Markov information matrix for $m \in \{1, 2, \cdots, M\}$ and constructed by the mth column of A as

$$\mathcal{A}_m = \left[\begin{array}{cccc} a_{1,m} & a_{1,m} & \cdots & a_{1,m} \\ \vdots & \vdots & \vdots & \vdots \\ a_{q_1,m} & a_{q_2,m} & \cdots & a_{q_N,m} \\ \vdots & \vdots & \vdots & \vdots \\ a_{M,m} & a_{M,m} & \cdots & a_{M,m} \end{array}\right], \tag{4.5}$$

where q_n indicates site n's status. Note that the tuple $(q_1, q_2, \cdots, q_N)$ corresponds to one of M^N possible network states. We denote the mappings between $\gamma = (D, A)$ and J as functions $\Gamma_J : \gamma \to J$ and $\Gamma_\gamma^{-1} : J \to \gamma$.

In heterogeneous IMs, J_n can be expressed using the parameters $\lambda = (D, \mathbb{A})$ where $\mathbb{A} = \{A_1, A_2, \cdots, A_N\}$ as

$$J_n = \begin{bmatrix} \mathcal{A}_{n_1} D' C_n & \mathcal{A}_{n_2} D' C_n & \cdots & \mathcal{A}_{n_M} D' C_n \end{bmatrix}, \tag{4.6}$$

where $\mathcal{A}_{n_m} \in \mathbb{R}^{M^N \times N}$ is the mth local Markov information matrix of site n for $m \in \{1, 2, \cdots, M\}$ and constructed by the mth column of A_n as

$$\mathcal{A}_{n_m} = \begin{bmatrix} a_{n_{1,m}} & a_{n_{1,m}} & \cdots & a_{n_{1,m}} \\ \vdots & \vdots & \vdots & \vdots \\ a_{n_{q_1,m}} & a_{n_{q_2,m}} & \cdots & a_{n_{q_N,m}} \\ \vdots & \vdots & \vdots & \vdots \\ a_{n_{M,m}} & a_{n_{M,m}} & \cdots & a_{n_{M,m}} \end{bmatrix}. \tag{4.7}$$

We denote the mappings between $\lambda = (D, \mathbb{A})$ and J as functions $\Lambda_J : \lambda \to J$ and $\Lambda_\lambda^{-1} : J \to \lambda$.

4.2.3 Problem Formulation

Given O_P independent observation sequences of POIMs as $Y_P = \{Y_P^{(1)}, Y_P^{(2)}, \cdots, Y_P^{(O_P)}\}$ where $Y_P^{(o)} = \left[S_P^{(o)}[1], S_P^{(o)}[2], \cdots, S_P^{(o)}[T]\right]$ with $o \in \{1, 2, \cdots, O_P\}$ and T is the length of observation sequences, the identifiability of the underlying POIM is defined as follows.

Definition 1: A POIM is identifiable if and only if the optimal solution to the following likelihood function is unique given Y_P with $O_P, T \to \infty$,

$$\hat{\phi}_P = \arg\max_{\phi_P} P(Y_P | \phi_P), \tag{4.8}$$

where ϕ_P indicates $\gamma_P = (D, A)$ for homogeneous POIMs and $\lambda_P = (D, \mathbb{A})$ for heterogeneous POIMs.

Let $\phi_{P_\mathcal{N}}$ denote a subset of parameters ϕ_P, i.e., $\phi_{P_\mathcal{N}} \subset \phi_P$. The identifiability of the underlying POIM with respect to $\phi_{P_\mathcal{N}}$ is defined as follows.

Definition 2: A POIM is identifiable for a subset of parameters $\phi_{P_\mathcal{N}}$ if and only if the optimal solution $\hat{\phi}_{P_\mathcal{N}}$ to (4.8) is unique given Y_P with $O_P, T \to \infty$, where $\phi_{P_\mathcal{N}}$ indicates $\gamma_{P_\mathcal{N}}$ for homogeneous POIMs and $\lambda_{P_\mathcal{N}}$ for heterogeneous POIMs.

A POIM is not identifiable if the corresponding fully-observed IM is not identifiable. Thus, we here only study the identifiability of homogeneous and heterogeneous POIMs whose corresponding fully-observed IMs are identifiable. In the homogeneous case, this is guaranteed by $rank(A) > 1$, and in the heterogeneous case by $rank(A_n) > 1 \ \forall n \in \{1, 2, \cdots, N\}$ [46]. This assumption generally holds in practical applications. The problems investigated in this chapter are summarized as follows.

Problem 1: Given Y_P with $O_P, T \to \infty$, estimate parameters $\gamma_P = (D, A)$ of the underlying homogeneous POIM.

Problem 2: Given Y_P with $O_P, T \to \infty$, estimate parameters $\lambda_P = (D, \mathbb{A})$ of the underlying heterogeneous POIM.

Problem 3: Given Y_P with $O_P, T \to \infty$, determine the identifiability of the underlying homogeneous POIM for parameters $\gamma_P = (D, A)$ and a subset of parameters $\gamma_{P_\mathcal{N}}$ if γ_P is not identifiable.

Problem 4: Given Y_P with $O_P, T \to \infty$, determine the identifiability of the underlying heterogeneous POIM for parameters $\lambda_P = (D, \mathbb{A})$ and a subset of parameters $\lambda_{P_\mathcal{N}}$ if λ_P is not identifiable.

4.3 Estimation of POIMs

In this section, we study the estimation of POIMs through the joint-margin matrix J. We develop a new estimation algorithm for POIMs, named EM-JMPE, where EM is first applied to estimate J and then the model parameters are retrieved from J using the JMPE.

We first present the EM algorithm to estimate J, which is consistent but biased. For the ease of presentation, we assume $O_P = 1$ and eliminate the superscript in $Y_P^{(o)}$. Let $X = [S_U[1], S_U[2], \cdots, S_U[T]]$ denote the state sequence of unobserved sites.

E-step: Calculate the expectation of the log likelihood function $\psi(\phi_P|\phi_P^t)$ where ϕ_P^t denotes the parameters estimated from the tth iteration.

$$\begin{aligned}
\psi(\phi_P|\phi_P^t) &= E_{(X|Y_P,\phi_P^t)}\left(log\ P(Y_P, X|\phi_P)\right) \\
&= \sum_X P(X|Y_P, \phi_P^t) log\ P(Y_P, X|\phi_P) \\
&= \sum_{i_U=1}^{M^{|\tilde{\mathcal{N}}|}} P(s[1] = i|Y_P, \phi_P^t) log\pi(s_U[1] = i_U) \\
&\quad + \sum_{k=1}^{T-1} \sum_{i=1}^{M^N} \sum_{m=1}^{M} \sum_{n=1}^{N} \left(P(s[k] = i, s_n[k+1] = m|Y_P, \phi_P^t) log J_{n_{i,m}}\right),
\end{aligned} \tag{4.9}$$

where $\pi(s_U[1])$ is the initial probability distribution of unobserved states. i_U is the unobserved states corresponding to network state i.

M-Step: Determine the parameters that maximize the expectation of the log likelihood function $\psi(\phi_P|\phi_P^t)$ with the constraints that J_n is a row stochastic matrix and $\pi(s_U[1])$ is a probability distribution, i.e.,

$$\begin{aligned}
&\phi_P^{t+1} = \arg\max_{\phi_P} \psi(\phi_P|\phi_P^t) \\
&s.t. \sum_{m=1}^{M} J_{n_{i,m}} = 1\ \forall i \in \{1, 2, \cdots, M^N\},\ \forall n \in \{1, 2, \cdots, N\} \\
&\sum_{i_U=1}^{M^{|\tilde{\mathcal{N}}|}} \pi(s_U[1] = i_U) = 1\ and\ \pi(s_U[1] = i_U) \geq 0.
\end{aligned} \tag{4.10}$$

The estimation of $\pi(s_U[1])$ and J at the $(t+1)$th iteration can be obtained by solving (4.10) as follows.

$$\hat{\pi}^{t+1}(s_U[1] = i_U) = \chi_i[1], \quad \hat{J}^{t+1}_{n_{i,m}} = \frac{\sum_{k=1}^{T-1} \xi_{n_{i,m}}[k]}{\sum_{k=1}^{T-1} \chi_i[k]}, \tag{4.11}$$

where $\chi_i[k] = P(s[k] = i|Y_P, \phi_P^t)$ and $\xi_{n_{i,m}}[k] = P(s[k] = i, s_n[k+1] = m|Y_P, \phi_P^t)$, which can be determined using the forward-backward algorithm as follows.

Forward-backward algorithm: For unobserved sites $n \in \bar{\mathcal{N}}$, let $\alpha_{i_U}[k]$ denote the global forward variables. $\alpha_{n_m}[k]$ and $\beta_{n_m}[k]$ denote the local forward and backward variables, respectively. Their definitions are given as follows.

$$\begin{aligned}
\alpha_{i_U}[k] &= P(s_U[k] = i_U, S_P[1] : S_P[k]|\phi_P), \\
\alpha_{n_m}[k] &= P(s_n[k] = m, S_P[1] : S_P[k]|\phi_P), \\
\beta_{n_m}[k] &= P(S_P[k+1] : S_P[T]|s_n[k] = m, S_P[k], \phi_P),
\end{aligned} \tag{4.12}$$

where $S_P[1] : S_P[k]$ denotes the observation sequence from initial time instant to k. Note that, when $|\bar{\mathcal{N}}| = 1$, $\alpha_{i_U}[k]$ and $\alpha_{n_m}[k]$ are the same.

The recursive calculation of $\alpha_{i_U}[k]$ is given as

$$\begin{aligned}
&\alpha_{i_U}[1] = \pi(s_U[1] = i_U), \\
&\alpha_{i_U}[k+1] = \sum_{j_U=1}^{M^{|\bar{\mathcal{N}}|}} \left(\alpha_{j_U}[k] \prod_{l \in \mathcal{N}} J_{l_{j,m_P}} \prod_{n \in \bar{\mathcal{N}}} J_{n_{j,m_i}} \right), \\
&for\ k \in \{1, 2, \cdots, T-1\}\ and\ i_U \in \{1, 2, \cdots, M^{|\bar{\mathcal{N}}|}\},
\end{aligned} \tag{4.13}$$

where m_P is the observed sites' status and m_i is unobserved sites' status corresponding to network state i at $k+1$.

The recursive calculation of $\alpha_{n_m}[k]$ is given as

$$\begin{aligned}
&\alpha_{n_m}[1] = \sum_{i_{U_m}} \pi(s_U[1] = i_{U_m}), \\
&\alpha_{n_m}[k+1] = \sum_{q=1}^{M} \left(\frac{\alpha_{n_q}[k]}{M^{(|\bar{\mathcal{N}}|-1)(|\mathcal{N}|+1)}} \left(\sum_{j_q} J_{n_{j_q,m}} \right) \prod_{l \in \mathcal{N}} \left(\sum_{j_q} J_{l_{j_q,m_P}} \right) \right), \\
&for\ k \in \{1, 2, \cdots, T-1\},\ m \in \{1, 2, \cdots, M\}\ and\ n \in \bar{\mathcal{N}},
\end{aligned} \tag{4.14}$$

where i_{U_m} denotes the unobserved state with site n's status as m. j_q is the network state with site n's status as q at k and the corresponding observed states. The detailed derivation follows a similar development as in [14] and hence is skipped here due to limited space. We refer interested readers to the appendix [86] for the details.

The recursive calculation of $\beta_{n_m}[k]$ is given as

$$\begin{aligned}
&\beta_{n_m}[T] = 1, \\
&\beta_{n_m}[k] = \sum_{q=1}^{M} \left(\frac{\beta_{n_q}[k+1]}{M^{(|\bar{\mathcal{N}}|-1)(|\mathcal{N}|+1)}} \left(\sum_{j_m} J_{n_{j_m,q}} \right) \prod_{l \in \mathcal{N}} \left(\sum_{j_m} J_{l_{j_m,m_P}} \right) \right), \\
&for\ k \in \{1, 2, \cdots, T-1\},\ m \in \{1, 2, \cdots, M\}\ and\ n \in \bar{\mathcal{N}}.
\end{aligned} \tag{4.15}$$

$\chi_i[k]$ can be expressed as

$$\chi_i[k] = \prod_{n \in \bar{\mathcal{N}}} \left(\frac{\alpha_{n_{m_i}}[k] \beta_{n_{m_i}}[k]}{\sum_{q=1}^{M} \alpha_{N_q}[k] \beta_{N_q}[k]} \right), \tag{4.16}$$

and $\xi_{n_{i,m}}[k]$ can be expressed as

$$\xi_{n_{i,m}}[k] = \begin{cases} 0, \quad if\ s_n[k+1] \neq m,\ for\ n \in \mathcal{N} \\ \chi_i[k], \quad if\ s_n[k+1] = m,\ for\ n \in \mathcal{N} \\ \frac{\alpha_{i_U}[k] J_{n_{i,m}} \prod_{l \in \mathcal{N}} J_{l_{i,m_P}} \beta_{n_m}[k+1]}{\sum_{q=1}^{M} \alpha_{N_q}[k] \beta_{N_q}[k]},\ for\ n \in \bar{\mathcal{N}} \end{cases}. \tag{4.17}$$

Once J is estimated from observation data, the model parameters of both homogeneous and heterogeneous POIMs exist and can be uniquely recovered from J,

using the JMPE approach guaranteed by theorems in [46]. For homogeneous POIMs, $\gamma_P = (D, A)$ can be obtained as follows.

$$a_{m,q} = J_{n\,\frac{(m-1)(M^N-1)}{M-1}+1,q}, \tag{4.18}$$

for any $n \in \{1, 2, \cdots, N\}$ where $m, q \in \{1, 2, \cdots, M\}$.

$$\mathcal{A}_m D' = JW, \tag{4.19}$$

where $\mathcal{A}_m$ is constructed as (4.5) by the mth column of A which has at least two nonidentical entries. $W \in \mathbb{R}^{MN \times N}$ is constructed as

$$W_{x,n} = \begin{cases} 1 & if\ x = (n-1)M + m \\ 0 & otherwise \end{cases} \tag{4.20}$$

where $x \in \{1, 2, \cdots, MN\}$ and $n \in \{1, 2, \cdots, N\}$. For heterogeneous POIMs, $\lambda_P = (D, \mathbb{A})$ can be determined from

$$a_{n_{m,q}} = J_{n\,\frac{(m-1)(M^N-1)}{M-1}+1,q} \tag{4.21}$$

$$\mathcal{A}_{n_m} D' C_n = J_n C_m, \tag{4.22}$$

where $\mathcal{A}_{n_m}$ is constructed as (4.7) by the mth column of A_n which has at least two nonidentical entries.

The EM-JMPE is summarized in the following algorithm.

Remark 3. *The EM was used in the literature together with the corresponding master Markov matrix G for the estimation of a POIM [14, 85]. Note that the JMPE approach that uses J in the estimation is more computationally efficient than the linear algebra-based estimation (LAE) using G because JMPE solves linear equations of smaller dimensions than LAE [46]. The challenge of integrating EM and JMPE for the estimation of POIMs is that J concerns local status given network state and hence*

Algorithm 3 EM-JMPE Algorithm for POIMs

Input:

Observation sequences Y_P.

Output:

Parameters of the underlying POIM ϕ_P.

for $|\phi_P^t - \phi_P^{t-1}| \geq \delta_P$ (a small preset threshold) **do**

  Apply EM algorithm in (4.9)-(4.17) to Y_P to obtain the estimated joint-margin matrix $\hat{J}$.

  if The POIM is homogeneous **then**

    Estimate A and D from $\hat{J}$ according to (4.18)-(4.20).

  end if

  if The POIM is heterogeneous **then**

    Estimate $\mathbb{A}$ and D from $\hat{J}$ according to (4.21)-(4.22).

  end if

end for

the conditional probabilities in J are not balanced with respect to the preceding and succeeding events. We introduce in the EM algorithm both global and local forward variables $\alpha_{i_U}[k]$ and $\alpha_{n_m}[k]$ to address this issue.

4.4 Identifiability of POIMs

In this section, we study the identifiability of both homogeneous and heterogeneous POIMs through a reduced-size joint-margin matrix R. We first construct R and then provide identifiability conditions for a subset of parameters to be identifiable from R.

4.4.1 Reduced-size joint-margin matrix R

The reduced-size joint-margin matrix $R \in \mathbb{R}^{M^{|\mathcal{N}|} \times M|\mathcal{N}|}$ is constructed for only the statuses of observed sites in a POIM. The relationship of R and the joint-margin matrix J is given in the following theorem.

Theorem 11. *The reduced-size joint-margin matrix R of POIMs and the joint-margin matrix J of the corresponding fully-observed IMs have the following relationship,*

$$R = \frac{1}{M^{|\bar{\mathcal{N}}|}} F J_P, \tag{4.23}$$

where $F = I_{M^{|\mathcal{N}|}} \otimes \mathbf{1}_{M^{|\bar{\mathcal{N}}|}}$. $I_{M^{|\mathcal{N}|}}$ denotes the identity matrix of dimension $M^{|\mathcal{N}|}$, and $\mathbf{1}_{M^{|\bar{\mathcal{N}}|}}$ denotes the all-ones row vector of length $M^{|\bar{\mathcal{N}}|}$. $\otimes$ is the Kronecker product. J_P is constructed from J by removing all blocks J_n for $n \in \bar{\mathcal{N}}$.

Proof. The blocks J_n in J for unobserved sites $n \in \bar{\mathcal{N}}$ are first removed because their statuses are unknown. We then partition the remaining part J_P into $M^{|\mathcal{N}|} \times M|\mathcal{N}|$ blocks with dimension $M^{|\bar{\mathcal{N}}|} \times 1$ for each block. Each element of R is a scaled sum of $M^{|\bar{\mathcal{N}}|}$ elements in the corresponding blocks of J_P so that the blocks in R corresponding to individual observed sites $n \in \mathcal{N}$ are row stochastic. Thus, (4.23) holds. □

Note that the observed state $S_P[k]$ does not necessarily evolve in a Markov way based on R due to the influence from unobserved sites.

4.4.2 Identifiability of homogeneous POIMs

To study the identifiability of homogeneous POIMs through R, we first show the uniqueness of the solution to $\Gamma_{\gamma_P}^{-1} : R \to \gamma_P$ is a sufficient condition for the identifiability of homogeneous POIMs.

Lemma 11. *Given Y_P with $O_P, T \to \infty$, the homogeneous POIM is identifiable if the solution to $\Gamma_{\gamma_P}^{-1}(R)$ is unique.*

Proof. Given a sufficient number of observations, each element of R can be uniquely obtained by counting the corresponding state transition frequency based on the law of large numbers [68]. Thus, the homogeneous POIM is identifiable if the solution to $\Gamma_{\gamma_P}^{-1}(R)$ is unique according to Definition 1. □

Now, we study the identifiability of homogeneous POIMs by analyzing the uniqueness of the solution to $\Gamma_{\gamma_P}^{-1}(R)$. According to (4.4) and (4.23), for unobserved sites $n \in \bar{\mathcal{N}}$, the nth rows of D cannot be recovered from R since the corresponding blocks J_n are removed when constructing R. Thus, $\Gamma_{\gamma_P}^{-1} : R \to D$ does not have a unique solution. That is, the homogeneous POIMs cannot be completely identified from the corresponding R. Therefore, we consider the identifiability of the parameters with respect to observed sites $\gamma_{P_\mathcal{N}}$ from R for homogeneous POIMs, where $\gamma_{P_\mathcal{N}} = (D_\mathcal{N}, A) \subset \gamma_P$ and $D_\mathcal{N} \in \mathbb{R}^{|\mathcal{N}|\times N}$ is a submatrix of D corresponding to observed sites.

Theorem 12. *Given the reduced-size joint-margin matrix R of a homogeneous POIM, $M(M-1)+|\mathcal{N}|(N-1) \leq M^{|\mathcal{N}|}(M-1)|\mathcal{N}|$ is a necessary condition for $\gamma_{P_\mathcal{N}}$ to be identifiable from R.*

Proof. The number of independent unknowns in $\gamma_{P_\mathcal{N}}$ is $M(M-1)+|\mathcal{N}|(N-1)$. The number of independent equations from R is $M^{|\mathcal{N}|}(M-1)|\mathcal{N}|$, which should be larger than or equal to the number of independent unknowns so that $\gamma_{P_\mathcal{N}}$ can be uniquely solved from R. The theorem is proved naturally. □

Remark 4. *Paper [14] provided a necessary condition for the identifiability of homogeneous POIMs, $M(M-1)+|\mathcal{N}|(N-1) \leq M^{|\mathcal{N}|}(M^{|\mathcal{N}|}-1)$, through exploring its master Markov representation. Theorem 12 provides a tighter or at least the same necessary condition through the construction of R. More specifically, the number of*

required independent equations here is less than or at least equal to that in [14] (see Fig. 4.2) because $(M-1)|\mathcal{N}| \leq M^{|\mathcal{N}|} - 1$ *and* $M^{|\mathcal{N}|} > 0\ \forall M, |\mathcal{N}| \in \mathbb{Z}^+$.

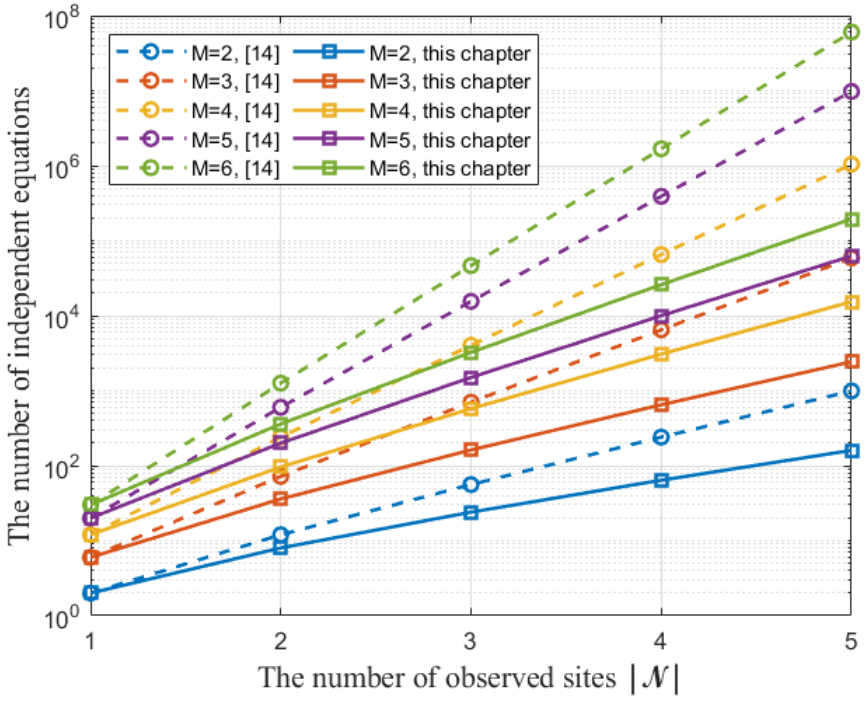

Figure 4.2: The number of required independent equations in the necessary condition for $\gamma_{P_\mathcal{N}}$ to be identified with multiple sets of $|\mathcal{N}|$ and M.

Note that, if $\gamma_{P_\mathcal{N}}$ is identifiable from R, $\gamma_{P_\mathcal{N}}$ can be obtained by solving the nonlinear equations (4.23) and (4.4) using, e.g., the least squares method.

4.4.3 Identifiability of heterogeneous POIMs

Similar results on the identifiability of heterogeneous POIMs can be obtained based on the reduced-size joint-margin matrix R. We first show that the uniqueness of the solution to $\Lambda_{\lambda_P}^{-1} : R \to \lambda_P$ is a sufficient condition for the identifiability of heterogeneous POIMs. The proof is similar to that of Lemma 11 and omitted here.

Lemma 12. *Given Y_P with $O_P, T \to \infty$, the heterogeneous POIM is identifiable if the solution to $\Lambda_{\lambda_P}^{-1}(R)$ is unique.*

Based on Lemma 12, we study the identifiability of heterogeneous POIMs by analyzing the uniqueness of the solution to $\Lambda_{\lambda_P}^{-1}(R)$. Similarly to the argument for the homogeneous case, the heterogeneous POIMs cannot be completely identified through the corresponding R. Note that neither $\Lambda_{\lambda_P}^{-1} : R \to D$ nor $\Lambda_{\lambda_P}^{-1} : R \to \mathbb{A}$ has a unique solution. We thus study the identifiability of the parameters with respect to observed sites $\lambda_{P_\mathcal{N}}$ from R for heterogeneous POIMs, where $\lambda_{P_\mathcal{N}} = (D_\mathcal{N}, \mathbb{A}_\mathcal{N}) \subset \lambda_P$ and $\mathbb{A}_\mathcal{N} = \{A_1, A_2, ..., A_{|\mathcal{N}|}\} \subset \mathbb{A}$ for observed sites.

Theorem 13. *Given the reduced-size joint-margin matrix R of a heterogeneous POIM, $M(M-1)+(N-1) \leq M^{|\mathcal{N}|}(M-1)$ is a necessary condition for $\lambda_{P_\mathcal{N}}$ to be identifiable from R.*

Proof. The number of independent unknowns in $\lambda_{P_\mathcal{N}}$ is $|\mathcal{N}|M(M-1) + |\mathcal{N}|(N-1)$. The number of independent equations from R is $M^{|\mathcal{N}|}(M-1)|\mathcal{N}|$, which should be larger than or equal to the number of independent unknowns so that $\lambda_{P_\mathcal{N}}$ can be uniquely solved from R. That is, $|\mathcal{N}|M(M-1) + |\mathcal{N}|(N-1) \leq M^{|\mathcal{N}|}(M-1)|\mathcal{N}|$. Multiplying both sides with $\frac{1}{|\mathcal{N}|} > 0$, the theorem is proved naturally. □

Note that, if $\lambda_{P_\mathcal{N}}$ is identifiable from R, $\lambda_{P_\mathcal{N}}$ can be obtained by solving the nonlinear equations (4.23) and (4.6) using, e.g., the least squares method.

4.5 Simulation Studies

In this section, simulation studies are conducted to validate the estimation and identifiability results. We use MATLAB R2021a on Dell Precision Tower 3620 with CPU clock speed up to 3.50 GHz.

4.5.1 Estimation of POIMs

First consider a homogeneous POIM with 2 sites and 2 statuses for each site. The second site is unobserved and the underlying parameters $\gamma_P = (D, A)$ are

$$A = \begin{bmatrix} 0.8 & 0.2 \\ 0.1 & 0.9 \end{bmatrix}, \; D = \begin{bmatrix} 0.0 & 1.0 \\ 0.6 & 0.4 \end{bmatrix}.$$

An observation sequence of length 320 is generated. We apply EM-JMPE in Algorithm 3 and also EM-LAE in [14] for comparison. The results are given as follows with subscripts denoting different methods. The mean squared errors (MSE) are 2.64×10^{-4} by EM-JMPE and 1.5×10^{-3} by EM-LAE. The execution time for EM-JMPE is 2.7560 seconds, which is less than the 5.2715 seconds for EM-LAE, showing reduced computation while maintaining the estimation accuracy.

$$\hat{A}_{JMPE} = \begin{bmatrix} 0.7916 & 0.2084 \\ 0.1170 & 0.8830 \end{bmatrix}, \; \hat{D}_{JMPE} = \begin{bmatrix} 0.0000 & 0.1000 \\ 0.5736 & 0.4264 \end{bmatrix},$$

$$\hat{A}_{LAE} = \begin{bmatrix} 0.7634 & 0.2366 \\ 0.0885 & 0.9115 \end{bmatrix}, \; \hat{D}_{LAE} = \begin{bmatrix} 0.0000 & 0.1000 \\ 0.6672 & 0.3328 \end{bmatrix}.$$

We also conduct 100 simulations with randomly generated 2-dimensional A and D. The average execution time for EM-JMPE is 2.2372 seconds, and for EM-LAE is 5.0358 seconds with a reduction of 2.7986 seconds. The average MSEs are 3.2×10^{-3} by EM-JMPE and 1.20×10^{-2} by EM-LAE, which are similar. The statistical results also verify the effectiveness of the EM-JMPE approach.

Consider a heterogeneous POIM with 2 sites and 2 statuses for each site. The second site is unobserved and the underlying parameters $\lambda_P = (D, \mathbb{A})$ are

$$A_1 = \begin{bmatrix} 0.8 & 0.2 \\ 0.1 & 0.9 \end{bmatrix}, \; A_2 = \begin{bmatrix} 1.0 & 0.0 \\ 0.2 & 0.8 \end{bmatrix}, \; D = \begin{bmatrix} 0.0 & 1.0 \\ 0.55 & 0.45 \end{bmatrix}.$$

An observation sequence of length 320 is generated. We apply EM-JMPE in Algorithm 3 to estimate the parameters and the results are given as follows with the MSE of 8.4919×10^{-4}.

$$\hat{A}_1 = \begin{bmatrix} 0.7974 & 0.2026 \\ 0.0341 & 0.9659 \end{bmatrix}, \ \hat{A}_2 = \begin{bmatrix} 0.9867 & 0.0133 \\ 0.2144 & 0.7856 \end{bmatrix}, \hat{D} = \begin{bmatrix} 0.0042 & 0.9958 \\ 0.5314 & 0.4686 \end{bmatrix}.$$

4.5.2 Identifiability of POIMs

First consider a homogeneous POIM with 3 sites and 2 statuses for each site. The last site is unobserved and the underlying parameters $\gamma_P = (D, A)$ are

$$A = \begin{bmatrix} 0.6 & 0.4 \\ 0.3 & 0.7 \end{bmatrix}, \ D = \begin{bmatrix} 0.55 & 0.20 & 0.25 \\ 0.25 & 0.45 & 0.30 \\ 0.30 & 0.20 & 0.50 \end{bmatrix}.$$

According to the necessary conditions for $\gamma_{P_\mathcal{N}}$ to be identifiable, the number of required independent equations in Theorem 12 is 8, smaller than 12 in [14]. The necessary condition is satisfied because there are 6 independent unknowns in $\gamma_{P_\mathcal{N}}$. Here we estimate $\gamma_{P_\mathcal{N}}$ by first obtaining R from an observation sequence of length $400,000$ and then solving nonlinear equations (4.23) and (4.4). Results are given as follows with the MSE of 7.1182×10^{-5}.

$$\hat{A} = \begin{bmatrix} 0.6015 & 0.3985 \\ 0.2891 & 0.7109 \end{bmatrix}, \ \hat{D} = \begin{bmatrix} 0.5423 & 0.1933 & 0.2643 \\ 0.2543 & 0.4396 & 0.3061 \\ * & * & * \end{bmatrix}.$$

Consider a heterogeneous POIM with 3 sites and 2 statuses for each site. The last site is unobserved and the underlying parameters $\lambda_P = (D, \mathbb{A})$ are

$$A_1 = \begin{bmatrix} 0.6 & 0.4 \\ 0.3 & 0.7 \end{bmatrix}, \ A_2 = \begin{bmatrix} 0.55 & 0.45 \\ 0.4 & 0.6 \end{bmatrix},$$

$$A_3 = \begin{bmatrix} 0.25 & 0.75 \\ 0.35 & 0.65 \end{bmatrix}, \; D = \begin{bmatrix} 0.48 & 0.27 & 0.25 \\ 0.25 & 0.45 & 0.30 \\ 0.30 & 0.20 & 0.50 \end{bmatrix}.$$

The necessary condition in Theorem 13 is satisfied for this heterogeneous POIM. Here we estimate $\lambda_{P_{\mathcal{N}}}$ by first obtaining R from an observation sequence of length $400,000$ and then solving nonlinear equations (4.23) and (4.6). Results are given as follows with the MSE of 1.4070×10^{-4}.

$$\hat{A}_1 = \begin{bmatrix} 0.5898 & 0.4102 \\ 0.2821 & 0.7179 \end{bmatrix}, \; \hat{A}_2 = \begin{bmatrix} 0.5440 & 0.4560 \\ 0.3917 & 0.6083 \end{bmatrix},$$

$$\hat{D} = \begin{bmatrix} 0.4657 & 0.2612 & 0.2730 \\ 0.2457 & 0.4582 & 0.2961 \\ * & * & * \end{bmatrix}.$$

4.6 Conclusion

In this chapter, we provided new results on the estimation and identifiability of homogeneous and heterogeneous POIMs. Through exploring the joint-margin matrix J, we developed a POIM estimation algorithm, EM-JMPE, which includes two steps, estimating J from observations and obtaining POIM parameters from J. We also provided new identifiability conditions for POIMs by introducing the reduced-size joint-margin matrix R. In the homogeneous case, we show that the new necessary condition is tighter or at least the same as that in [14]. The necessary condition for the heterogeneous case is the first in the literature.

CHAPTER 5

DISTRIBUTED SCHEDULING SCHEME FOR SUB-6 GHZ V2X-ASSISTED MMWAVE COMMUNICATION UNDER LONG HIGHWAY TRAFFIC

5.1 Introduction

Vehicle-to-Everything (V2X) communication in vehicular networks plays an important role in the safety and efficiency of the intelligent transportation systems (ITS) [22–24]. A wide range of ITS applications, e.g., collective perception of environment, vehicle platooning and automated driving assistance benefit from V2X technologies [25, 26]. In V2X communication, extensive exchange of information requires large bandwidth that can be provided by millimeter wave (mmWave) communication in the wireless frequencies range between 30 and 300 GHz [87]. However, mmWave communication is vulnerable to blockage and suffers from severe path loss [27]. The link budget for beamforming of highly directional antennas can be expensive, which is even more challenging considering the highly dynamic environment in the vehicular ad-hoc networks (VANETs) [88]. Sub-6 GHz V2X-assisted mmWave communication has been proposed to address such challenge, where the sub-6 GHz broadcasts omni-directional V2X communication for the control panel and the directional mmWave communication for the data panel [27, 29, 30].

In sub-6 GHz V2X-assisted mmWave transmission, vehicles in VANETs share mmWave channel, and inappropriate channel use can lead to collisions and thus, a waste of bandwidth resources [89]. MmWave transmission scheduling arranges mmWave links for transmission to achieve an optimized mmWave channel utilization [28]. We have conducted significant efforts to design mmWave scheduling algorithms

that consider realistic VANET data features, e.g., data importance, data freshness and data size heterogeneity from various ITS applications [29,30]. Our previous study [30] considered these data features by formulating the scheduling problem into a mixed-integer nonlinear programming (MINLP) problem. The mmWave scheduling scheme in [30] requires a head node, i.e., a roadside unit (RSU) or vehicle, to collect mmWave link requests within the sub-6 GHz communication range and conduct scheduling. However, for long highway traffic, such scheduling scheme is not applicable considering the communication and computing scalability. First, control information exchange beyond the sub-6 GHz communication range requires multi-hop packet forwarding and large control signalling overhead [31–33]. The computational complexity of solving the MINLP problem can also be high if there is heavy communication load for the long highway [30,34–36]. As such, we consider in this chapter a distributed scheduling scheme. In [31, 33], distributed scheduling schemes at each node were developed for large-scale networks to avoid multi-hop packet forwarding for information exchange. Compared to scheduling schemes with one head node, distributed schemes have lower implementation complexity and better flexibility and adaptability to varying vehicular network conditions, at the cost of possible performance degradation [90, 91].

Distributed scheduling is NP-hard [92]. We consider in this chapter the distributed scheduling with multiple head nodes and coordinations in between. Coordination aims to resolve the conflicts among individual schedulers to achieve an overall conflict-free transmission schedule. For example, coordination can be conducted at the medium access control (MAC) protocol level [93–97]. Head nodes can arrange link transmissions within their pre-assigned time slots using the time division multiple access (TDMA) [94, 95]. Distinct pre-assigned radio frequencies and orthogonal coding are leveraged for various head nodes in the frequency division multiple access (FDMA) and code division multiple access (CDMA), respectively [93]. Another type

of methods, namely the interference localization, considers limited interference range of communication links to isolate conflicts among head nodes [90, 98–100]. However, such interference localization approach is not applicable for highway traffic due to the specific chain-like coupling of link interference range along the highway. Game-theoretic approaches in the literature provide a strategical mathematical model for decision-making in both cooperative and non-cooperative systems [101], and have been used in distributed scheduling [91, 102–104]. However, the constraints for individual game players are decoupled and this is not the case for our distributed scheduling in which coupling conflict constraints exist among multiple head nodes. In [105], the game-theoretic distributed scheduling requires heavy control overhead to achieve conflict-free schedules, which is also not applicable for wireless communication in sub-6 GHz channel.

In this chapter, we propose a distributed scheduling scheme with multiple head nodes for sub-6 GHz V2X-assisted mmWave transmission for long highway traffic. We address the two challenges, including the communication scalability for multiple head nodes to coordinate across sections, and the computational scalability for individual head node to solve the scheduling problem within a section. The contributions of this chapter are summarized as follows.

- In the proposed distributed scheduling scheme, the long highway is divided into contiguous and non-overlapping sections, inside of which a head node solves the scheduling problem and coordinates with other head nodes to achieve an overall conflict-free mmWave schedule. Extensive simulation studies are conducted to validate the effectiveness of the proposed distributed scheduling scheme. The performance degradation of channel utilization is small with respect to that by one head node.

- To address the computational scalability challenge for individual head node within a section, we develop a decomposition-based approximate solution. The scheduling problem for each head node is decomposed into sub-problems with minimal dependencies by leveraging the spectral analysis of the mmWave link conflicts. Remaining dependencies are addressed through a permutation and enumeration procedure.
- To address the communication scalability challenge for coordination among multiple head nodes, we first propose highway division scheme to confine the cross-section conflicts to adjacent head nodes. Based on this, we design two coordination schemes, namely the rule-based coordination and section-parity-based coordination, both of which are simple to implement. An overall conflict-free schedule is achieved with low control overhead for sub-6 GHz channel.

The rest of this chapter is structured as follows. In Section 5.2, the distributed scheduling problem is motivated and formulated. Section 5.3 describes the decomposition-based approximate solution for individual head node within a section, and the coordination schemes among multiple head nodes. Section 5.4 presents the simulation studies and Section 5.5 concludes this chapter.

5.2 System Model and Problem Formulation

5.2.1 Scheduling for Sub-6 GHz V2X-assisted MmWave Communication

Consider a network of N_v vehicles on an M-lane highway of length L, as illustrated in Fig. 5.1. Sub-6 GHz V2X radio devices and mmWave transceivers are mounted on vehicles. The sub-6 GHz V2X radio works as the control panel for data exchange over mmWave radio. Through sub-6 GHz channel, vehicles broadcast N

mmWave link requests during the time span $[0, T_c]$, along with basic safety message (BSM) such as their positions and velocities. The ith requested link is attached with a tag $\{TX_i, RX_i, w_i, d_i, o_i\}$ denoting the transmitter vehicle ID, receiver vehicle ID, data weight, transmission duration and data generation time, respectively, where $w_i, d_i, o_i \in \mathbb{R}^+$ and $i \in \{1, 2, \cdots, N\}$. Without loss of generality (WLOG), we assume that $d_i \leq T_c$ is satisfied for all links.

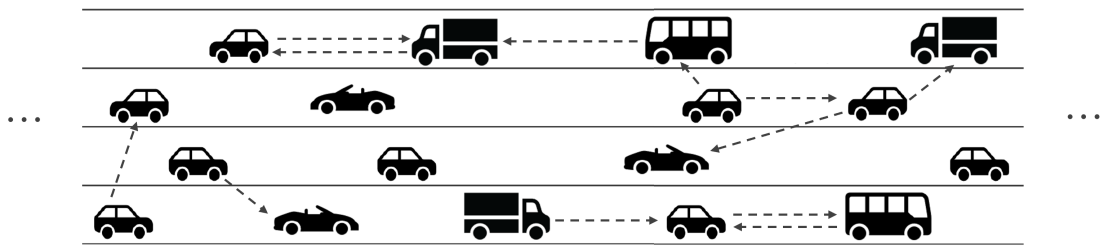

Figure 5.1: An example of the vehicular network on highway, where the dashed lines denote mmWave transmission link requests, with arrows pointing from the transmitters to receivers.

Note that the requested mmWave links may not be transmitted concurrently. The mmWave communication properties, i.e., the *point-to-point communication*, *half-duplex* and the specific *in-lane interference* for highway scenario [29] can lead to transmission conflicts among the requested mmWave links, as illustrated in Fig. 5.2. The point-to-point and half-duplex conflicts result in the constraint that any two concurrently transmitted mmWave links cannot share a common transmitter or receiver. The in-lane interference conflict says that two receivers in the same lane cannot be within the mmWave communication range for successful reception. This conflict cannot be neglected for the highway traffic due to the specific highway structure and the directionality of mmWave transmission. These conflicts can be integratedly captured by a symmetric binary matrix $C \in \mathbb{R}^{N \times N}$ with the ith row and jth column entry

$C_{i,j} = 1$ denoting existing conflicts between links i and j, and 0 otherwise. Vehicles or the roadside units (RSUs) selected as head nodes collect mmWave link requests as well as BSM during $[0, T_c]$, arrange data transmission with conflict constraints for $[T_c, 2T_c]$, and disseminate schedules through sub-6 GHz radio. Vehicles in the network build mmWave links according to the received schedules and conduct data exchange.

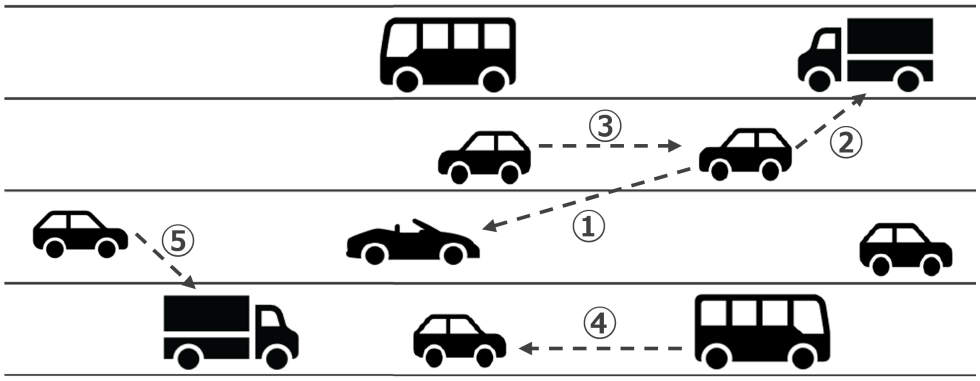

Figure 5.2: An illustration of the conflicts in highway traffic. Requested mmWave links ① and ② have conflict considering the point-to-point communication property. Links ① and ③, or links ② and ③ cannot be transmitted concurrently due to the half-duplex constraint. The conflict for links ④ and ⑤ arises due to the non-negligible in-lane interference where the transmission of link ④ can lead to reception failure for the receiver of link ⑤ because that the two receivers are in the same lane within the mmWave communication range.

Head nodes consider the following three important V2X data features in a conflict-free mmWave transmission schedule to facilitate vehicles' real-time decision-making and support diverse applications. The first feature is *data importance*. The more important the data is (captured by a larger w_i), the higher transmission priority it should be given. The second feature is *data freshness*, because longer delays will diminish the value of data. As such, achieving a small transmission finish time f_i for link i in the schedule is desired. Thus, the ratio $\frac{w_i}{f_i - o_i}$, namely the *link utility* is utilized to capture these V2X data features. Correspondingly, the mmWave channel

utilization can be characterized by the sum of the link utilities of all scheduled links, namely *network utility*. We aim to maximize the network utility when scheduling the mmWave link transmission, subject to the above three conflicts. We also note that to handle data transmission demands from various vehicular applications, flexible data size is involved, i.e., d_i can be different for all links and $T_c + d_i \leq f_i \leq 2T_c$. Mathematically, the scheduling by head nodes is to find the optimal solution to the following MINLP problem [30],

$$\max_{x_i, f_i} \sum_{i=1}^{N} \frac{w_i x_i}{f_i - o_i},$$
$$s.t. : \begin{cases} x_i \in \{0, 1\}; \\ f_i \in \mathbb{R}^+; \\ T_c + d_i \leq f_i \leq 2T_c; \\ if\ x_i = x_j = C_{ij} = 1, \\ f_i \leq f_j - d_j\ or\ f_j \leq f_i - d_i; \\ i, j \in \{1, 2, \cdots, N\}\ and\ i < j. \end{cases} \tag{5.1}$$

The MINLP problem (5.1) is NP-complete. Existing approaches to solve such MINLP problem, e.g., the branch and bound method in [106, 107] incur high computational cost with low convergence rate. Our previous work [30] transformed (5.1) into an equivalent parametric mixed-integer linear programming (MILP) problem

$$\max_{x_i, f_i} \sum_{i=1}^{N} \mu_i^* (w_i x_i - \beta_i^* (f_i - o_i)), \tag{5.2}$$

where $\mu_i^* = \frac{x_i^*}{f_i^* - o_i}$ and $\beta_i^* = \frac{w_i x_i^*}{f_i^* - o_i}$ with x_i^* and f_i^* denoting the optimal solution to (5.1). To achieve the global optimal solution, a scheduling algorithm named the Parameterization-based Iterative Algorithm (PIA) was developed in [30], where the

MILP problem (5.3) with random parameters μ_i and β_i is solved iteratively with updated parameters under multiple sets of initial parameters μ_i^0 and β_i^0.

$$\max_{x_i, f_i} \sum_{i=1}^{N} \mu_i (w_i x_i - \beta_i (f_i - o_i)). \tag{5.3}$$

The linear convergence rate of the PIA for any random set of initial parameters μ_i^0 and β_i^0 was proved in [30]. Despite the efficiency, We note that PIA does not scale with the number of mmWave link requests N. This is because for each set of initial parameters, multiple MILP problems with updated parameters are solved, resulting in expensive computational cost when N is large. The efficiency of PIA decreases with the increase of the number of links N, motivating this work to address the scalability problem of the mmWave scheduling for vehicular scenarios with large N.

5.2.2 Distributed Scheduling for Long Highway Traffic

In this chapter, we consider mmWave link scheduling in a long highway traffic scenario. We note that the use of one head node, as illustrated in Section 5.2.1 for the small-scale vehicular network [30], does not apply for long highway traffic because the multi-hop packet forwarding over sub-6 GHz channel can induce significant transmission delay of mmWave channel over the large communication range. To address this challenge, we propose a distributed scheduling scheme with multiple head nodes for the long highway traffic as shown in Fig. 5.3. The long highway is divided into contiguous and non-overlapping N_s sections, each within the sub-6 GHz communication range. The mmWave link requests to be scheduled within a section are determined by the section ID of their receivers. For each section j, where $j \in \{1, 2, \cdots, N_s\}$, a head node H_j collects all mmWave link requests within section j, runs the mmWave link scheduler (e.g., by adopting the PIA that solves the MINLP problem (5.1)), and disseminates the optimized transmission schedules.

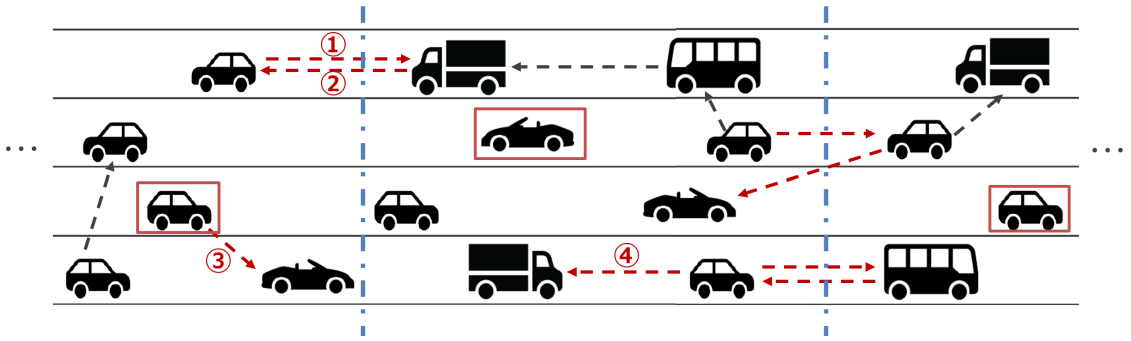

Figure 5.3: An example of the long highway division. The blue dashed lines denote section boundaries and vehicles with red frames indicate the head nodes for each section.

This chapter addresses two challenges of the distributed scheduling scheme:

1. For individual head node within a large section, the computation of scheduler that solves the MINLP problem (5.1), e.g., using the PIA, needs to be reduced. In particular, these optimal scheduling algorithms do not scale with the number of mmWave link requests.
2. A mechanism is needed to coordinate the distributed schedulers at the multiple head nodes to resolve the potential conflicts across sections.

To address the intra-section computational challenge 1) for an individual head node, decomposition is a promising technique where a large-scale problem is divided into several small-scale sub-problems [108–110]. Designing decomposition schemes for scheduling algorithms needs to consider the tight coupling in the constraints of transmission conflicts and the dependencies among sub-problems. We address this in Section 5.3.1.

An example of inter-section challenge 2) with regard to the cross-section conflict is shown in Fig. 5.3, where links ① and ② cannot be transmitted concurrently because they share two common nodes. Similarly, links ③ and ④ have in-lane interference conflict because the distance between the two receivers is smaller than

the mmWave communication range R_M. More specifically, such pairs of conflicted links, if scheduled by their individual sections to transmit concurrently, will result in cross-section conflict considering the receivers' positions. We will develop a coordination scheme among multiple head nodes to achieve an overall conflict-free mmWave transmission schedule in Section 5.3.2.

5.3 Our Proposed Distributed Scheduling Scheme

In this section, we develop solutions to address the intra- and inter- section challenges of the proposed distributed scheduling scheme to solve the scheduling problem (5.1) respectively in the two subsections.

5.3.1 Decomposition-based Efficient Scheduling by Individual Head Node within a Section

An efficient decomposition-based approximate solution is developed in this subsection to solve the MINLP scheduling problem (5.1) for an individual head node within a section. Based on available computing resources, the proposed solution reduces the computation using three steps, i.e., clustering, permutation and enumeration, and selection, elaborated as follows. In clustering, the problem (5.1) is decomposed into sub-problems with minimal dependencies. The permutation and enumeration step handles remaining dependencies among the sub-problems. In the selection step, the solution with the highest overall network utility is chosen as the final schedule.

Step 1: Clustering. The clustering step utilizes the conflict table C to decompose the scheduling problem (5.1) into sub-problems with minimal dependencies. In particular, given that each sub-problem corresponds to a link cluster (a set of links i with $i \in \{1, 2, \cdots, N\}$), the number of link conflicts within individual link clusters

should be maximized while that between any two link clusters should be minimized. Considering that more '1's in a row (or column) in C indicate more conflicts the corresponding link has with other links and vice versa, we are inspired to leverage a graph-theoretic approach for the decomposition using the conflict table C.

C can be represented by an undirected graph $\mathcal{G} = (\mathcal{V}, \mathcal{E})$, namely the conflict graph. $\mathcal{V}$ is the set of vertices, representing the requested links, and $\mathcal{E}$ is the set of edges, representing the existing conflicts between links and $\mathcal{E} \subseteq \{\{V_i, V_j\} | V_i, V_j \in \mathcal{V},\ and\ C_{ij} = 1\}$. In the following, we define direct conflict, disconnected cluster and connected cluster to facilitate presenting our decomposition approach (see Fig. 5.4 for examples).

Definition 1: Direct conflict. Links i and j are said to have direct conflict if there exists an edge between vertices V_i and V_j in $\mathcal{G}$. Link clusters m and n are said to have direct conflict if there exist link i in cluster m and link j in cluster n that have direct conflict.

Definition 2: Disconnected cluster. A link cluster is said to be a disconnected cluster if it has no direct conflict with all other clusters.

Definition 3: Connected cluster. A link cluster is said to be a connected cluster if there exists a link cluster with which it has direct conflict.

With the above definitions for conflict graph $\mathcal{G}$, the clustering step groups the vertices in $\mathcal{G}$ into clusters to maximize the number of disconnected clusters, and minimize direct conflicts among connected clusters.

We propose an eigen-structure approach for clustering. The positive-semidefinite Laplacian matrix $L \in \mathbb{R}^{N \times N}$ of the graph $\mathcal{G}$ is calculated as

$$L = D - C, \tag{5.4}$$

where $D \in \mathbb{R}^{N \times N}$ is the degree matrix,

$$D = diag\left(\sum_{j=1}^{N} C_{ij}\right), \tag{5.5}$$

and $diag(\cdot)$ denotes diagonalization [111]. Lemma 13 shows the use of L's eigenvalues to determine the number of link clusters K in an adaptive way [112].

Lemma 13. *The eigenvalues of L are non-negative.*

1. *The algebraic multiplicity of L's '0' eigenvalue indicates the number of disconnected clusters in graph $\mathcal{G}$. If L has more than one '0' eigenvalues, the scheduling problem* (5.1) *can be decomposed into completely decoupled sub-problems.*
2. *The smaller the corresponding non-zero eigenvalues are, the less direct conflicts exist between connected clusters. If L has small non-zero eigenvalues, our problem* (5.1) *can be decomposed into sub-problems with low dependencies.*

Consider the example in Fig. 5.4 to illustrate the Lemma 13. Here $N = 15$ and the conflict table is given as follows.

$$C = \begin{bmatrix} C_1 & \mathcal{O} & \mathcal{O} & \mathcal{O} & \mathcal{O} \\ \mathcal{O} & C_2 & C_5 & \mathcal{O} & \mathcal{O} \\ \mathcal{O} & C_5^{\mathrm{T}} & C_1 & \mathcal{O} & \mathcal{O} \\ \mathcal{O} & \mathcal{O} & \mathcal{O} & C_3 & C_6 \\ \mathcal{O} & \mathcal{O} & \mathcal{O} & C_6^{\mathrm{T}} & C_4 \end{bmatrix},$$

where $\mathcal{O} \in \mathbb{R}^{3 \times 3}$ is the all-zero matrix, $^{\mathrm{T}}$ denotes the transpose operation and

$$C_1 = \begin{bmatrix} 0 & 1 & 0 \\ 1 & 0 & 1 \\ 0 & 1 & 0 \end{bmatrix}, C_2 = \begin{bmatrix} 0 & 1 & 1 \\ 1 & 0 & 1 \\ 1 & 1 & 0 \end{bmatrix}, C_3 = \begin{bmatrix} 0 & 1 & 1 \\ 1 & 0 & 0 \\ 1 & 0 & 0 \end{bmatrix},$$

$$C_4 = \begin{bmatrix} 0 & 0 & 1 \\ 0 & 0 & 1 \\ 1 & 1 & 0 \end{bmatrix}, C_5 = \begin{bmatrix} 0 & 0 & 1 \\ 0 & 0 & 0 \\ 0 & 0 & 0 \end{bmatrix}, C_6 = \begin{bmatrix} 0 & 0 & 0 \\ 0 & 1 & 0 \\ 0 & 0 & 0 \end{bmatrix}.$$

The corresponding Laplacian matrix L's first 7 eigenvalues in the ascending order are $\{0, 0, 0, 0.2679, 0.3249, 1, 1\}$. Based on these eigenvalues, we can group all links into 3 disconnected clusters as in Fig. 5.4(a), or 5 clusters of smaller cluster sizes including 1 disconnected cluster and 4 connected clusters as in Fig. 5.4(b).

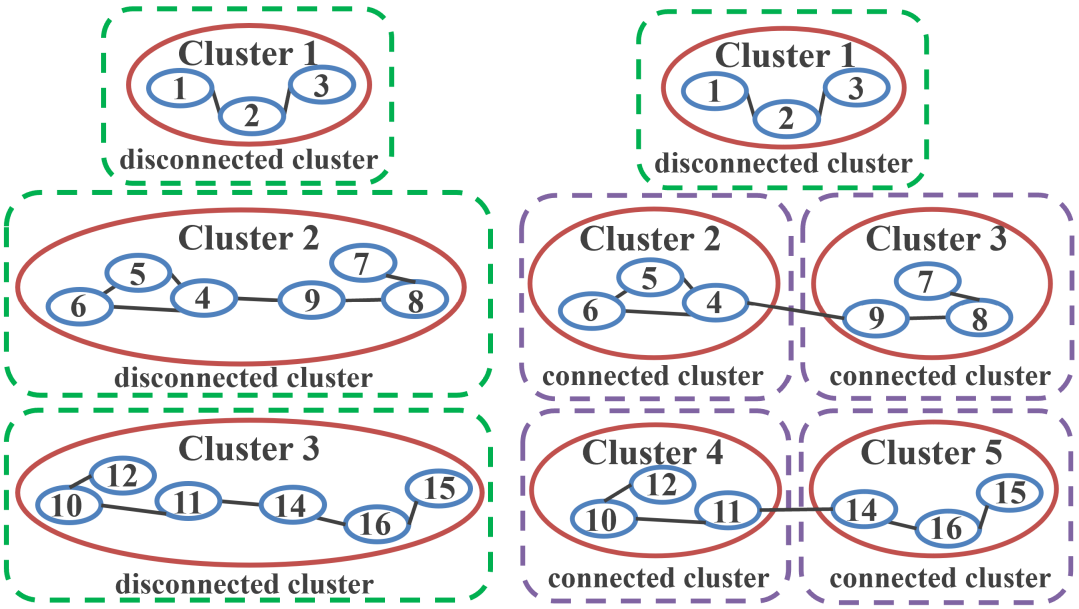

Figure 5.4: Clustering of the illustrative example. (a) 3 disconnected clusters. (b) 5 clusters with 1 disconnected cluster and 4 connected clusters.

The spectral clustering algorithm summarized in Algorithm 4 uses the eigenstructure approach to group N links into K link clusters.

Step 2: Permutation and enumeration. The remaining dependencies among sub-problems are handled in the permutation and enumeration step. In partic-

Algorithm 4 Spectral Clustering Algorithm [111]

Input: The conflict table C of N requested mmWave links, and the number of link clusters K.

Output: The membership of N links in K clusters.

1: Compute the graph Laplacian matrix L according to (5.4) and (5.5).

2: Obtain L's top K eigenvectors $f_1, f_2, \cdots, f_K$, where $f_i \in \mathbb{R}^N$ with $i \in \{1, 2, \cdots, K\}$. Here, by 'top', we refer to the eigenvectors associated with the smallest K eigenvalues.

3: Construct matrix $F \in \mathbb{R}^{N \times K}$ by stacking all f_i in a row.

4: Treat each row of F as a vertex in $\mathbb{R}^K$ and partition these vertices into K clusters via the K-means algorithm.

ular, the direct conflicts among connected clusters, e.g., clusters 2 and 3 in Fig. 5.4(b) are resolved by scheduling each of these connected clusters with modified constraints in order. Specifically, to achieve a conflict-free schedule, the completed schedules of the connected clusters modify the finish time constraints of the next connected clusters to be scheduled, and the scheduling of a connected cluster becomes to find the optimal solution subject to the sub-intervals in $[T_c, 2T_c]$ that have not been scheduled by the previous connected clusters. Note that, the modified constraint for f_i of link i in the connected cluster may include several sub-intervals in $[T_c + d_i, 2T_c]$. If there exists no sub-interval with length larger than or equal to d_i, the link i is assigned $x_i = 0$ and filtered out in the corresponding sub-problem to reduce computation.

The scheduling order of the connected clusters with direct conflict can have impact on network utility. All possible permutations of these connected clusters are enumerated to search for the highest achievable network utility. This procedure can be implemented through parallel computing. For example, in Fig. 5.5, all links are

grouped into 7 clusters given available computing resources. Let LC_i denote the ith link cluster with $i \in \{1, 2, \cdots, 7\}$. These clusters include 2 disconnected clusters LC_1 and LC_2, and 5 connected clusters. Due to the direct conflicts among LC_3, LC_4 and LC_5, their 6 permutations of scheduling order are considered, while for LC_6 and LC_7 there are 2 permutations.

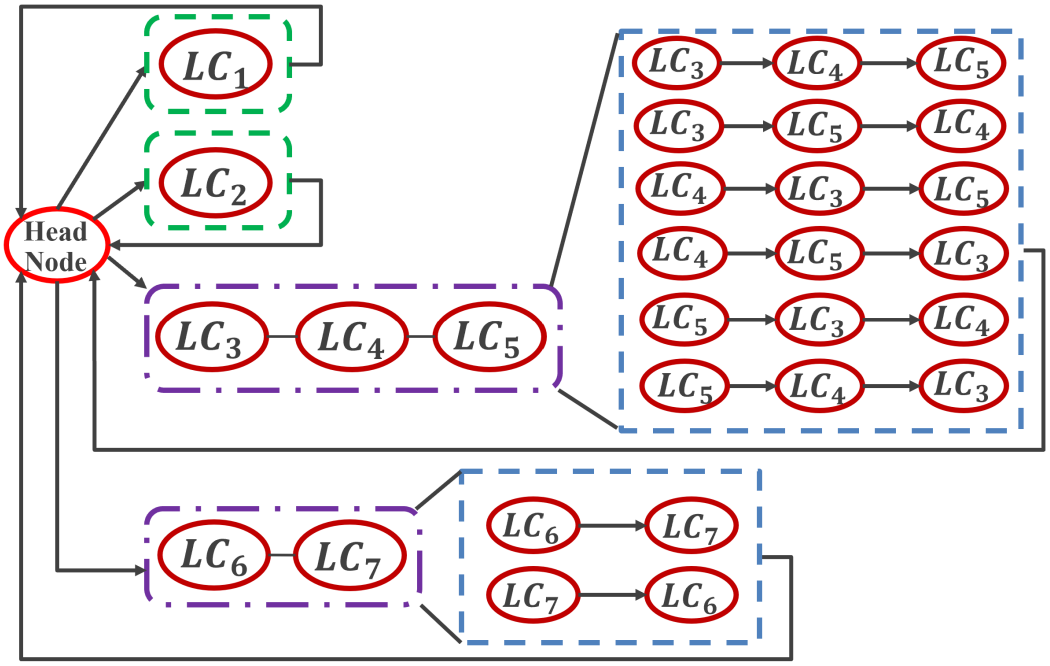

Figure 5.5: An example to show the permutation and enumeration step for link clusters. The purple dashed-line boxes denote the connected clusters with direct conflicts. The blue dashed-line boxes include the permutations of scheduling order.

Step 3: Selection. In the selection step, the individual head node within a section selects the schedule with the highest network utility from the permutation and enumeration step as the final solution to our scheduling problem (5.1).

Remark 5. *The number of link clusters K is a trade-off between the cluster size and the computational complexity in the permutation and enumeration step. At the extremes, $K = 1$ implies no decomposition for the scheduling problem and $K = N$*

denotes a brute-force approach. As shown in Fig. 5.6, the global optimal solution is guaranteed to be achieved when $K = 1$ and $K = N$, but with high computational cost [30]. When $1 < K < N$, the global optimal solution can be achieved with lower computational cost.

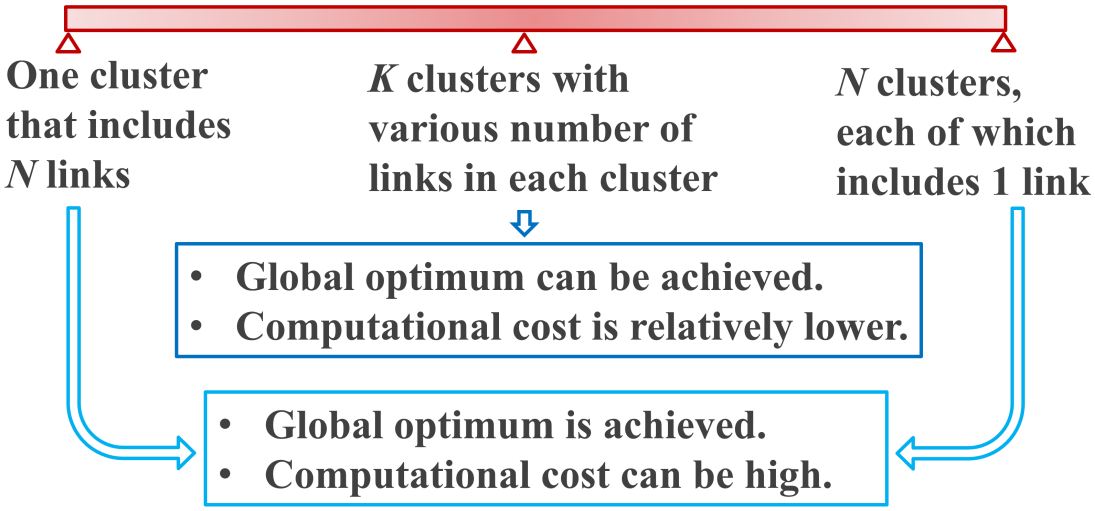

Figure 5.6: The trade-off between the cluster size and the computational complexity in the permutation and enumeration step.

The proposed decomposition-based approximate solution with three steps is summarized in Fig. 5.7.

Remark 6. *Note that our developed solution in Fig. 7 is not limited to using the PIA to solve the MINLP problem. Other scheduling algorithms, e.g., the branch and bound method, can also be used.*

5.3.2 Coordination among Multiple Head Nodes

In this subsection, we first show that an appropriate division of the long highway can confine cross-section conflicts to reside only within adjacent sections (i.e., one-hop

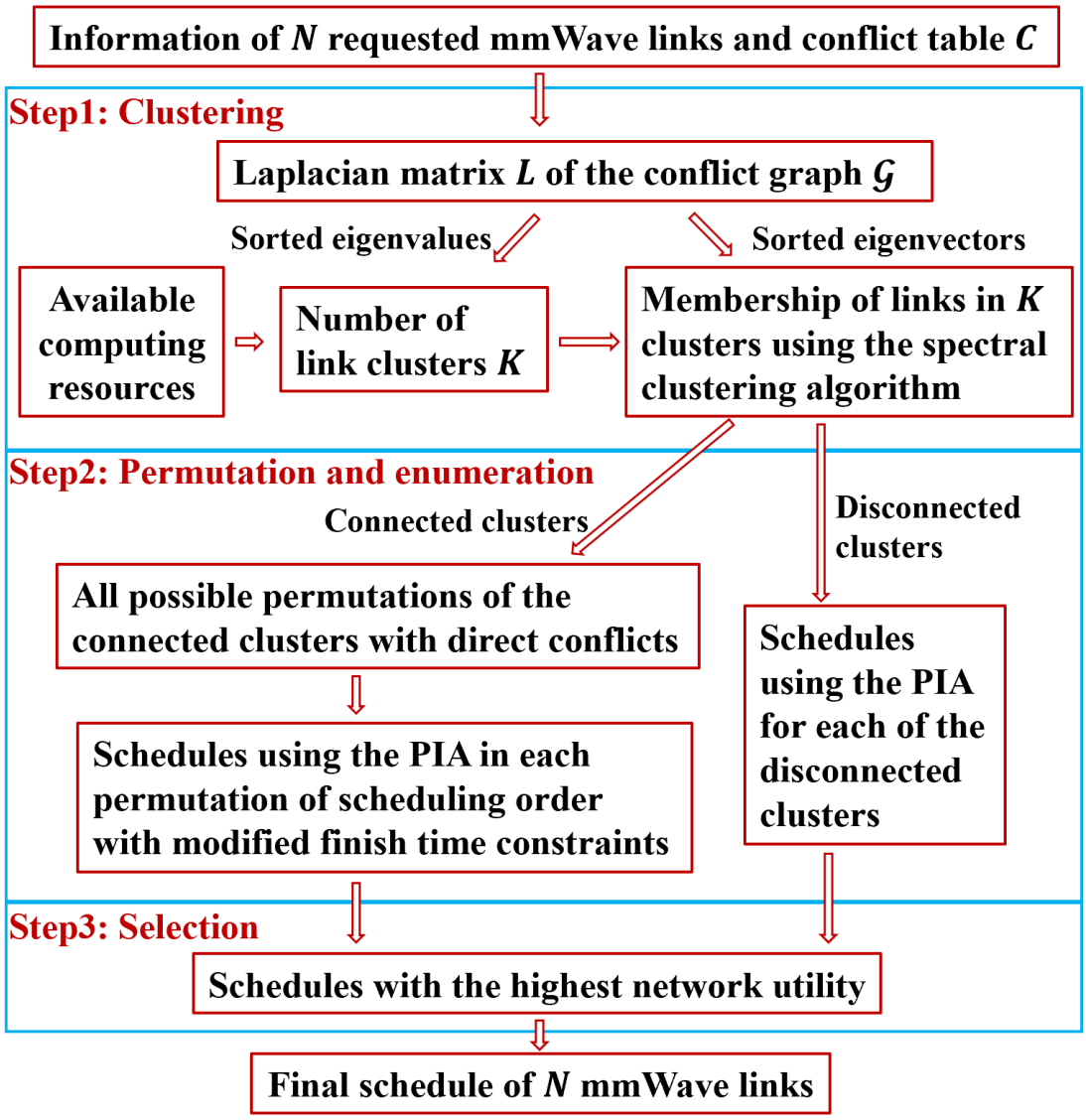

Figure 5.7: The proposed decomposition-based approximate solution with three steps for scheduling problem (5.1).

neighbor of head nodes). This helps to avoid complex coordination schemes among multi-hop head nodes and achieve low control overhead for sub-6 GHz channel.

Theorem 14. *Consider the communication conflicts resulted from mmWave communication properties, i.e., the point-to-point communication, half-duplex and in-lane interference for highway traffic, as illustrated in Section 5.2.1. If the range*

of each highway section R_S is at least twice of the mmWave communication range, i.e., $R_S \geq 2R_M$, link conflicts exist only in an individual section or in two adjacent sections.

Proof. We prove this theorem by considering the conflicts caused by three mmWave communication properties separately and show that in each case, the conflicted links are to be scheduled by an individual head node in one section or two head nodes in two adjacent sections. For point-to-point communication, the links cannot share a common transmitter or receiver. The maximum distance between two receivers of the conflicted links along highway is $2R_M$ with maximum link length R_M, as in Fig. 5.8(a). As a result, if $R_S \geq 2R_M$, the two conflicted links with a common transmitter are guaranteed to be scheduled by an individual head node or two adjacent head nodes regardless of the position of their common transmitter (see Figs. 5.8(b)-5.8(d)). Conflicted links with common receivers are to be scheduled by an individual head node. For half-duplex, a node cannot be the transmitter and receiver at the same time. The maximum distance between two receivers of the conflicted links along highway is R_M for this conflict, as in Fig. 5.9(a). If $R_S \geq 2R_M$, the two conflicted links are also guaranteed to be scheduled by an individual head node or two adjacent head nodes (see Figs. 5.9(b)-5.9(d)). For in-lane interference, the maximum distance between two receivers of the conflicted links along highway is R_M, as in Fig. 5.10(a). A similar argument as for half-duplex guarantees that the two conflicted links are to be scheduled by an individual head node or two adjacent head nodes under the condition $R_S \geq 2R_M$ (see Figs. 5.10(b)-5.10(d)). □

Now consider to resolve the cross-section conflicts confined within adjacent sections guaranteed by Theorem 14. Two coordination schemes are described below.

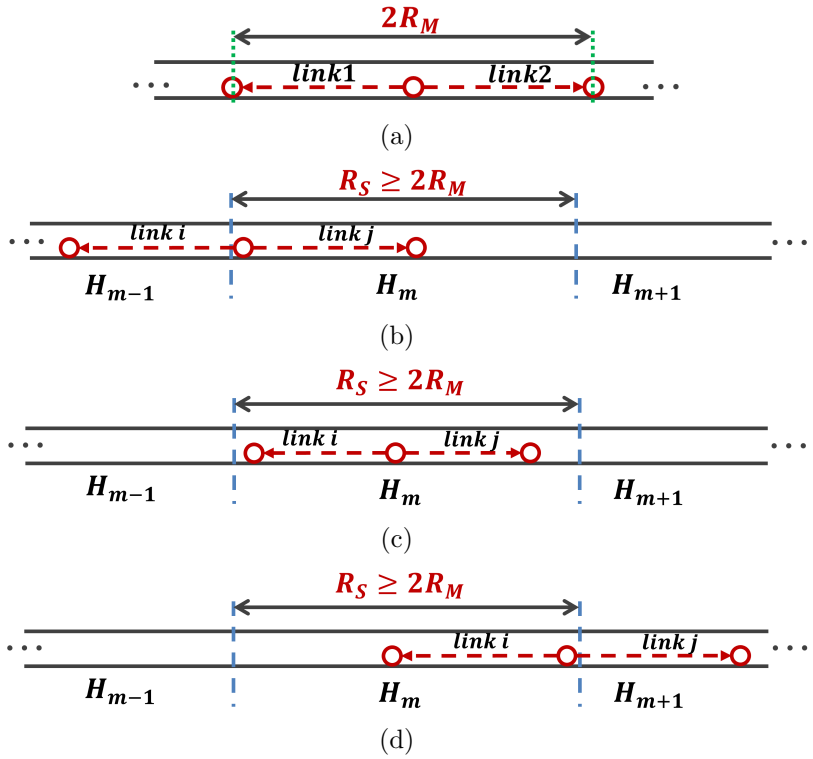

Figure 5.8: For point-to-point communication, (a) shows the maximum distance between two receivers of a pair of conflicted links. Two conflicted links are to be scheduled by (b) two adjacent head nodes, (c) one individual head node and (d) two adjacent head nodes, respectively, considering various position of the common transmitter.

Coordination scheme 1: Rule-based Coordination. In the proposed rule-based coordination scheme, multiple head nodes resolve cross-section conflicts using two steps (see Fig. 5.11). In step 1, each head node within a section conducts scheduling as in Section 5.3.1 and then shares the computed schedules with its adjacent head node(s). In step 2, each head node compares the schedules received and self-computed, and eliminate the conflicted links in schedules according to the following predefined rules:

a) For two conflicted links with different link utilities, the one with a smaller link utility is labeled with elimination.

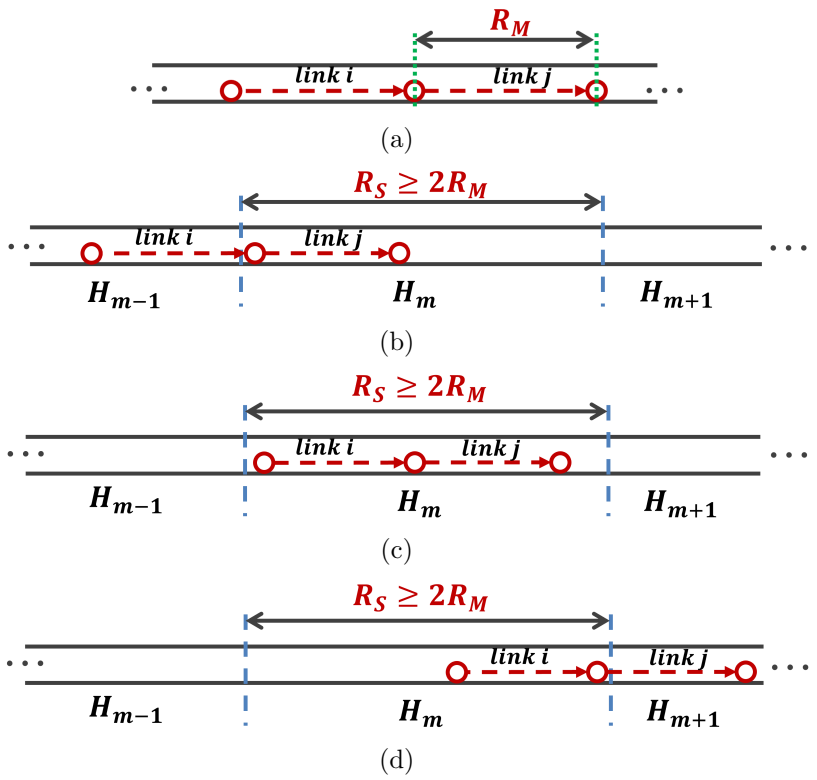

Figure 5.9: For half-duplex, (a) shows the maximum distance between two receivers of a pair of conflicted links. Two conflicted links are to be scheduled by (b) one individual head node, (c) one individual head node and (d) two adjacent head nodes, respectively, considering various position of the common node.

b) For two conflicted links with identical link utility, the one belonging to the odd (or even) section is labeled with elimination.

c) The links with at least one elimination label will be eliminated in the final schedules to be disseminated.

The rules are designed to retain the scheduled links with higher link utilities and abandon the conflicted ones with lower link utilities to achieve a high overall network utility, i.e., the sum of all network utilities by multiple head nodes. Following the predefined rules, all head nodes are able to eliminate the same conflicted links in their

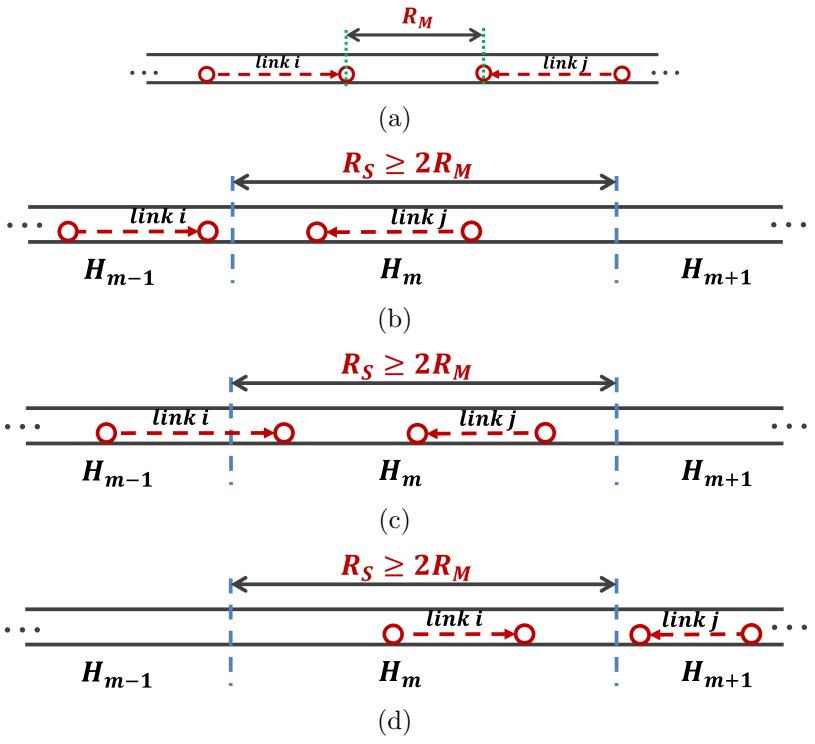

Figure 5.10: For in-lane interference, (a) shows the maximum distance between two receivers of a pair of conflicted links. Two conflicted links are to be scheduled by (b) two adjacent head nodes, (c) one individual head node and (d) two adjacent head nodes, respectively, considering various positions of the two receivers.

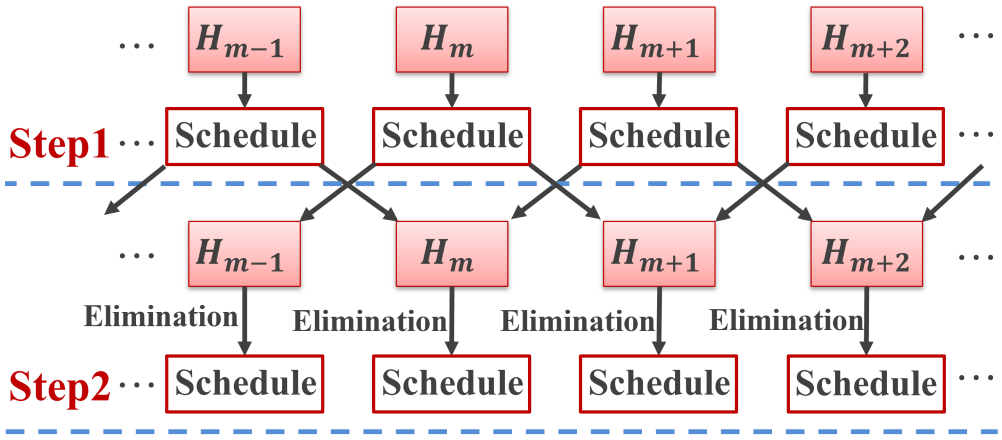

Figure 5.11: The rule-based coordination scheme for multiple head nodes.

schedules without additional control message exchange. In addition, these rules are simple to implement in practice.

Remark 7. *We notice that the rule-based coordination may result in unnecessary elimination of conflicted links in schedules, i.e., a pair of conflicted links are both eliminated. However, the overall conflict-free schedule can be achieved without heavy control overhead.*

Coordination Scheme 2: Section-parity-based Coordination. In this coordination scheme, we leverage Theorem 14 that cross-section conflicts are confined within adjacent sections. We consider head nodes divided into two groups based on the parity of their section IDs. Clearly, head nodes in the same group do not have conflicts. The cross-section conflicts are resolved by the two groups of head nodes following the two steps in Fig. 5.12. In step 1, all head nodes in the group of odd (or even) section IDs conduct scheduling as in Section 5.3.1 and then share the computed schedules with their adjacent head node(s). In step 2, all head nodes in the other group of even (or odd) section IDs modify the link finish time constraints in their MINLP problems based on the received schedules, as illustrated in the permutation and enumeration step in Section 5.3.1, and then conduct scheduling accordingly.

The developed section-parity-based coordination scheme allows half of the head nodes to schedule first and the rest to modify the constraints of their scheduling problems and resolve the cross-section conflicts. Compared with the rule-based coordination scheme, sharing computed schedules is only required for half of the head nodes, reducing the control overhead in sub-6 GHz channel. However, there is a delay introduced because the second group has to wait for its scheduling until the first group finishes.

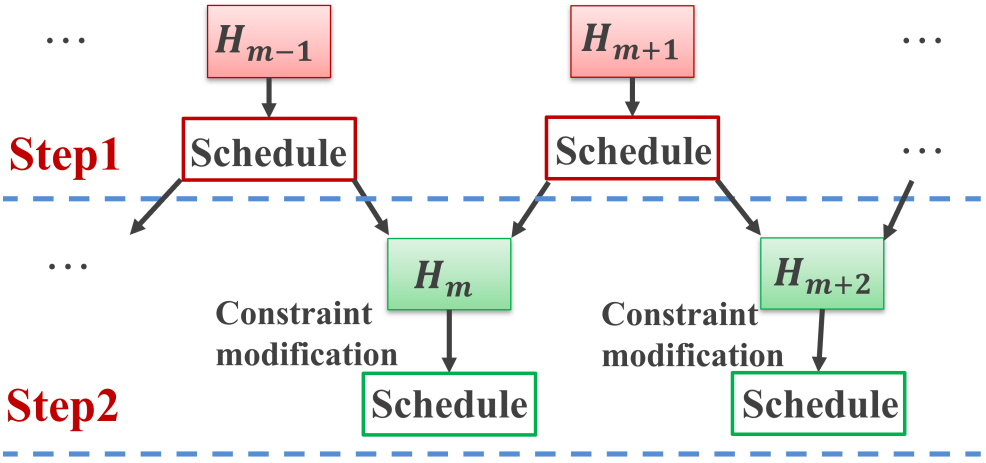

Figure 5.12: The section-parity-based coordination scheme for multiple head nodes.

5.4 Simulation Studies

In this section, simulation studies are conducted to show the performance of the proposed distributed scheduling scheme for long highway traffic. We first show performance of the decomposed PIA, which integrates the decomposition-based approximate solution with the PIA for individual head node within a section, and then the coordination schemes among multiple head nodes.

5.4.1 Decomposed PIA by Individual Head Node within a Section

Consider N link requests where link information and conflict tables are randomly generated with $w_i, d_i, o_i \in (0, 100]$ for $i \in \{1, 2, \cdots, N\}$ and $T_c = 100$ milliseconds (ms). Two studies are presented in the following.

Study 1: In this study, we show that if the conflict table is fully decomposable, the computational cost can be significantly reduced by clustering requested links, i.e., all link clusters are disconnected clusters. In this case, the global optimum is achieved. The execution time (ET) of algorithms is used as the performance metric. Consider N requested links where $N \in \{30, 40, \cdots, 100\}$, and the corresponding

number of clusters is $K \in \{3, 4, \cdots, 10\}$. As such, 10 links per disconnected cluster is maintained for the scalability study. We apply the PIA, the decomposed PIA and the decomposed PIA with parallel computing to solve the MINLP problem (5.1).

The result is shown in Fig. 5.13. When N is smaller than or equal to 50, the computational cost of the decomposed PIA is larger than that of the PIA. This is because the final schedule of the decomposed PIA approach is obtained only after schedules of all disconnected clusters are ready. The difference gets smaller with the increase of N. When N is larger than 50, the superiority of the decomposed PIA over the PIA in computing reduction becomes more significant. Furthermore, with parallel computing enacted, the ET of the decomposed PIA is the least for all N.

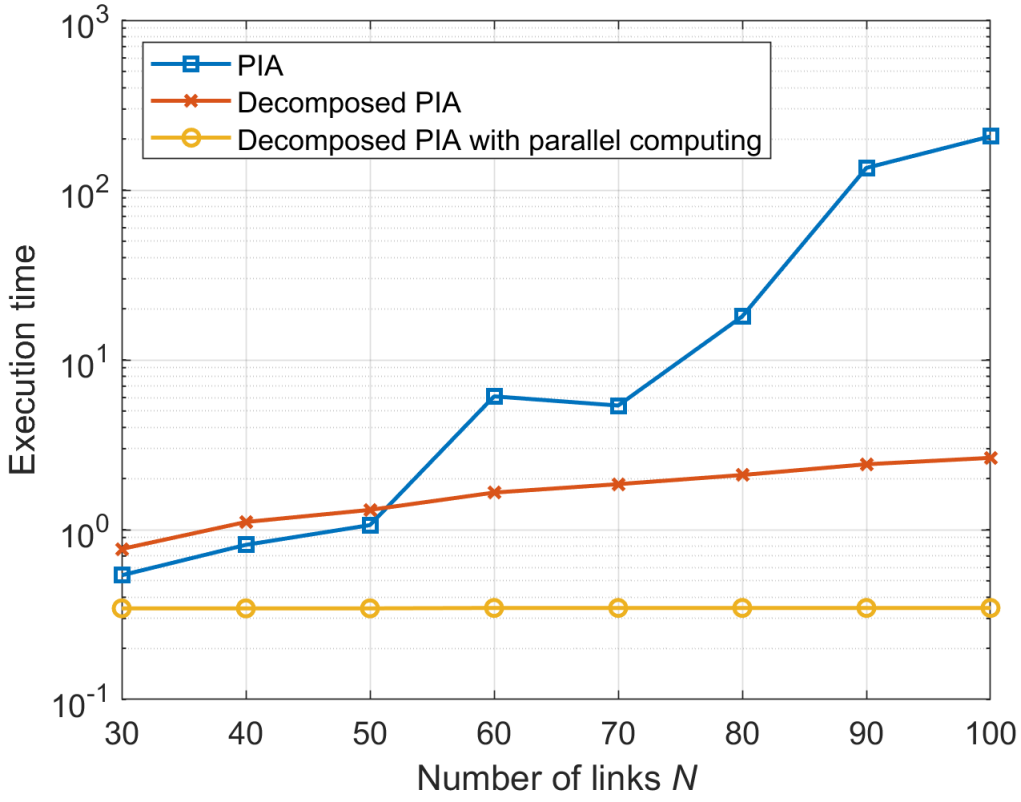

Figure 5.13: Algorithm execution time for an individual head node with fully decomposable conflict tables as illustrated in *Study 1*.

Study 2: In this study, we show that for general conflict tables, the decomposed PIA performs well in obtaining the global optimal solution, while the performance can be different for different numbers of clusters K. We define performance in percentage (PP) with respect to the global optimal solution obtained by the PIA as follows.

$$PP(\%) = \frac{NU_{decPIA}}{NU_{PIA}} \times 100, \tag{5.6}$$

where NU_{decPIA} and NU_{PIA} denote the network utilities by the decomposed PIA and the PIA, respectively. Consider $N = 15$ and $K \in \{2, 3\}$. 50 simulations are conducted with randomly generated link requests and conflicted tables.

The results are presented in Fig. 5.14 with $K = 2$ and $K = 3$. It can be seen that the global optimal network utility, i.e., $PP = 100\%$, can be achieved using the decomposed PIA in the majority of simulations. When $K = 2$, 70% (35 out of 50) can achieve the global optimal solution, and all can achieve the PP over 86% except one simulation run with $PP = 71.29\%$. When $K = 3$, 44% (22 out of 50) can achieve the global optimal solution, and all can achieve the PP over 84%. The distribution of PP for $K = 2$ is further to the right compared to that for $K = 3$. The decomposed PIA with $K = 2$ has a better performance in this example.

5.4.2 Coordination among Multiple Head Nodes

In this subsection, the range of a highway section for each head node is set as $2R_M$, according to Theorem 14, to mitigate computational burden. $R_M = 200m$.

Study 3: This study considers the performance degradation using the proposed coordination schemes. We define performance loss (PL) as follows.

$$PL(\%) = \frac{NU_g - NU_{dis}}{NU_g} \times 100, \tag{5.7}$$

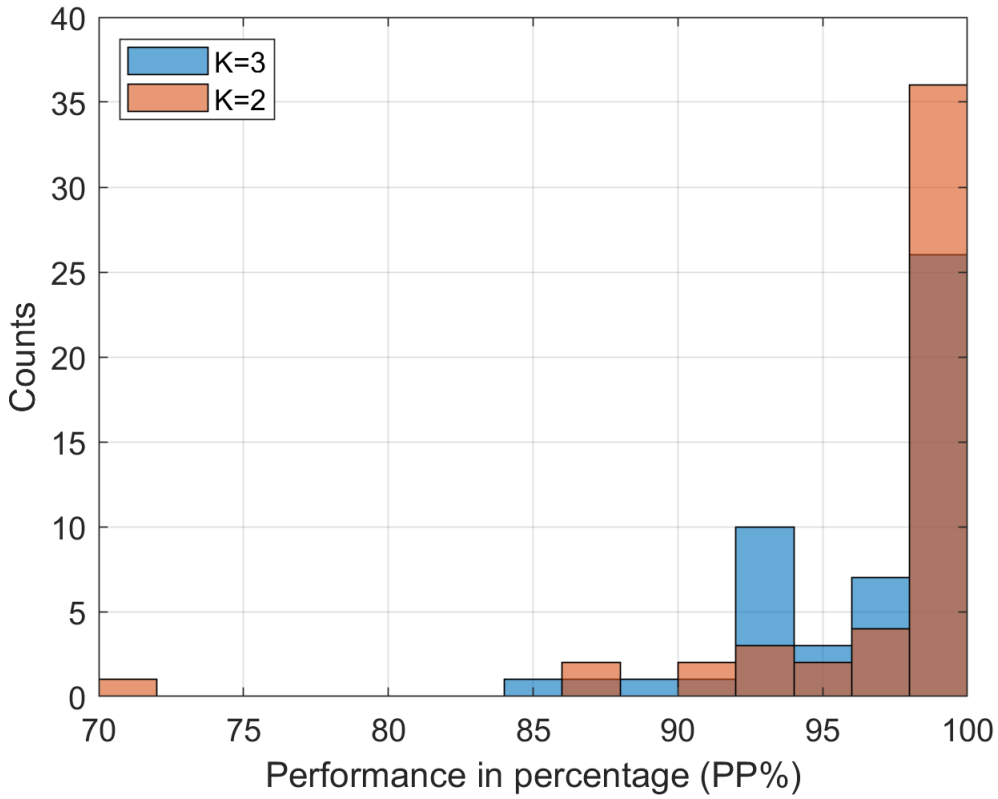

Figure 5.14: Histogram of PPs by the decomposed PIA for $N = 15$ in *Study 2*.

where NU_g is the global optimal network utility obtained by applying the PIA to process all the requested links for the whole highway, and NU_{dis} is the overall network utility using the proposed coordination scheme.

Consider a vehicular network on a 4-lane highway of length $2,000m$. The highway is segmented into 5 sections. 100 vehicles have random locations on the highway, and 80 of them are randomly selected to be equipped with the sub-6 GHz and mmWave devices. The number of link requests per vehicle N_{int} ranges between 10 and 20 with a step size of 2 over the time interval $[0, T_c]$. The link information, w_i, d_i and o_i, is generated randomly as in Section 5.4.1. The conflict tables are constructed for

the specific vehicular networks under highway traffic considering the three mmWave communication conflicts illustrated in Section 5.2.1.

We compare the rule-based and section-parity-based coordination schemes, and for the latter, we also investigate the impact of scheduling orders of the two head node groups on the overall network utility. 100 simulations are conducted with randomly generated link information and vehicular networks.

The result is shown in Fig. 5.15. For both coordination schemes, the average PL can be small ($< 6\%$), and increases with the increase of N_{int}. In addition, there is no significant performance difference between the two coordination schemes. For the section-parity-based coordination scheme, the scheduling order of two head node groups also shows negligible impact on the average PL.

Study 4: In this study, we show the performance of the proposed distributed scheduling scheme with varying highway length. Note that, as illustrated in Section 5.2.2, it is not feasible for one head node to perform scheduling, when the highway length is beyond the sub-6 GHz communication range. As such, a distributed scheduling scheme must be applied. The configuration for vehicular networks and mmWave links is the same as in *Study 3* except that the length of highway ranges between $1200m$ and $2800m$ with a step size of $400m$. As such, the number of highway sections N_s ranges between 3 and 7 with a step size of 1. The corresponding number of vehicles ranges between 60 and 140 with a step size 20 to maintain the vehicle density per section. 100 random simulations are conducted.

The average NU_{dis} with varying N_{int} using the rule-based coordination scheme is shown in Fig. 5.16. The average NU_{dis} increases with the increase of N_{int}. For a given N_{int}, the average NU_{dis} increases with the length of highway L. The same results are observed using the section-parity-based coordination scheme. The difference of the average NU_{dis} between two coordination schemes is not significant for all pair

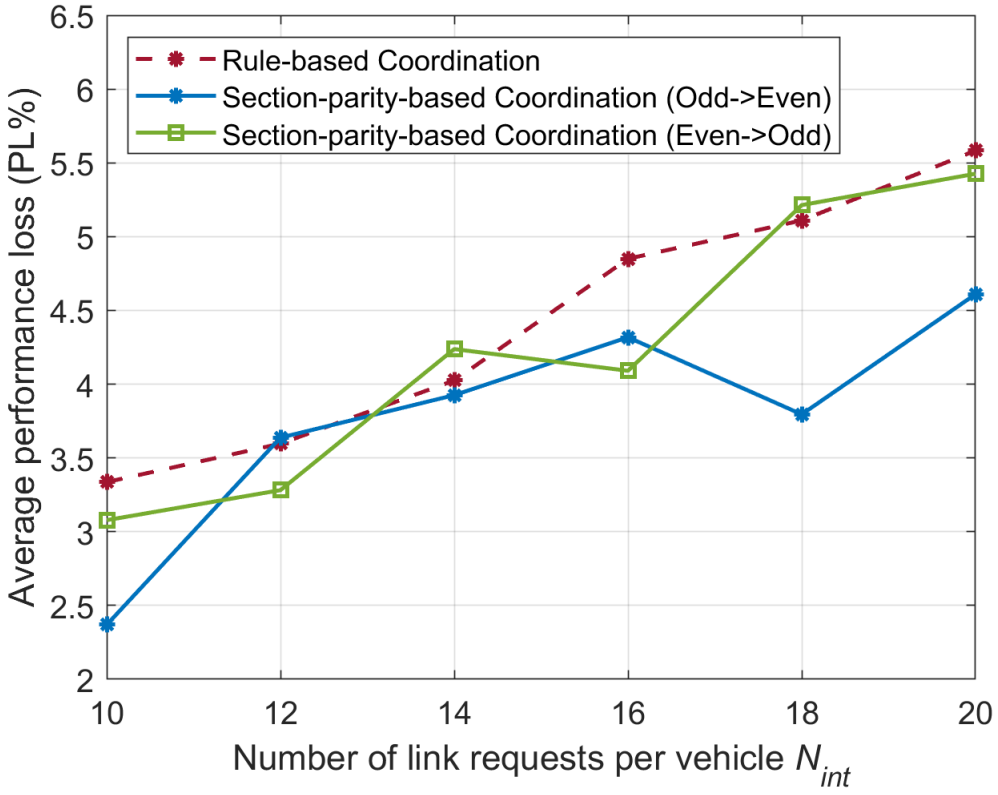

Figure 5.15: Average PL by the coordination schemes with varying N_{int} in *Study 3*.

of N_{int} and L (see the three lines on top of Fig. 5.17 for $L = 2800m$), consistent with the observation in *Study 3*. The scheduling order of two head node groups in the section-parity-based coordination scheme shows no significant influence on the average NU_{dis} achieved as in *Study 3*.

Study 5: In this study, we compare the effectiveness of the proposed distributed scheduling scheme with that of a decentralized solution without coordination. The decentralized solution has a head node within each highway section of range R_M. The head node schedules links only within the section and there is no coordination among them. The length of highway and the number of vehicles are the same as in *Study 4*. As such, the number of highway sections N_s ranges between 6 and 14 with a step size

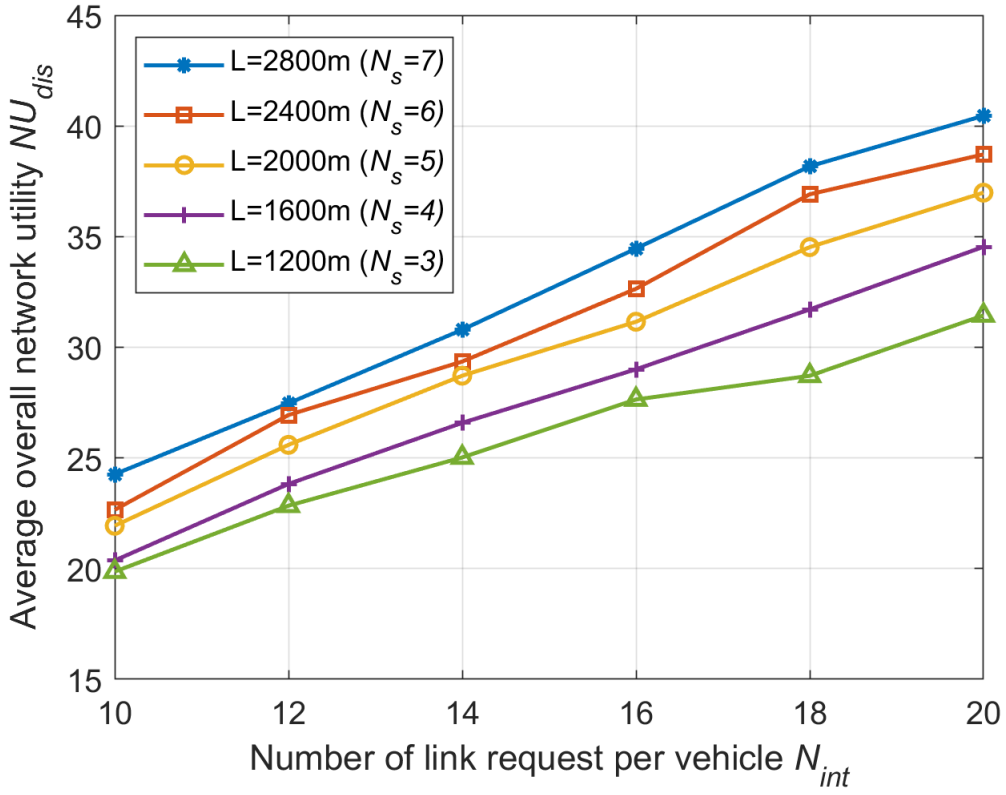

Figure 5.16: Average overall network utility NU_{dis} using the rule-based coordination scheme with varying N_{int} in *Study 4*.

of 2. The link utilities of conflicted links in schedules of multiple head nodes are not counted in NU_{dis} due to transmission failure. 100 random simulation are conducted.

As shown in Fig. 5.17 for $L = 2800m$, distributed scheduling with the two coordination schemes all achieves higher average NU_{dis} compared to the decentralized solution. The same comparative result is observed for all L. The results are not surprising because our design for highway division confines link conflicts within adjacent head nodes, which are then resolved by the coordination schemes to improve channel utilization. In addition, the superiority of the proposed distributed scheduling scheme becomes more significant with the increase of N_{int}.

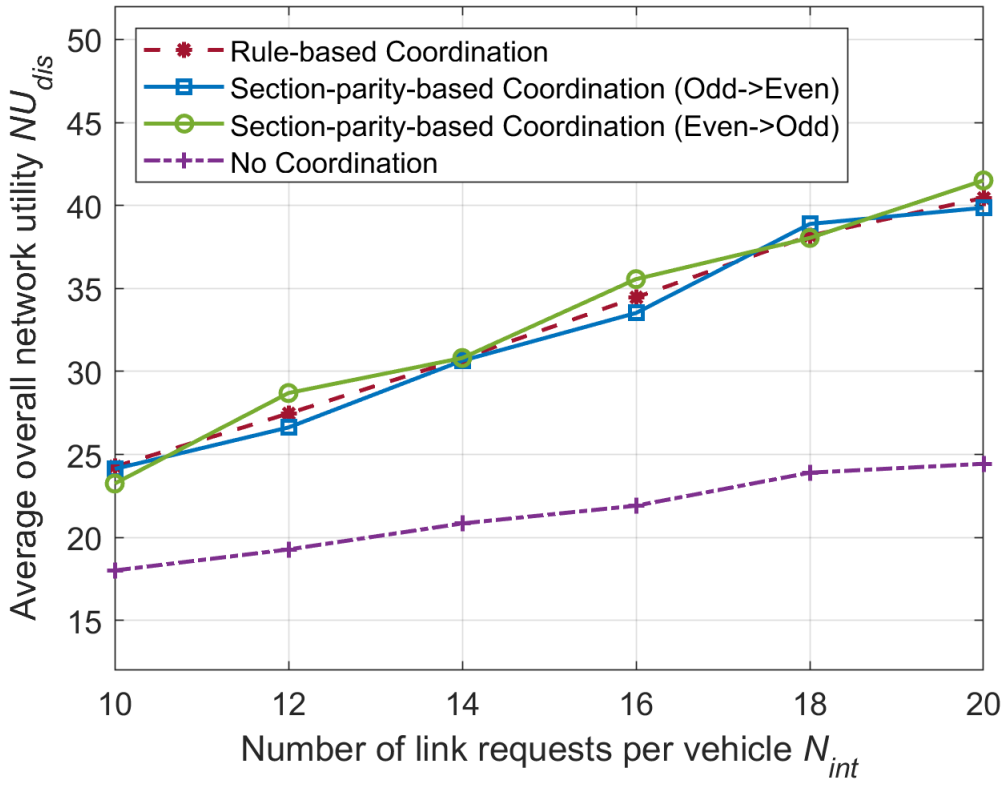

Figure 5.17: Average overall network utility NU_{dis} for $L = 2800m$ with varying N_{int} in *Study 5*.

5.5 Conclusion

In this chapter, we studied the sub-6 GHz V2X-assisted mmWave link scheduling for long highway traffic. A distributed scheduling scheme was proposed. The long highway is divided into contiguous and non-overlapping sections. For each section, a head node collects mmWave link requests and determines a conflict-free transmission schedule through coordinating with other head nodes. We addressed both the computational challenge for individual head node to solve the scheduling problem in a section, and the communication challenge for multiple head nodes to resolve cross-section conflicts. To address the intra-section computational challenge, we developed a decomposition-based approximate solution, which leverages the spectral analysis

of conflict table to decompose the scheduling problem in a section with minimal dependencies among sub-problems. Remaining dependencies are addressed through a permutation and enumeration procedure. To address the inter-section communication challenge, two coordination schemes were designed to avoid heavy control overhead for an overall conflict-free transmission schedule. The rule-based scheme uses predefined rules to eliminate conflicted links. The section-parity-based scheme groups head nodes based on the parity of their section IDs, and head nodes from two groups conduct scheduling with modified constraints in order. Both schemes are simple to implement. Simulation studies using MATLAB validated the effectiveness of the proposed distributed scheduling scheme.

CHAPTER 6

STOCHASTIC HIERARCHICAL GAME (SHG) FOR MULTIAGENT AUTONOMOUS DRIVING

6.1 Introduction

Autonomous vehicles (AVs) can transform the way people live and work, for example, by reducing traffic deaths, improving fuel economy, and maximizing travel efficiency [113]. Decision-making, which navigates the AVs through complex traffic scenarios safely and efficiently, plays a critical role to achieve these goals [114,115]. It is challenging for the AVs to make decisions in diverse traffic environments because of the presence of, e.g., multiple interactive agents and the inherent uncertainty [116, 117]. Various uncertainties are involved in the decision-making process of AVs, e.g., observation uncertainty due to inaccuracy perception [118] and intention uncertainty of human drivers and pedestrians [119]. In this chapter, we consider the uncertain intentions of traffic participants in multiagent decision-making for AVs.

The partially observable Markov decision process (POMDP) has been studied to consider the inherent uncertainty of dynamic environments in AVs' decision-making [120, 121]. However, finding optimal solutions of general POMDPs under multiagent traffic environments can be intractable [122, 123]. Approximate solutions are developed at the cost of sacrificing optimality [124, 125]. An alternative approach to considering uncertain intentions of complex traffic participants is to formulate the problem as a planning problem that includes prediction and decision-making [126,127]. To predict trajectories resulting from uncertain intentions to enable probabilistic safety guarantees in complex dynamic environments, most recent studies

in the literature implement uncertainty models to approximate uncertain trajectory as random processes [40]. Uncertainty models of specific distributions include the Gaussian process and its several variants [37, 128] and a noise rational model [38, 129]. Distribution-free uncertainty models include quantile regression [39], scenario optimization [130, 131], generative models (e.g., generative adversarial models) [132, 133], and hidden Markov models [134, 135]. The limitations of these uncertainty models lie in the inaccurate probabilities of rare trajectory scenarios learned with finite data (e.g., abrupt intention changes) and inaccurate confidence bounds for making safe decisions [40].

The random mobility model (RMM) is a promising model because it has been proved to be effective in capturing the stochastic movement characteristics of mobile agents in realistic scenarios, e.g., ground and airborne vehicles [136, 137]. Classic RMMs include random waypoint/walk/direction models, Manhattan mobility model and smooth-turn RMMs [138, 139]. In [140], the RMM models random movement of agents as a random switching system with two types of random variables, where one type of random variable characterizes the specific maneuver executions and the other type accounts for maneuver-changing behaviors. Compared with the uncertainty models, the RMM can capture both uncertain low-level movements resulting from intentions as well as uncertain changes of intentions. RMMs can leverage discrete or continuous probabilistic information. Because a discrete hypothesis set can be inadequate to cover all behavior variations emerging in real-world tasks [141], in this chapter, we consider continuous RMM to capture the uncertain intentions of interactive agents to facilitate the decision-making of AVs.

Regarding the multiagent decision-making of AVs, game theoretic-based approaches provide a good framework to model interactions among multiple traffic participants and to solve for optimal payoffs in non-cooperative traffic environments

[142, 143]. Various types of games (e.g., the normal-form games and the Stackelberg games) are applied for decision-making under specific traffic scenarios, such as lane-changing and intersection-crossing [41, 42]. A three-level decision-making framework has been proposed in [43] to generalize the universality of game theoretic-based methods for diverse traffic scenarios. In [144, 145], the pairwise game is applied to address the computational scalability issue in multiagent decision-making where each pair of game players makes the decision independently. However, such decisions can be inefficient and lead to deadlock because the interactions among multiple agents are not considered. [146] proposed a hierarchical game (HG) for safe and efficient multi-agent decision-making by leveraging an interaction graph. The game theoretic-based approaches usually assume that the intentions of traffic participants are known to AVs, but this assumption does not hold in realistic traffic scenarios, especially when human drivers are involved. A Bayesian game is generally used to consider the incomplete information of agents, such as their uncertain intentions [44]. However, fixed players with uncertain intentions are required in the Bayesian games, which is not scalable with the number of game players and high computational cost is inevitable. Simulation for all possible scenarios with uncertain intentions is also time-consuming. Therefore, in this chapter, we leverage an efficient uncertainty evaluation technique, named the multivariate probabilistic collocation method with the orthogonal fractional factorial design (MPCM-OFFD) [147, 148], to integrate uncertain intentions with the HG in [146] to achieve safe decisions efficiently.

We propose a stochastic hierarchical game (SHG) to consider uncertain intentions in multiagent decision-making. We address two challenges, including capturing uncertain intentions as well as their random changing behavior and integrating uncertain intentions in decision-making using HG efficiently. The main contributions of this chapter are summarized as follows.

- In the proposed SHG, an RMM with two types of continuous random variables is used to capture uncertain intentions of interactive agents and their random changing behavior under realistic traffic scenarios.
- A smart sampling-based uncertainty evaluation approach (the MPCM-OFFD) is used to solve the proposed SHG efficiently given the probability information in the RMM. Both conservative and progressive decision-making for the ego can be characterized.
- Extensive simulation studies are conducted to validate the effectiveness of the proposed SHG by comparing the performance with the HG that does not consider uncertain intentions. The ego can make safe and efficient decisions with reduced frequency of repeated game play, realistic braking maneuver, and timely response to emergencies.

The rest of this chapter is organized as follows. In Section 6.2, the problem for multiagent decision-making considering uncertain intentions of interactive agents is motivated and formulated. The SHG is elaborated upon in Section 6.3. Comparative simulation studies are presented in Section 6.4. Section 6.5 concludes this chapter.

6.2 Preliminaries and Problem Formulation

6.2.1 HG for Multiagent Decision-Making

The HG was proposed in [146] for efficient multiagent decision-making. In HG, the ego vehicle considers its game players based on an interaction graph (see Fig. 6.1), which captures its interaction level with the surrounding agents, e.g., AVs, human-driven vehicles and pedestrians. We illustrate the HG in the intersection-crossing traffic scenarios.

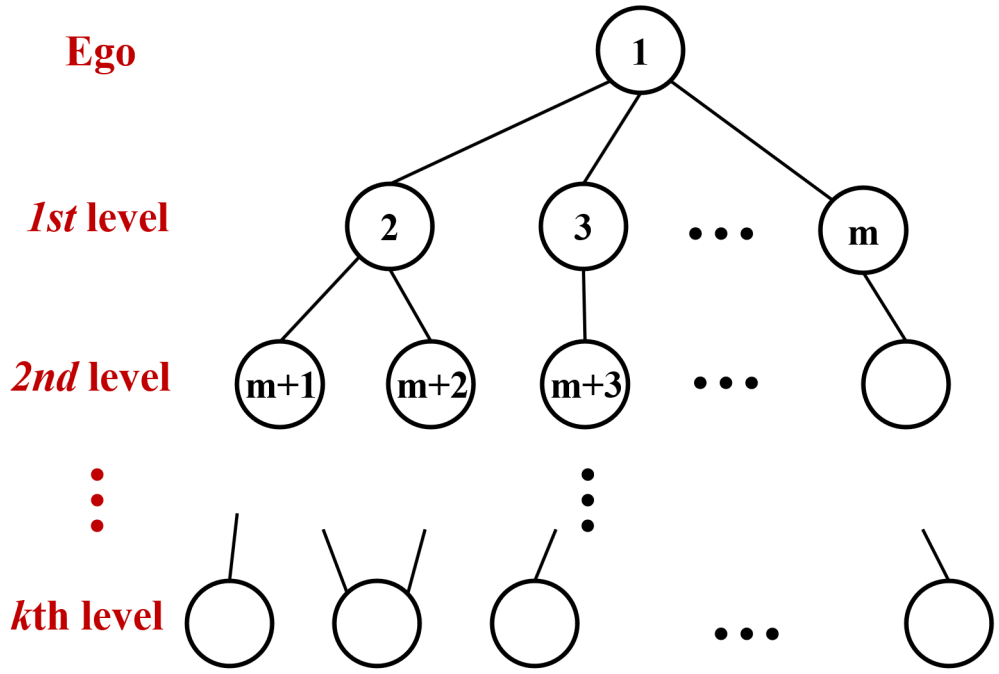

Figure 6.1: A general interaction graph in the HG. Circles with numbers denote agents. Ego is labeled as agent 1. Edges between nodes indicate the existence of trajectory conflicts.

Considering that agents with intersecting trajectories have trajectory conflicts, we define the ego's kth level neighbors as the agents that have trajectory conflicts with its $(k-1)$th level neighbors. The $1st$ level neighbors, also called the direct neighbors, are the agents that have trajectory conflicts with the ego. An agent cluster $\mathcal{C}_n$ is the set of agents with parallel trajectories. Among agent i's direct neighbors, an agent j is said to be the representative of $\mathcal{C}_n$ if $j = \text{argmin}_{j \in \mathcal{C}_n} |T_{ij}^c - T_{ji}^c|$, where T_{ij}^c is the time that agent i takes to reach the relative position of agent j, namely, time-to-collision (TTC) of agent i against agent j (see Fig. 6.2). Note that the TTC for agents without trajectory conflicts is infinite. Based on the above definitions, an interaction graph is constructed using cluster representatives as nodes and trajectory conflicts as edges, as in Fig. 6.1. The ego can play a multiagent game with its first K levels of neighbors in the HG. To further reduce the computational complexity, we consider a branch in

the interaction graph, which is defined as an interaction tree with one direct neighbor of the ego as the root node and all agents that have a path to the root are involved. Then the multiagent game can be decomposed into separate subgames with respect to the branches without common nodes. The ego then plays several subgames and selects the most conservative Nash equilibrium decision as the solution of the HG.

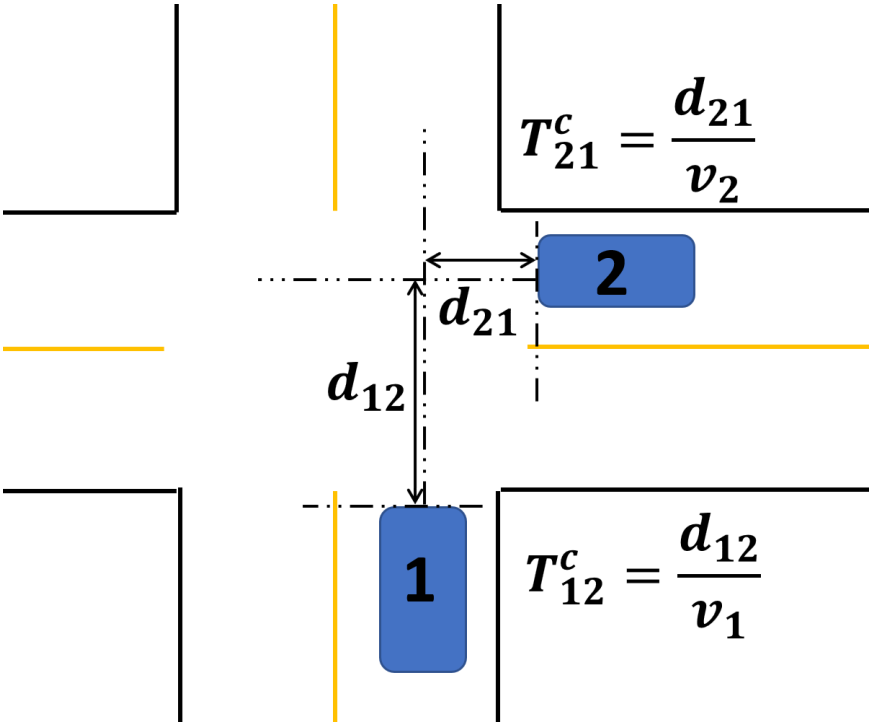

Figure 6.2: Time-to-collision (TTC) between agents 1 and 2, T_{ij}^c where $i, j \in \{1, 2\}$, d_{ij} denotes the longitudinal distance with respect to road geometry from agent i' forepart to the relative position of agent j's forepart, and v_i denotes the velocity of agent i.

An example of seven interactive agents is given in Fig. 6.3 to illustrate the HG. Agents 3 and 4 and agents 5 and 7 are grouped into two clusters, respectively, with agents 3 and 5 as the corresponding representatives. The interaction graph with the ego's first two levels of neighbors is shown in Fig. 6.3. The ego plays two

subgames, a two-player game with agent 2, and a three-player game with agents 3 and 5. Compared with a seven-player game, the computational cost can be significantly reduced by using the HG.

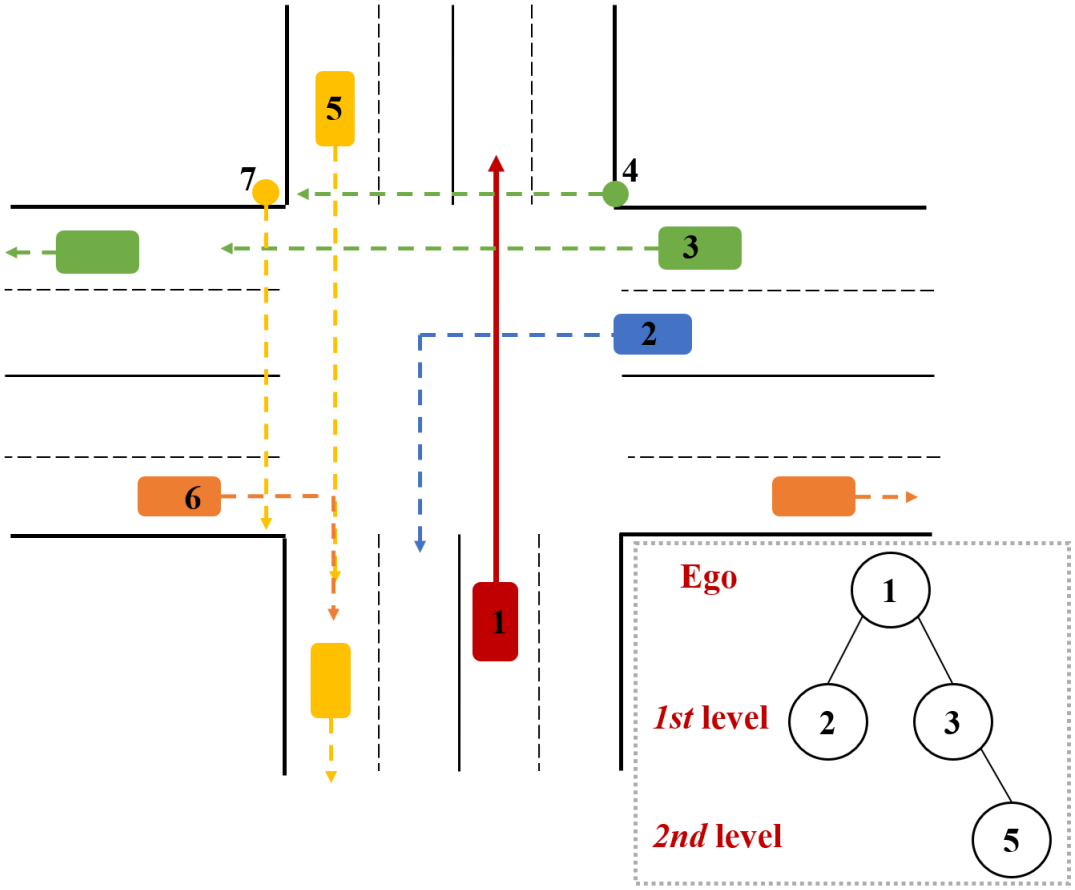

Figure 6.3: An example of an intersection-crossing traffic scenario and the interaction graph with the first two levels of neighbors.

6.2.2 Multiagent Decision-Making Considering Uncertain Intentions

In general traffic scenarios, the intentions of interactive agents are often uncertain to the ego; therefore, uncertain trajectories in the interaction graph to determine the game players. For example, as in Fig. 6.4, each of agents 2 and 3 with uncer-

tain intentions can have two possible future trajectories for the ego to consider in its decision-making. Thus, the HG in Section 6.2.1 cannot be directly applied for multiple interactive agents with uncertain intentions. Furthermore, a sudden intention change of interactive agents can lead to serious safety concerns to the ego; for example, vehicles on highway may perform sudden lane-changing to avoid missing a desired exit. Therefore, in this chapter, we are motivated to capture the uncertain intentions of interactive agents and incorporate them into the ego's decision-making using HG to improve its safety and efficiency.

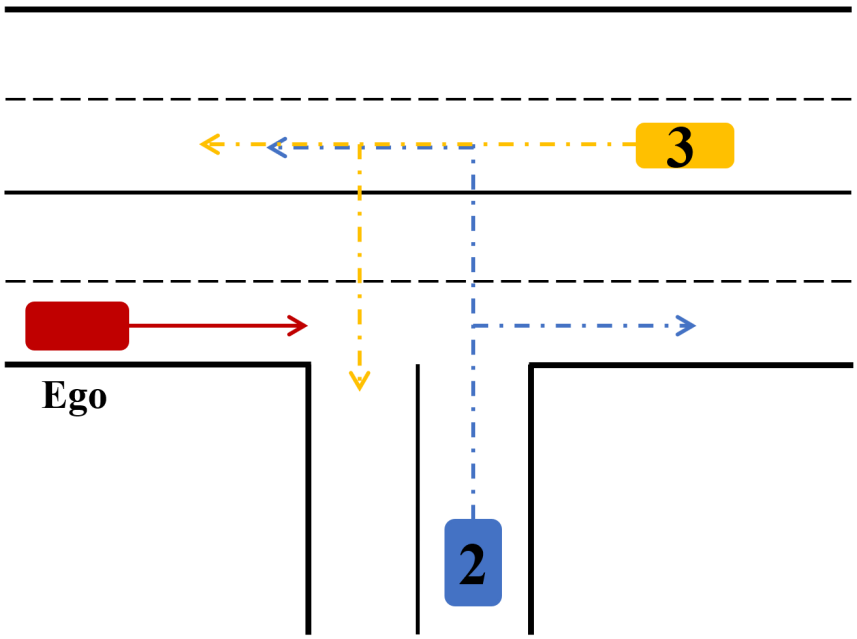

Figure 6.4: A traffic scenario in which the intentions of agents 2 and 3 are uncertain to the ego. Two possible trajectories for each agent should be considered in the ego's decision-making.

Capturing uncertain intentions can be challenging because realistic intentions are often affected by multiple factors, exhibiting temporal, spatial and geographic dependencies. These dependencies of realistic intentions modulate the probabilities

of possible future trajectories, namely, intention-oriented trajectories. Let Tr_i with $i = 1, 2$ denote the intention-oriented trajectories. Fig. 6.5(a) shows an example of temporal dependency, where the probability of Tr_1 is higher than that of Tr_2 if the blue vehicle finished lane-changing just a moment ago. Fig. 6.5(b) shows an example of spatial dependency, where the probability of Tr_1 can be lower than that of Tr_2 for the blue vehicle if the green vehicle on the top lane has a lower speed. One example for geographic dependency is shown in Fig. 6.5(c), where the probability of Tr_1 for the blue vehicle can become larger when it gets close to the intersection. However, it is also essential to consider random switching from uncertain intentions.

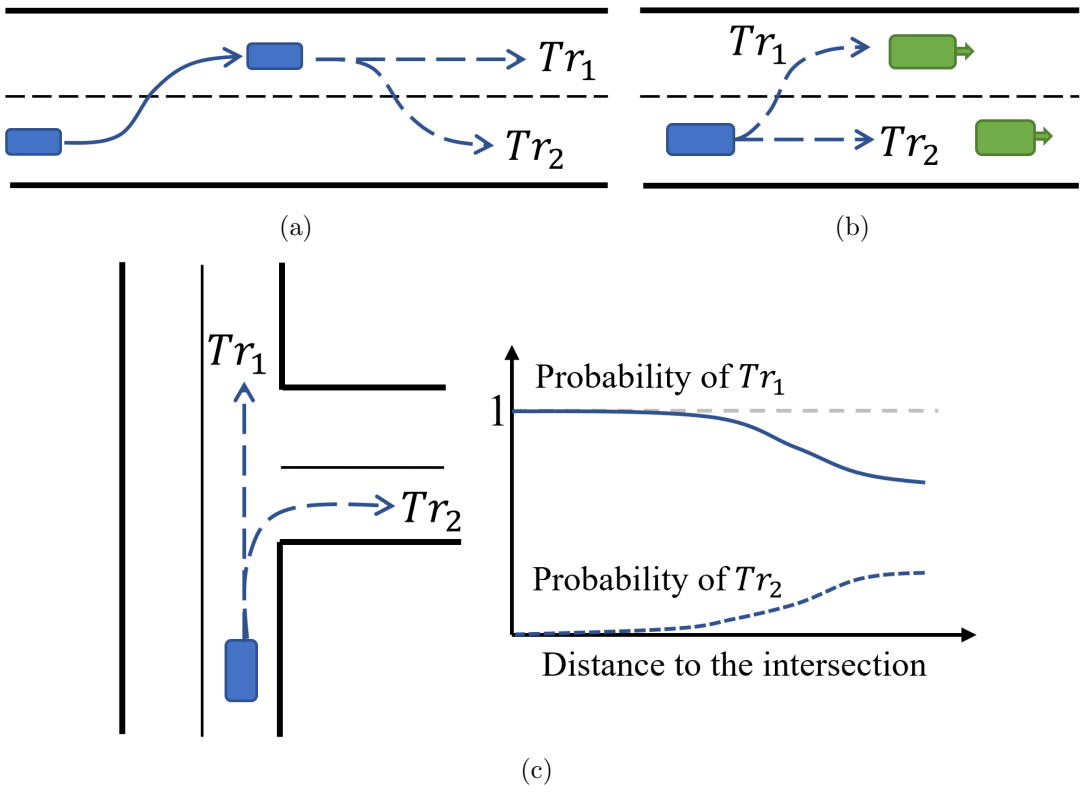

Figure 6.5: For realistic intentions, examples of (a) temporal dependency, (b) spatial dependency, and (c) geographic dependency.

Incorporating uncertain intentions in the HG can also be challenging with respect to safety and efficiency. First, determining the solution of HG with uncertain intentions to guarantee the ego's safety is challenging. Bayesian Nash equilibrium (BNE) is the solution of a Bayesian game, which is able to consider the uncertain intentions of interactive agents [44]. As an analogous concept to Nash equilibrium in the non-Bayesian games, BNE is the strategy profile that maximizes the expected payoff for each player given the probabilities of their intentions, with the other players' strategies fixed [149]. However, fixed players are required in a Bayesian game, which is not the case in HG with uncertain intentions. As shown in Fig. 6.6, uncertain intentions of interactive agents generate different interaction graphs for the HG, leading to different game players. Therefore, BNE is not applicable as the solution of HG considering uncertain intentions. In addition, it is computationally expensive and time-consuming to simulate all possible scenarios with uncertain intentions in the HG.

In this chapter, we propose an SHG to consider the uncertain intentions of interactive agents in multiagent decision-making with HG. In the SHG, we address the following two challenges.

1) Find an appropriate mobility model to succinctly and effectively characterize traffic agents' uncertain intentions.
2) Incorporate the efficient uncertainty quantification model into the ego's decision-making such that the ego's expected decisions in the presence of others' uncertain intentions can be derived both accurately and computationally efficiently.

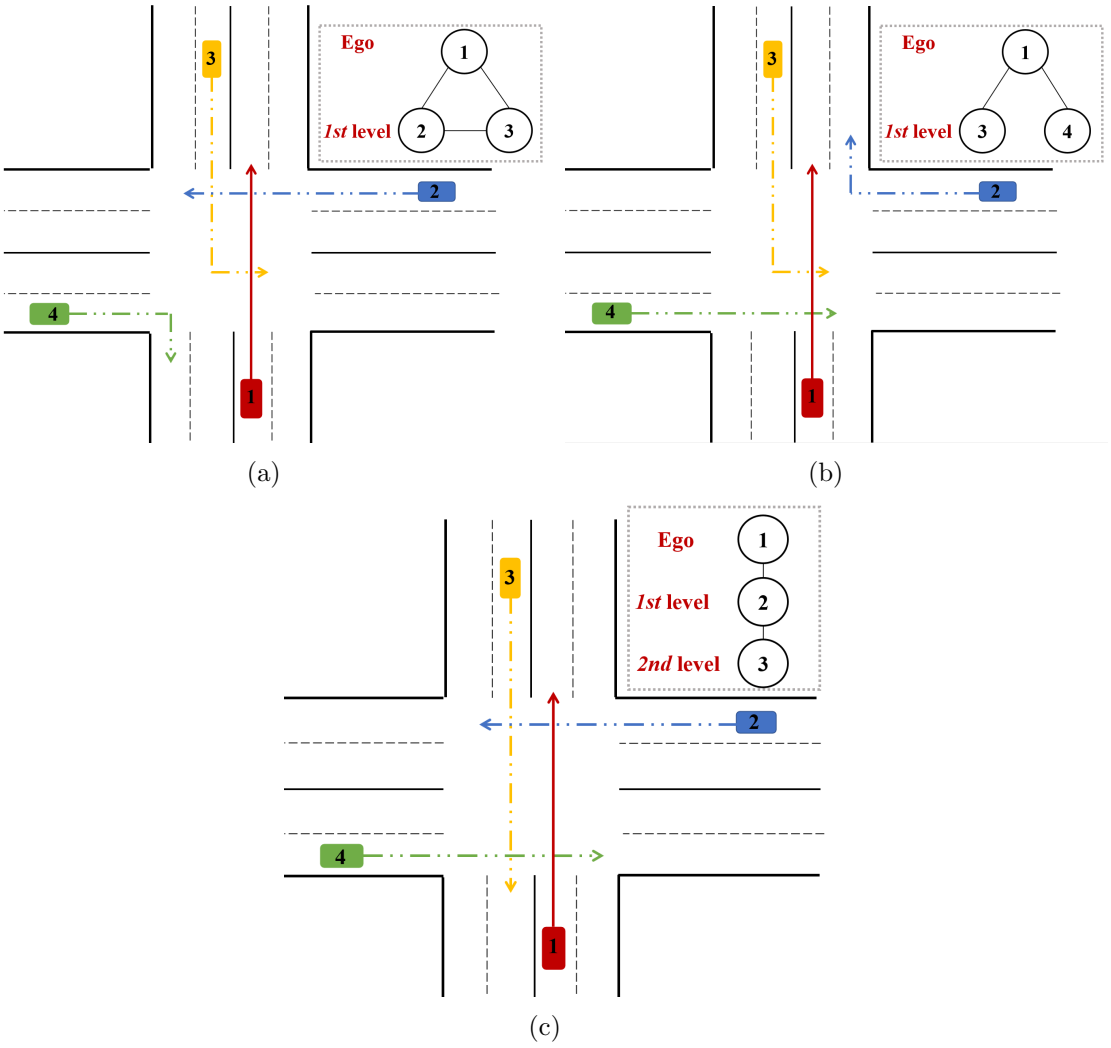

Figure 6.6: Various trajectory scenarios with corresponding interaction graphs. The ego (agent 1) has the trajectory of going straight. Agents 2 and 4 have possible trajectories of going straight and turning right. Agent 3 can go straight or turn left. In each sample trajectory scenario, the ego plays (a) a 3-player game with agents 2 and 3; (b) two 2-player games with agents 3 and 4 respectively; and (c) a 3-player game with agents 2 (cluster representative) and 3 if the first two levels of neighbors are considered.

6.3 SHG for Multiagent Decision-making

This section addresses the two challenges in the SHG, including capturing uncertain intentions with its random changing behavior using a succinct random mobility model and solving the SHG using an efficient uncertainty evaluation technique for the ego's decision-making.

6.3.1 RMM to Capture Uncertain Intentions

Specific maneuvers like acceleration and deceleration in the movements of traffic agents can reflect their high-level motion intentions, e.g., turn right, turn left, and go straight. Thus, the uncertain intentions can be captured by describing the random maneuvers of the moving agents and then mapping the specific maneuvers to intentions. In the following, we first show how to use an appropriate mobility model to characterize the traffic agents' random maneuvers.

We propose to use RMM in the SHG to capture the movement patterns of mobile agents as random switching systems. Two types of random variables are involved in the RMM [140]. Type 1 random variables describe the movement characteristics for specific maneuvers, e.g., the velocities of vehicles. Type 2 random variables describe the frequency of the switching behaviors for the type 1 random variables, e.g., how often a driver will change the velocity. In this way, the random change of maneuvers can be characterized. We leverage the RMM with continuous probability distributions to cover the maneuver variations as much as possible. Consider the velocity as the type 1 random variable, denoted by $v_i(t)$ for agent i at time t. Note that other maneuvers in the vehicular dynamics (e.g., steering angle) can be type 1 random

variables. Let T_i^k denote the kth time instant at which the agent i changes its velocity, and $0 = T_i^0 < T_i^1 < T_i^2 < \cdots$. For $v_i(t)$, we have

$$v_i(t) = \begin{cases} v_i(t^-), & if\ t \neq T_i^k,\ \forall k \in \{0, 1, 2, \cdots\} \\ v_i(T_i^k), & if\ t = T_i^k,\ \exists k \in \{0, 1, 2, \cdots\} \end{cases}, \tag{6.1}$$

when it is not time to change the velocity, i.e., $t \neq T_i^k$, agent i remains its velocity as before $v_i(t^-)$. When it is time to change the velocity, agent i obtains its new velocity $v_i(T_i^k)$ by sampling a specific probability distribution characterized by several parameters. To capture the switching behavior, we represent the type 2 random variable using the interval between two consecutive switching instants, i.e.,

$$\tau_i \left[T_i^k\right] = T_i^{k+1} - T_i^k, \tag{6.2}$$

where $\tau_i \left[T_i^k\right]$ follows a specific probability distribution characterized by several parameters. In this way, the RMM captures the temporal dependency of uncertain intentions succinctly and efficiently.

Remark 8. *The Markov chain can also capture the temporal dependency of intentions. However, the RMM is much more succinct and efficient than the Markov chain. Consider the state of an agent after T_p time steps $S[k + T_p]$ given the current state $S[k]$. In the RMM, for $\delta \in \{1, 2, \cdots, T_p\}$,*

$$S[k + \delta] = \begin{cases} S[k + \delta - 1],\ if\ \forall l \in \{0, 1, 2, \cdots\}, \delta \neq T_l \\ S[T_l],\ if\ \exists l \in \{0, 1, 2, \cdots\}, \delta = T_l \end{cases},$$

where T_l is the randomly selected lth state switching instant. The joint state space depends on the number of switches during T_p in the RMM. However, the Markov chain requires an ordered T_p-tuples of the states $(S[k], S[k + 1], \cdots, S[k + T_p - 1])$. The joint state space is the multiplication of T_p marginal state spaces and increases exponentially with T_p.

Note that the parameters in the probability distributions of the two types of random variables in the RMM can be modulated by factors such as road geometry, traffic rules, specific maneuvers, relative locations within intersection region, etc. Thus, spatial and geographic dependencies can be considered. In addition, we claim that these parameters can be estimated by, for example, training a neural network offline from data.

Given the random maneuver described by the RMM, we can indicate the uncertain intentions correspondingly. Specifically, we notice that different turning intentions often correspond to different velocity changes when a vehicle approaches an intersection. For example, compared to going straight, a vehicle that intends to turn is more likely to slow down. Moreover, the turning velocities of left- and right- turns are often different as well, due to the different turning radius. Therefore, the change of velocity can indicate a vehicle's turning intention, and such a maneuver-to-intention mapping can be learned by supervised learning from a realistic traffic dataset.

6.3.2 MPCM-OFFD to Solve SHG

We leverage the MPCM integrated with the OFFD in the proposed SHG to help the ego obtain the expected decisions efficiently and accurately in the presence of other agents' uncertain intentions.

The MPCM is a systematic design procedure to select a very limited number of simulation samples to create a low-order polynomial model that has the same mean statistics as the original model [150]. The OFFD selects a subset of experimental combinations that best estimate the main effects and low-order interaction effects [147], which can further reduce the number of the samples while maintaining the computing accuracy for the system statistics. The integration of MPCM with the statistical experimental design OFFD (i.e., MPCM-OFFD) can break the curse of

dimensionality for the uncertainty evaluation in the multiagent setting. Compared with the Monte Carlo simulation, the MPCM-OFFD is more effective and scalable for uncertainty evaluation [147]. Compared with other existing approaches in estimating the mean statistics of the system output (e.g., MPCM and stochastic response surface method), the MPCM-OFFD can achieve the best performance with the fewest number of simulation samples [148]. In addition, the MPCM-OFFD is the most robust to numerical errors for designs of the same size among the approaches [148].

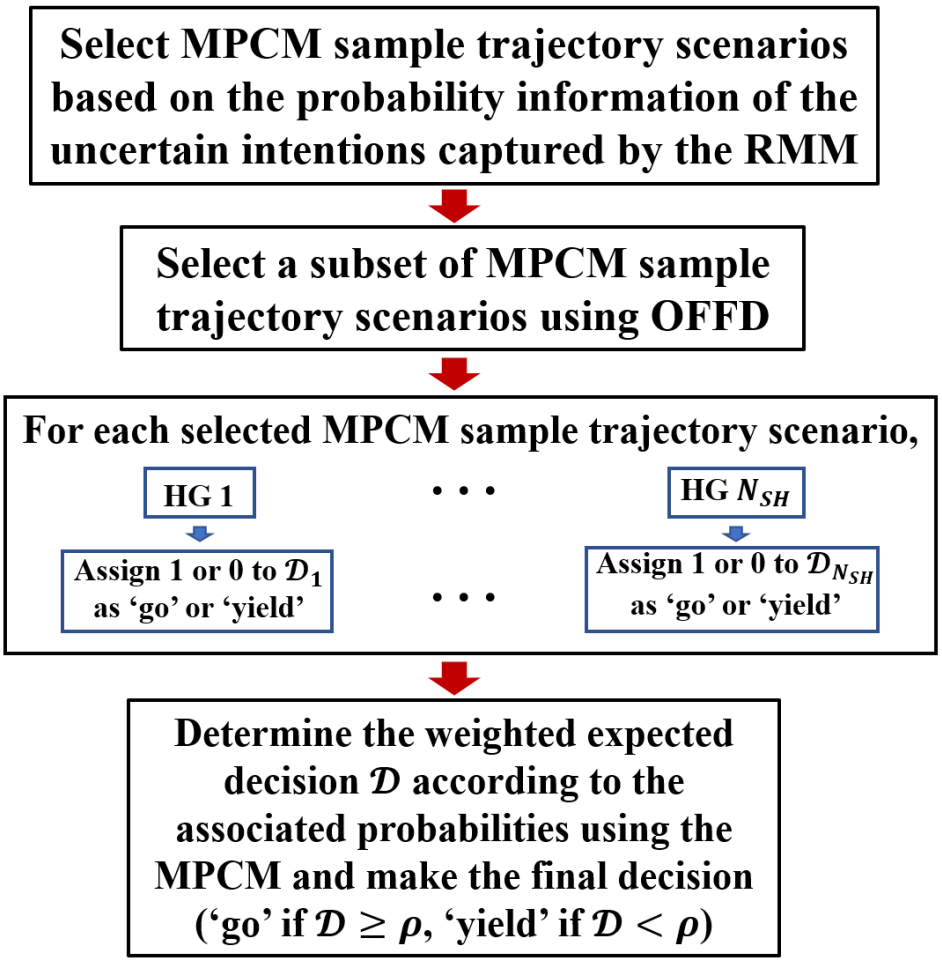

Figure 6.7: Solve the SHG by using MPCM-OFFD.

The procedure to use the MPCM-OFFD for solving the SHG efficiently is summarized in Fig. 6.7 and illustrated as follows.

1. MPCM is first used to sample a certain number of trajectory scenarios consisting of the intention-oriented trajectories of interactive agents based on the uncertain intentions captured by the RMM as described in Section 6.3.1.
2. OFFD is then applied to select a subset of the above MPCM samples to further reduce the number of sample trajectory scenarios to N_{SH}.
3. For each selected sample trajectory scenario $n \in \{1, 2, \cdots, N_{SH}\}$, the ego plays a HG as described in Section 6.2.1. A binary is assigned to the corresponding decision $\mathcal{D}_n$, in particular, '1' for 'go' and '0' for 'yield'.
4. The expected decision $\mathcal{D}$ is determined according to the associated probabilities using the MPCM. The ego makes the final decision as 'go' if $\mathcal{D} \geq \rho$ and 'yield' if $\mathcal{D} < \rho$ where $\rho \in [0, 1]$ is a predefined threshold.

Note that, the parameter ρ can be used to capture ego's decision characterization. For example, ego makes conservative decisions by choosing large ρ, but aggressive decisions using small ρ. $\rho = 1$ indicates that the ego make the final decision by selecting the most conservative solution among all individual HGs. In this case, we see that the proposed SHG provides a general solution.

6.4 Simulation Studies using Four-Vehicle Scenarios

In this section, we compare the performance of the proposed SHG which considers uncertain intentions to those of the HG in Section 6.2.1 without uncertain intentions.

Consider the traffic scenario in Fig. 6.8, where agents 2, 3, and 4 have uncertain intentions captured by the RMM. The parameters of the random variables' probability

distributions in the RMM are assumed to be known and are summarized in Table 6.1. The v_i follows a skew normal distribution with various parameters for $i \in \{2, 3, 4\}$ to imply a velocity preference of different vehicles at distinct switching instants, as shown in Fig. 6.9(a). The τ_i follows an Erlang distribution with identical parameters for $i \in \{2, 3, 4\}$ as shown in Fig 6.9(b), considering that the Erlang distribution counts the amount of time until the occurrence of a fixed number of events [151], i.e., switching the velocity here. The parameters are set as constants for simplicity. Regarding the mapping from maneuvers to intentions (i.e., velocity change to turning behavior), we assume that agents 2 and 4 will go straight if they decelerate (switch to a lower velocity) and turn right if they accelerate when approaching the intersection region and that agent 3 will go straight if it accelerates and turn left if it decelerates. In addition, the number of agents with uncertain intentions decreases over simulation time to mimic the realistic scenario where uncertainty fades away if the agents show their intention explicitly, e.g., turning on the signal light. The true intentions are going straight and going straight and turning right for agents 2, 3, and 4, respectively. For simulations using HG without uncertain intentions, vehicles' future trajectories are determined by the velocity direction at the instant when playing the game. We also let agent 2 suddenly speed up at the location marked by a purple triangle in Fig. 6.8 to test whether the developed solution can provide the ego a safe response to emergencies.

Using the MPCM, we selected two switching time instants; and at each switching instant, we selected two values for vehicle velocity, as shown in Fig. 6.9. Thus, the four most representative trajectories were obtained for each vehicle and 64-sample trajectory scenarios. Then, by applying the OFFD, we eventually selected eight sample trajectory scenarios, a significant reduction compared with 64 by using MPCM only. We see the efficiency of leveraging the MPCM-OFFD in the proposed SHG.

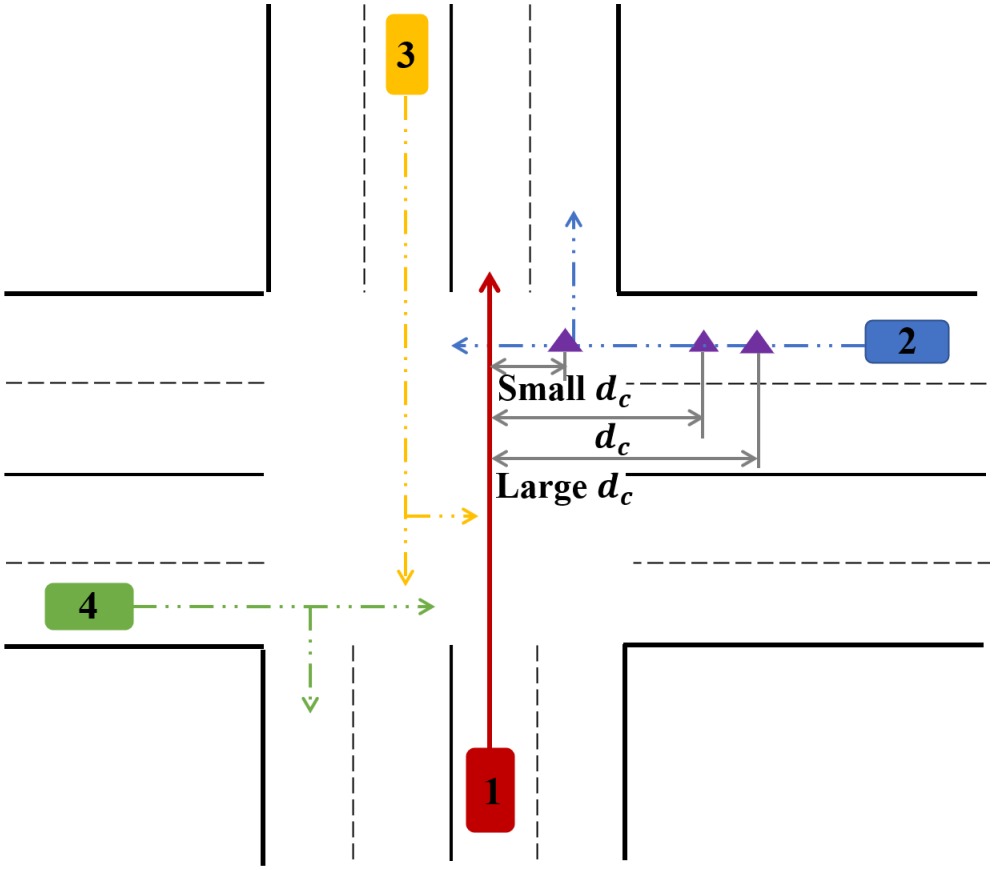

Figure 6.8: An uncontrolled intersection-crossing scenario with four agents. The arrows with solid bold line and dash lines indicate the deterministic trajectory of the ego and possible intention-oriented trajectories of the interactive agents, respectively. The purple triangle marks the position where agent 2 speeds up abruptly.

In the following subsections, we show that the developed SHG can help to reduce the frequency of repeated game play, consider a more realistic vehicle velocity profile (e.g., a slow stop maneuver for 'yield') and provide safe response to emergencies.

6.4.1 Study 1: Frequency of repeated play

Repeated game play by the ego with changing payoffs has been introduced in the decision-making process for reliable and efficient solutions [144]. It enables the ego to respond in a timely manner to traffic environment changes. Because

Table 6.1: PDFs in the RMM for Simulation Studies.

	Type 1	Type 2
PDF	$f(v_i;\xi,\omega,\eta_i^k) = \frac{2}{\omega}\phi\left(\frac{v_i-\xi}{\omega}\right)\Phi\left(\eta_i^k\left(\frac{v_i-\xi}{\omega}\right)\right)$, where $\phi(\cdot)$ and $\Phi(\cdot)$ denote the standard normal PDF and CDF, respectively. k denotes the switching time instant.	$f(\tau_i;\kappa,\lambda) = \frac{\lambda^\kappa \tau_i^{\kappa-1} e^{-\lambda\tau_i}}{(\kappa-1)!}$
Parameters	$\xi = 5, \omega = 1\ \forall\ i \in \{2,3,4\}$, $\eta_i^1 = \begin{cases} -1 & i = 2 \\ 1 & i = \{3,4\} \end{cases}$, $\eta_i^2 = \begin{cases} -4 & i = 2 \\ 4 & i = \{3,4\} \end{cases}$	$\kappa = 2, \lambda = 12\ \forall\ i \in \{2,3,4\}$

the proposed SHG leverages the RMM to capture the random changing behavior of uncertain intentions, we show that the frequency of repeated play can be reduced for SHG while the safety of the ego is guaranteed. Let Δt denote the time interval between two consecutive repeated plays in second(s) and we consider $\Delta t = 0.01s$, $0.1s$ and $1s$. The ego is assumed to conduct a sharp stop for the decision 'yield'. The results are summarized in Table 6.2, and more details are discussed as follows.

Table 6.2: Results of study 1.

	Δt	HG	SHG
Sharp stop for 'yield'	0.01s	Safe	Safe
	0.1s	Safe	Safe
	1s	Not Safe	Safe

(1) $\Delta t = 0.01s$. It can be seen in Figs. 6.10 and 6.11 that with frequent repeated play, the ego can safely cross the intersection by both HG and SHG, and the ego yields to agent 2 earlier in SHG than in HG. In addition, comparing the ego's positions at the same time instant as in Figs. 6.10(b) and 6.11(b), the ego travels

a longer distance in SHG than in HG, indicating that the decision by SHG is more efficient than that by HG.

(2) $\Delta t = 0.1s$. Increase Δt to $0.1s$ to see whether the ego can still make safe decisions with SHG and HG. As shown in Figs. 6.12 and 6.13, it is safe for the ego to cross the intersection by both SHG and HG, and the decision by SHG is more efficient than that by HG, the same observation as for $\Delta t = 0.01$s. We notice that when the ego yields to agent 2 by HG as in Fig. 6.12(a), their distance is still not very large, which can be unsafe for the ego with a slow stop for decision 'yield', discussed in the next study.

(3) $\Delta t = 1s$. Increase Δt to $1s$. As shown in Fig. 6.14, the ego cannot safely cross the intersection by HG considering its close distance to agent 2. In contrast, it shows in Fig. 6.15 that, by the SHG, the ego's safety is guaranteed with the reduced repeated play frequency.

6.4.2 Study 2: Impact of slow stop for decision 'yield'

Braking distance is critical considering limited deceleration of vehicles under realistic traffic environments. In this subsection, we show the performance of SHG and HG if the ego conducts a slow stop for its decision 'yield'. More specifically, the velocity of the ego times a coefficient of 0.5 each time for its decision as 'yield'. $\Delta t = 0.1s$. The results are summarized in Table 6.3. As shown in Fig. 6.16, using HG, the ego cannot stop completely to avoid collision with agent 2. However, with SHG, the safety of ego can still be achieved with a realistic braking maneuver. The superiority of the SHG over HG lies in that its prediction capability allows the ego to make possible responses in advance and reserves certain 'space' to avoid accidents.

Table 6.3: Results of study 2.

	Δt	HG	SHG
Slow stop for 'yield'	0.1s	Not Safe	Safe

6.4.3 Study 3: Impact of safety buffer in the payoffs

The SHG allows the ego to reserve certain space in advance for possible intention changes of interactive agents based on its prior knowledge. A safety buffer can also provide similar functionality. In this subsection, we show that the SHG cannot be replaced by a safety buffer in dealing with emergencies. A collision region (see the red shaded square in Fig. 6.17), is introduced as a safety buffer when calculating the TTC. Compared with Fig. 6.2, T_{ij}^c is calculated with a smaller relative collision distance. Note that we consider TTC with a safety buffer because it is critical in both the construction of the interaction graph and the design of payoff functions [146]. Consider a collision region with a side length of 5 meters. Let d_c denote the distance from agent 2's speed-up point to its trajectory intersecting point with the ego (see Fig. 6.8). Large d_c and small d_c (see Fig. 6.8) are applied to evaluate the performance of SHG and HG with a safety buffer in TTC in handling emergencies.

The results are summarized in Table 6.4, and additional details follow.

Table 6.4: Results of study 3.

Safety buffer in payoffs, slow stop for 'yield', $\Delta t = 0.1$s	d_c	HG	SHG
	Large	Safe	Safe
	Small	Not Safe	Safe

(1) Large d_c. As shown in Figs. 6.18 and 6.19, it is safe for the ego to cross the intersection by both HG and SHG with a safety buffer in TTC. Comparing Fig. 6.18(a) and 6.19(a), the ego yields earlier in the SHG than in HG . In addition, the

superiority of the SHG in making more efficient decisions is not observed in this case considering similar travel distance after $6s$ as in Fig. 6.18(b) and 6.19(b). With regard to a large d_c, a safety buffer can improve the ego's safety.

(2) Small d_c. As shown in Fig. 6.20, the ego cannot safely cross the intersection by the HG. The 'space' reserved by introducing a safety buffer in TTC is not enough in an HG for a small d_c. However, in the SHG, the ego yields earlier during its travel based on its prediction of the possible intention changes of agent 2 (see Fig. 6.21(a)). Thus, the ego can respond in a timely manner to the emergency (see Fig. 6.21(b)). The safety buffer has a limit in improving the safety of the ego, and the SHG cannot be replaced by a safety buffer in handling emergencies.

6.5 Conclusions

In this chapter, we proposed a novel SHG for autonomous driving, where the uncertain intentions of drivers are captured. The proposed SHG uses the RMM to capture uncertain driver intentions of random switching behavior, and uses the MPCM-OFFD to solve the SHG efficiently. Comparative simulation studies have been conducted to validate the effectiveness of the proposed SHG. Comparing the performances of the SHG to the HG that does not consider uncertain intentions, the safety of the ego is achieved with reduced repeated play frequency, realistic braking maneuver, and timely response to abrupt intention changes in emergencies.

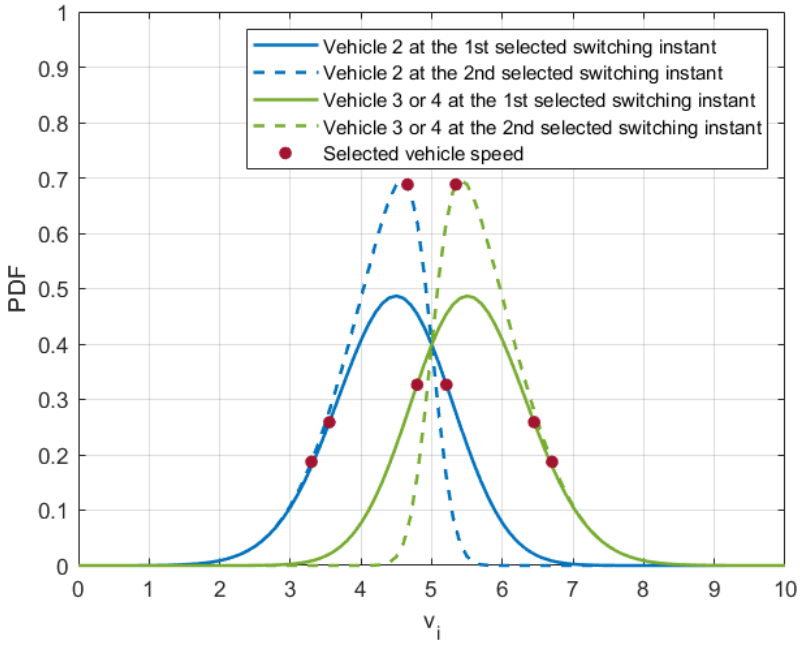

(a)

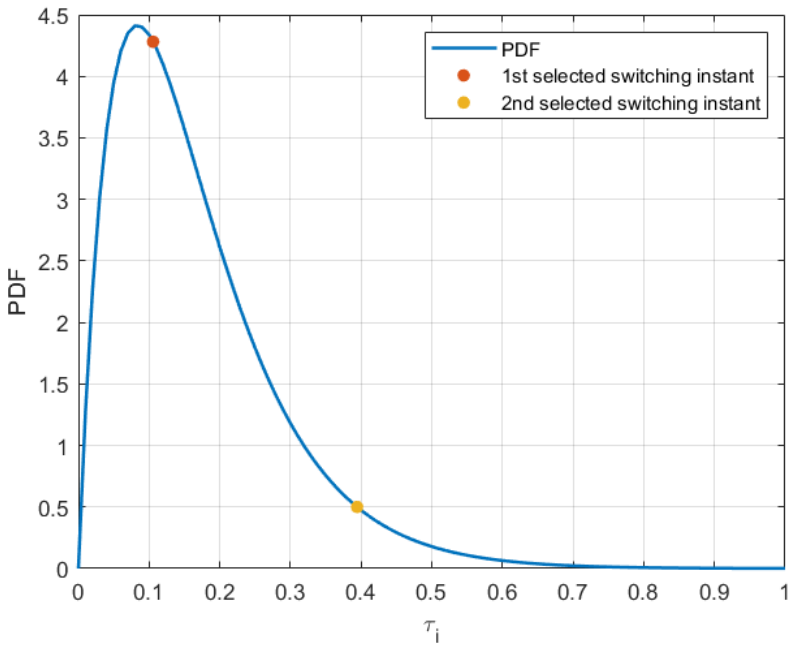

(b)

Figure 6.9: PDFs of the random variables in the RMM. (a) PDF of v_i with selected points by MPCM-OFFD. (b) PDF of τ_i with selected points by MPCM-OFFD.

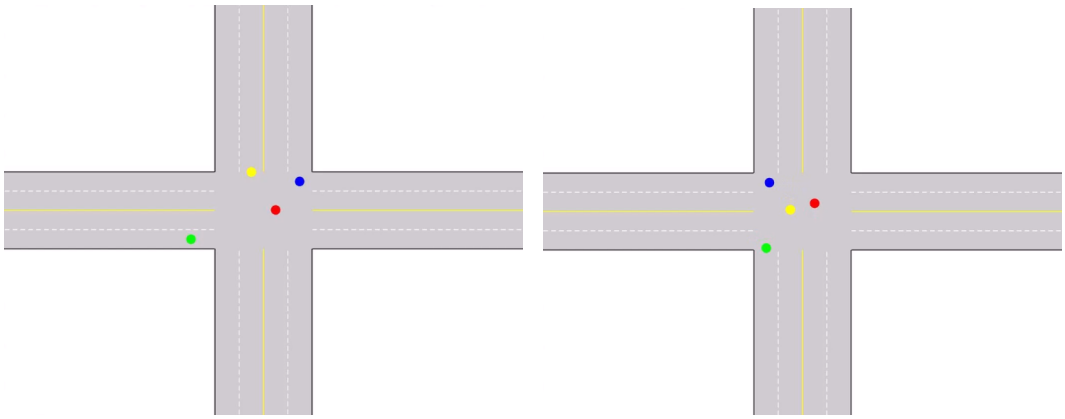

(a) (b)

Figure 6.10: The ego's decision in HG with $\Delta t = 0.01s$s. (a) At $4s$, the ego yields to agent 2. (b) At $6s$, the ego crosses the intersection safely.

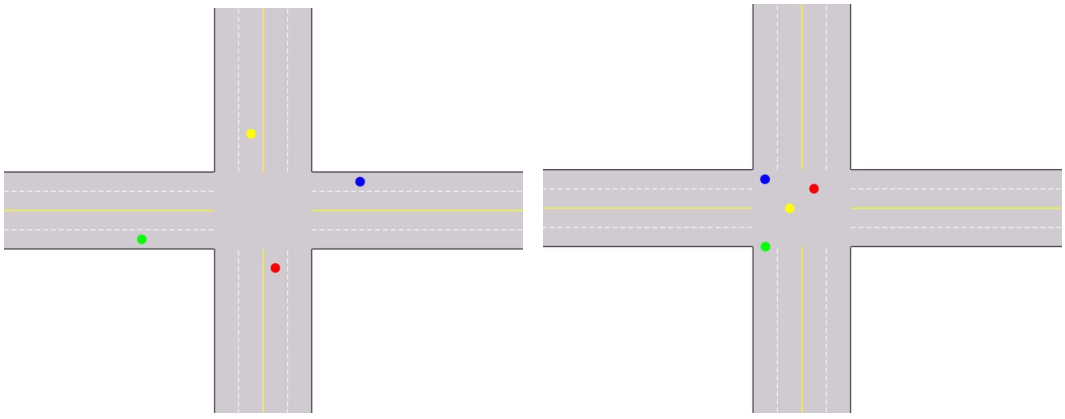

(a) (b)

Figure 6.11: The ego's decision in SHG with $\Delta t = 0.01s$. (a) At $2s$, the ego yields to agent 2. (b) At $6s$, the ego crosses the intersection safely.

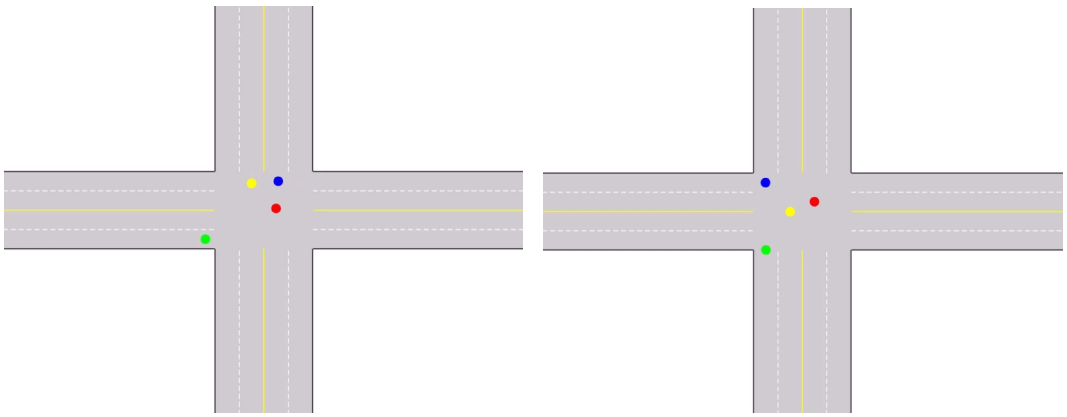

(a) (b)

Figure 6.12: The ego's decision in HG with $\Delta t = 0.1s$. (a) At $4.6s$, the ego yields to agent 2. (b) At $6s$, the ego crosses the intersection safely.

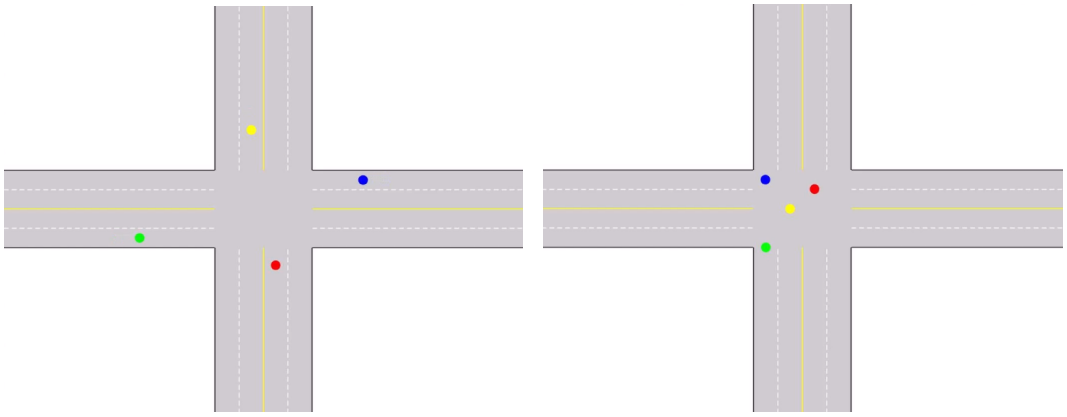

(a) (b)

Figure 6.13: The ego's decision in SHG with $\Delta t = 0.1s$. (a) At $2s$, the ego yields to agent 2. (b) At $6s$, the ego crosses the intersection safely.

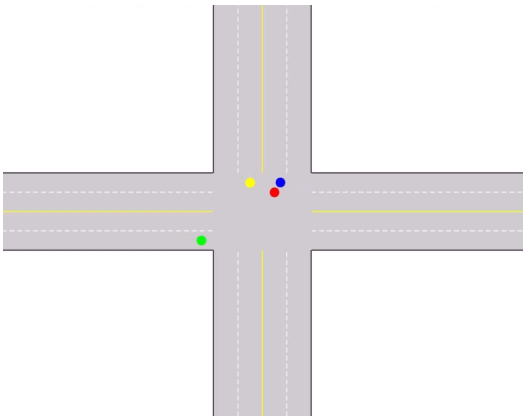

Figure 6.14: The ego's decision at $4.5s$ in HG with $\Delta t = 1s$. The ego does not yield to agent 2 in time to avoid a collision.

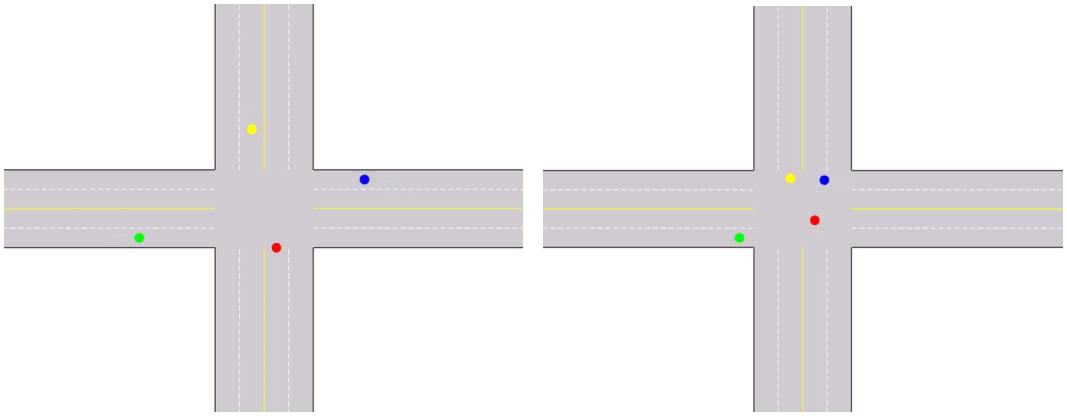

(a) (b)

Figure 6.15: The ego's decision in SHG with $\Delta t = 1s$. (a) At $2s$, the ego yields to agent 2. (b) At $4.5s$, the ego is crossing the intersection safely.

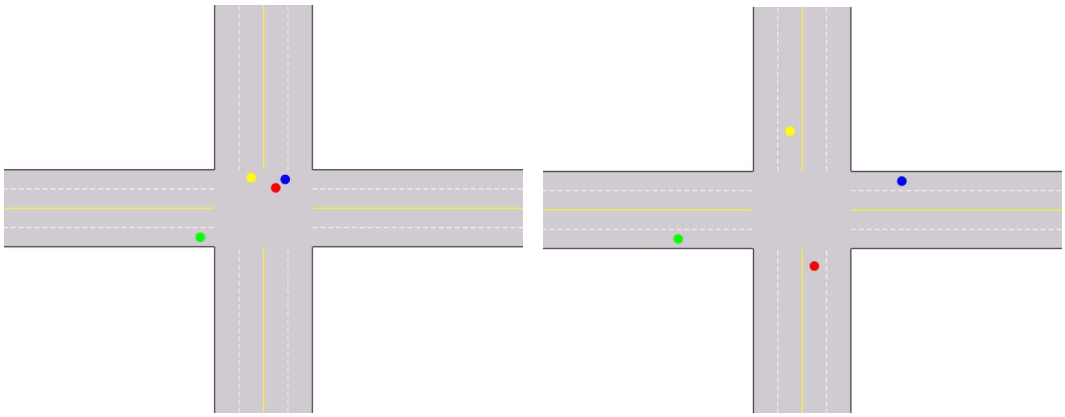

(a) (b)

Figure 6.16: The ego's decision with $\Delta t = 0.1s$ and slow stop for 'yield'. (a) By the HG, the ego yields to agent 2 with a non-zero velocity at $4.5s$ and a collision occurs. (b) By the SHG, the ego yields to agent 2 with zero velocity at $2s$.

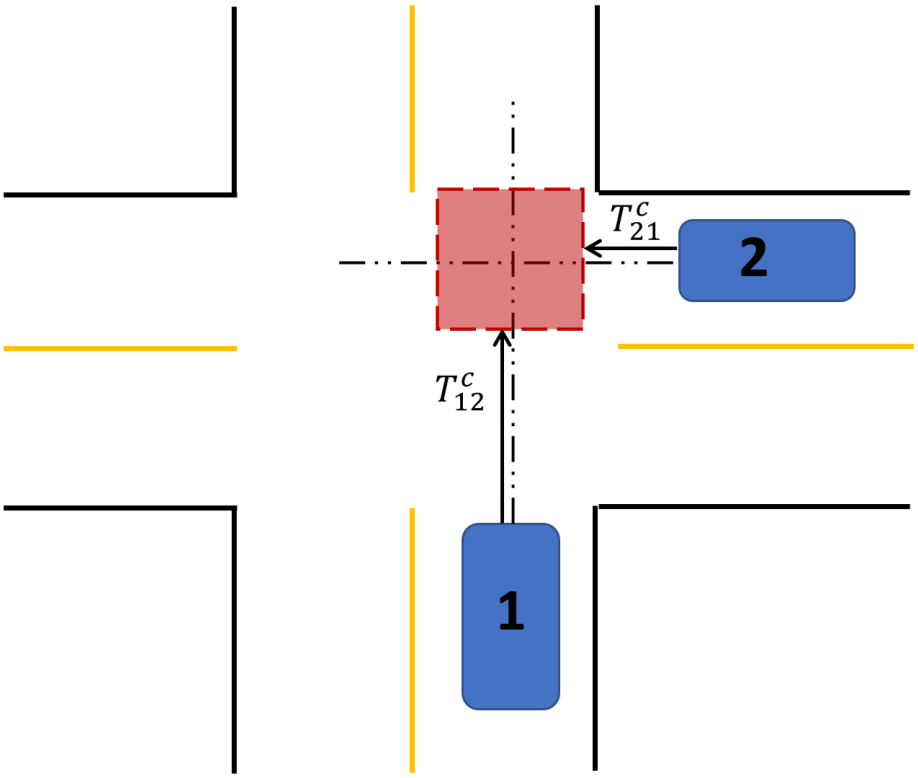

Figure 6.17: TTC with a safety buffer.

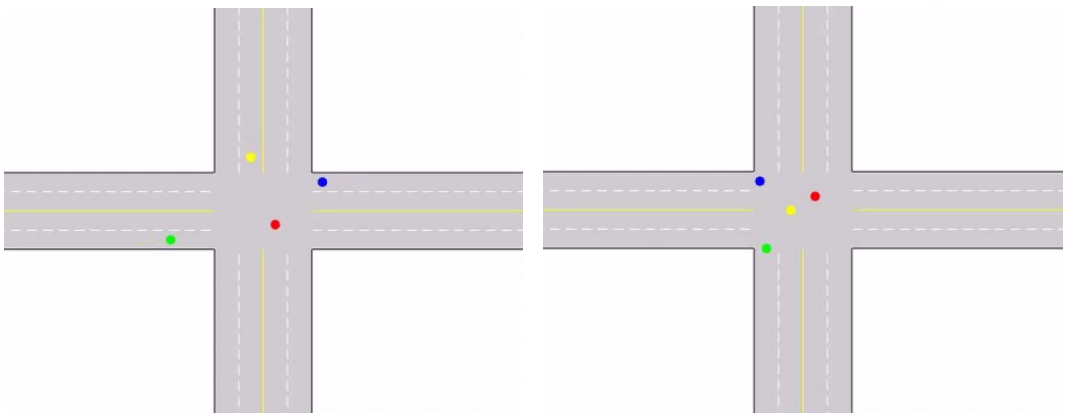

(a) (b)

Figure 6.18: The ego's decision in HG with a safety buffer in TTC for large d_c. (a) At $3.2s$, the ego yields to agent 2. (b) At $6s$, the ego crosses the intersection safely.

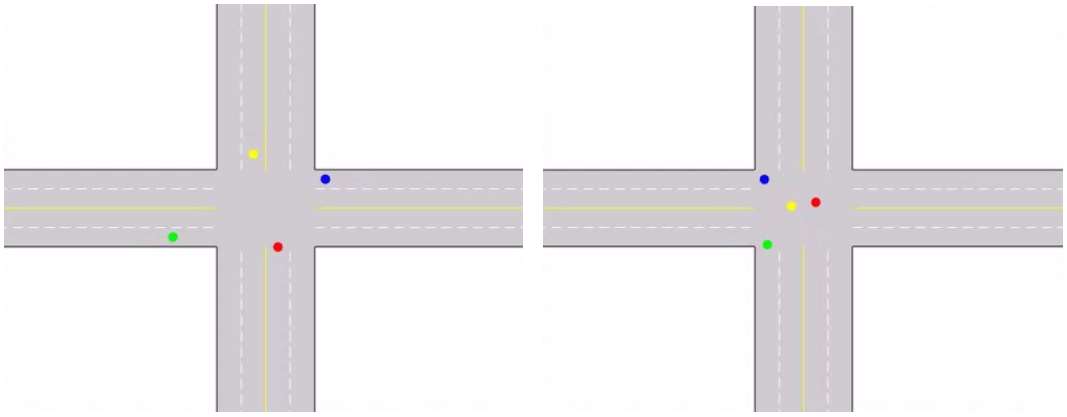

(a) (b)

Figure 6.19: The ego's decision in SHG with a safety buffer in TTC for large d_c. (a) At $3.2s$, the ego yields to agent 2. (b) At $6s$, the ego crosses the intersection safely.

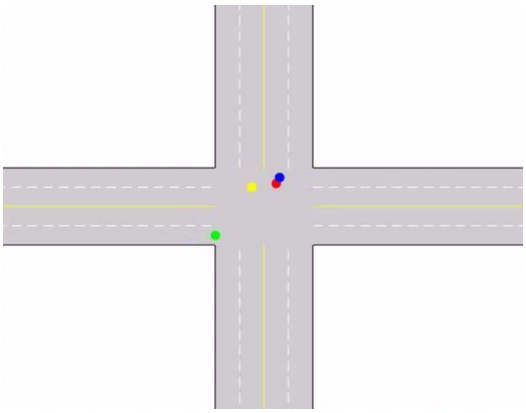

Figure 6.20: The ego's decision in HG with a safety buffer in TTC for small d_c. At $5s$, the ego yields to agent 2 by stopping completely very close to the collision point and a collision occurs.

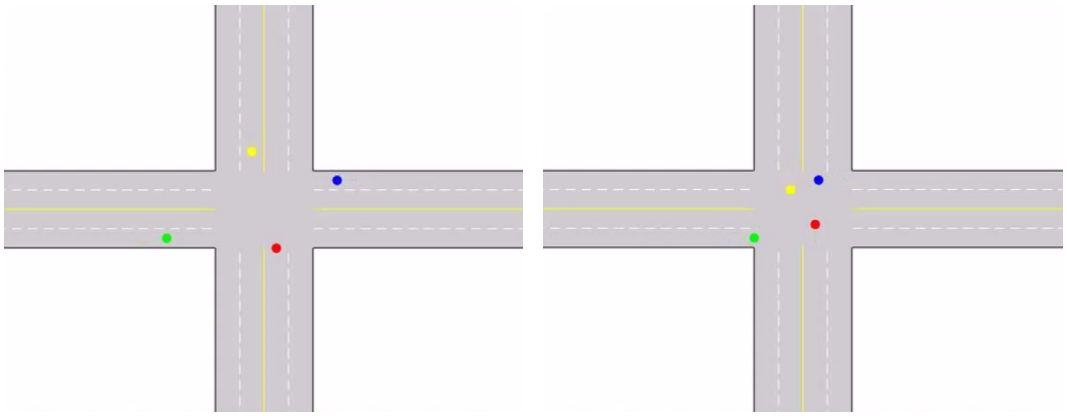

(a) (b)

Figure 6.21: The ego's decision in SHG with a safety buffer in TTC for small d_c. (a) At $3s$, the ego yields to agent 2. (b) At $5s$, the ego crosses the intersection safely.

CHAPTER 7

CONCLUSIONS AND FUTURE WORK

This dissertation addressed the challenges in the study of environment, communication and decision for MAS. First, this dissertation studied the IMs which capture the stochastic spatiotemporal environment of MAS, and provided succinct identifiability conditions and efficient estimation algorithms. Then, for sub-6 GHz V2X-assisted mmWave communication, the dissertation proposed a distributed multi-section scheduling scheme under long highway traffic to address the intra-section computational scalability issue and inter-section communication scalability issues. Finally, this dissertation developed a SHG to support safe and efficient decisions of AVs considering uncertain intentions of interactive traffic participants.

7.1 Conclusions

In Chapter 2, we studied the reduced-order estimation of IMs. For UCC-HIM, a canonical class of IM, we proved that it is identifiable. Then we constructed a reduced-order Markov chain to facilitate the estimation study. The dimension of this reduced-order Markov chain is far less than the master Markov chain and we find the one-to-one mapping between these two Markov chains. By using the proposed reduced-order Markov chain, an efficient parameter estimation algorithm is developed. Compared with the master Markov chain approach, the same accuracy is achieved but with significant reduction of computational load. Simulation studies verify efficiency of our proposed parameter estimation algorithm and demonstrate its practical value in real applications.

In Chapter 3, we took a structural approach to study the identifiability and estimation of both the homogeneous IMs and the heterogeneous IMs with reduced computation. To facilitate the identifiability analysis, we introduced the joint-margin matrix J which connects the first-order and highest-order representations of IMs. Based on J, we find that the local Markov chain transition matrices are always identifiable and their ranks determine the identifiability of the network influence matrix D. The if-and-only-if identifiability condition identified in this chapter for the homogeneous IMs is much simpler to check compared to that in [14]. For heterogeneous IMs, the if-and-only-if identifiability condition identified is the first in the literature and shows that the individual local Markov chain transition matrix determines the identifiability of the corresponding row of D. Based on the identifiability analysis, we developed the joint-margin probability based estimation (JMPE) methods for both the homogeneous IMs and heterogeneous IMs. The effectiveness of the proposed methods is validated through simulation studies. Compared to the maximum likelihood estimation and the linear algebra based estimation approaches, we find that the JMPE method retains accuracy with significantly reduced computation.

In Chapter 4, we provided new results on the estimation and identifiability of homogeneous and heterogeneous POIMs. Through exploring the joint-margin matrix J introduced in Chapter 3, we developed a POIM estimation algorithm, EM-JMPE, which includes two steps, estimating J from observations and obtaining POIM parameters from J. We also provided new identifiability conditions for POIMs by introducing the reduced-size joint-margin matrix R. In the homogeneous case, we show that the new necessary condition is tighter or at least the same as that in [14]. The necessary condition for the heterogeneous case is the first in the literature. Simulation studies demonstrate the use of the results and validate their effectiveness.

In Chapter 5, we studied the sub-6 GHz V2X-assisted mmWave link scheduling for long highway traffic. A distributed scheduling scheme was proposed. The long highway is divided into contiguous and non-overlapping sections. For each section, a head node collects mmWave link requests and determines a conflict-free transmission schedule through coordinating with other head nodes. We address both the computational challenge for individual head node to solve the scheduling problem in a section, and the communication challenge for multiple head nodes to resolve cross-section conflicts. To address the intra-section computational challenge, we developed a decomposition-based approximate solution, which leverages the spectral analysis of conflict table to decompose the scheduling problem in a section with minimal dependencies among sub-problems. Remaining dependencies are addressed through a permutation and enumeration procedure. To address the inter-section communication challenge, two coordination schemes were designed to avoid heavy control overhead for an overall conflict-free transmission schedule. The rule-based scheme uses predefined rules to eliminate conflicted links. The section-parity-based scheme groups head nodes based on the parity of their section IDs, and head nodes from two groups conduct scheduling with modified constraints in order. Both schemes are simple to implement. Simulation studies using MATLAB validated the effectiveness of the proposed distributed scheduling scheme.

In Chapter 6, we proposed a novel SHG for autonomous driving, where the uncertain intentions of drivers are captured. The proposed SHG uses the RMM to capture uncertain driver intentions of random switching behavior, and uses the MPCM-OFFD to solve the SHG efficiently. Comparative simulation studies have been conducted to validate the effectiveness of the proposed SHG. Comparing the performances of the SHG to those of the HG that does not consider uncertain inten-

tions, the safety of the ego is achieved with reduced repeated play frequency, realistic braking maneuver, and timely response to abrupt intention changes in emergencies.

7.2 Future Work

We plan to explore multiple directions in the future. First, we will study the if-and-only-if conditions for POIMs by leveraging specific classes of network topology. Second, we will investigate scheduling schemes under other practical traffic scenarios and evaluate performance using, e.g., the ns-3 simulator. Finally, we will extend the proposed SHG to other challenging traffic scenarios, e.g., multiple-lane changing.

APPENDIX A

DERIVATION OF THE FORWARD-BACKWARD ALGORITHM FOR POIM ESTIMATION

Here we provide the detailed derivation of the forward-backward algorithm in (4.12)-(4.17) in Chapter 4.

Given the definitions of $\alpha_{i_U}[k]$, $\alpha_{n_m}[k]$ and $\beta_{n_m}[k]$ in (4.12) as

$$\alpha_{i_U}[k] = P(s_U[k] = i_U, S_P[1] : S_P[k]|\phi_P),$$

$$\alpha_{n_m}[k] = P(s_n[k] = m, S_P[1] : S_P[k]|\phi_P),$$

$$\beta_{n_m}[k] = P(S_P[k+1] : S_P[T]|s_n[k] = m, S_P[k], \phi_P),$$

the corresponding recursive calculations are derived as follows.

To derive (4.13) for $\alpha_{i_U}[k]$, we have

$$\begin{aligned}
\alpha_{i_U}[k+1] &= P(s_U[k+1] = i_U, S_P[1] : S_P[k+1]|\phi_P) \\
&= P(s_U[k+1] = i_U, S_P[1] : S_P[k], S_P[k+1]|\phi_P) \\
&= \sum_{j_U=1}^{M^{|\bar{\mathcal{N}}|}} P(s_U[k] = j_U, S_P[1] : S_P[k], s_U[k+1] = i_U, S_P[k+1]|\phi_P) \\
&= \sum_{j_U=1}^{M^{|\bar{\mathcal{N}}|}} P(s_U[k] = j_U, S_P[1] : S_P[k]|\phi_P) \\
&\qquad P(s_U[k+1] = i_U, S_P[k+1]|s_U[k] = j_U, S_P[1] : S_P[k], \phi_P) \\
&= \sum_{j_U=1}^{M^{|\bar{\mathcal{N}}|}} P(s_U[k] = j_U, S_P[1] : S_P[k]|\phi_P) \\
&\qquad P(s_U[k+1] = i_U, S_P[k+1]|s_U[k] = j_U, S_P[k], \phi_P) \\
&= \sum_{j_U=1}^{M^{|\bar{\mathcal{N}}|}} \left(\alpha_{j_U}[k] \prod_{l \in \mathcal{N}} J_{l_{j,m_P}} \prod_{n \in \bar{\mathcal{N}}} J_{n_{j,m_i}} \right),
\end{aligned}$$

where m_P is the observed sites' status at $k+1$ and m_i is the unobserved sites' status corresponding to network state i. The penultimate equality holds because of the Markov property, and the last one holds because the statuses of all sites evolve independently.

To derive (4.14) for $\alpha_{n_m}[k]$, we have

$$
\begin{aligned}
\alpha_{n_m}[k+1] &= P(s_n[k+1]=m, S_P[1]:S_P[k+1]|\phi_P) \\
&= P(s_n[k+1]=m, S_P[1]:S_P[k], S_P[k+1]|\phi_P) \\
&= \sum_{q=1}^{M} P(s_n[k]=q, s_n[k+1]=m, S_P[1]:S_P[k], S_P[k+1]|\phi_P) \\
&= \sum_{q=1}^{M} P(s_n[k]=q, S_P[1]:S_P[k]|\phi_P) \\
&\qquad P(s_n[k+1]=m, S_P[k+1]|s_n[k]=q, S_P[1]:S_P[k], \phi_P) \\
&= \sum_{q=1}^{M} P(s_n[k]=q, S_P[1]:S_P[k]|\phi_P) P(s_n[k+1]=m, S_P[k+1]|s_n[k]=q, S_P[k], \phi_P) \\
&= \sum_{q=1}^{M} P(s_n[k]=q, S_P[1]:S_P[k]|\phi_P) \\
&\qquad P(s_n[k+1]=m|s_n[k]=q, S_P[k], \phi_P) P(S_P[k+1]|s_n[k]=q, S_P[k], \phi_P) \\
&= \sum_{q=1}^{M} \left(\alpha_{n_q}[k] \left(\frac{\sum_{j_q} J_{n_{j_q,m}}}{M^{|\bar{\mathcal{N}}|-1}} \right) \prod_{l\in\mathcal{N}} \left(\frac{\sum_{j_q} J_{l_{j_q,m_P}}}{M^{|\bar{\mathcal{N}}|-1}} \right) \right) \\
&= \sum_{q=1}^{M} \left(\frac{\alpha_{n_q}[k]}{M^{(|\bar{\mathcal{N}}|-1)(|\mathcal{N}|+1)}} \left(\sum_{j_q} J_{n_{j_q,m}} \right) \prod_{l\in\mathcal{N}} \left(\sum_{j_q} J_{l_{j_q,m_P}} \right) \right),
\end{aligned}
$$

where j_q is the network state with site n's status as q at k and the corresponding observed states as m_P. The fifth and sixth equalities hold due to the Markov property and independent evolution of all sites' statuses respectively. In the penultimate equality, the conditional probabilities are scaled by $\frac{1}{M^{|\bar{\mathcal{N}}|-1}}$ because only site n's status and the observed states are concerned in the condition.

Similarly, to derive (4.15) for $\beta_{n_m}[k]$, we have

$$\begin{aligned}
\beta_{n_m}[k] &= P(S_P[k+1]:S_P[T]|s_n[k]=m,S_P[k],\phi_P)\\
&= P(S_P[k+1],S_P[k+2]:S_P[T]|s_n[k]=m,S_P[k],\phi_P)\\
&= \sum_{q=1}^{M} P(s_n[k+1]=q,S_P[k+1],S_P[k+2]:S_P[T]|s_n[k]=m,S_P[k],\phi_P)\\
&= \sum_{q=1}^{M} P(s_n[k+1]=q,S_P[k+1]|s_n[k]=m,S_P[k],\phi_P)\\
&\qquad P(S_P[k+2]:S_P[T]|s_n[k+1]=q,S_P[k+1],s_n[k]=m,S_P[k],\phi_P)\\
&= \sum_{q=1}^{M} P(s_n[k+1]=q,S_P[k+1]|s_n[k]=m,S_P[k],\phi_P)\\
&\qquad P(S_P[k+2]:S_P[T]|s_n[k+1]=q,S_P[k+1],\phi_P)\\
&= \sum_{q=1}^{M} P(s_n[k+1]=q|s_n[k]=m,S_P[k],\phi_P)P(S_P[k+1]|s_n[k]=m,S_P[k],\phi_P)\\
&\qquad P(S_P[k+2]:S_P[T]|s_n[k+1]=q,S_P[k+1],\phi_P)\\
&= \sum_{q=1}^{M}\left(\left(\frac{\sum_{j_m} J_{n_{j_m},q}}{M^{|\bar{\mathcal{N}}|-1}}\right)\prod_{l\in\mathcal{N}}\left(\frac{\sum_{j_m} J_{l_{j_m},m_P}}{M^{|\bar{\mathcal{N}}|-1}}\right)\beta_{n_q}[k+1]\right)\\
&= \sum_{q=1}^{M}\left(\frac{\beta_{n_q}[k+1]}{M^{(|\bar{\mathcal{N}}|-1)(|\mathcal{N}|+1)}}\left(\sum_{j_m} J_{n_{j_m},q}\right)\prod_{l\in\mathcal{N}}\left(\sum_{j_m} J_{l_{j_m},m_P}\right)\right).
\end{aligned}$$

Given $\alpha_{n_m}[k]$ and $\beta_{n_m}[k]$, the following probabilities can be obtained as

$$\begin{aligned}
\alpha_{n_m}[k]\beta_{n_m}[k] &= P(s_n[k]=m,S_P[1]:S_P[k]|\phi_P)P(S_P[k+1]:S_P[T]|s_n[k]=m,S_P[k],\phi_P)\\
&= P(s_n[k]=m,S_P[1]:S_P[k]|\phi_P)P(S_P[k+1]:S_P[T]|s_n[k]=m,S_P[1]:S_P[k],\phi_P)\\
&= P(s_n[k]=m,S_P[1]:S_P[k],S_P[k+1]:S_P[T]|\phi_P)\\
&= P(s_n[k]=m,Y_P|\phi_P),\\
P(Y_P|\phi_P) &= \sum_{m=1}^{M} P(s_n[k]=m,Y_P|\phi_P) = \sum_{m=1}^{M}\alpha_{n_m}[k]\beta_{n_m}[k].
\end{aligned}$$

Note that any unobserved site n in the network can be used to calculate $P(Y_P|\phi_P)$. Thus, $\chi_i[k]$ in (4.16) is derived as

$$\chi_i[k] = P(s[k]=i|Y_P,\phi_P) = P(s_U[k]=i_U|Y_P,\phi_P) = \prod_{n\in\bar{\mathcal{N}}} P(s_n[k]=m_i|Y_P,\phi_P)$$
$$= \prod_{n\in\bar{\mathcal{N}}}\left(\frac{P(s_n[k]=m_i,Y_P|\phi_P)}{P(Y_P|\phi_P)}\right) = \prod_{n\in\bar{\mathcal{N}}}\left(\frac{\alpha_{n_{m_i}}[k]\beta_{n_{m_i}}[k]}{\sum_{q=1}^{M}\alpha_{l_q}[k]\beta_{l_q}[k]}\right),$$

where l_q in the denominator indicates that site l has local status as q and l here can be any unobserved sites in the network.

Because $\xi_{n_{i,m}}[k]$ is defined for all sites in the network, in the following, we show the derivation of $\xi_{n_{i,m}}[k]$ for observed and unobserved sites respectively. For observed site $n\in\mathcal{N}$, $\xi_{n_{i,m}}[k]$ can be expressed as

$$\xi_{n_{i,m}}[k] = P(s[k]=i,s_n[k+1]=m|Y_P,\phi_P) = \begin{cases} 0, & if\ s_n[k+1]\neq m \\ P(s[k]=i|Y_P,\phi_P)=\chi_i[k], & if\ s_n[k+1]=m \end{cases}.$$

For unobserved site $n\in\bar{\mathcal{N}}$, $\xi_{n_{i,m}}[k]$ can be expressed as

$$\begin{aligned}
\xi_{n_{i,m}}[k] &= P(s[k]=i,s_n[k+1]=m|Y_P,\phi_P) = P(s_U[k]=i_U,s_n[k+1]=m|Y_P,\phi_P)\\
&= \frac{P(s_U[k]=i_U,s_n[k+1]=m,Y_P|\phi_P)}{P(Y_P|\phi_P)}\\
&= \frac{P(s_U[k]=i_U,s_n[k+1]=m,S_P[1]:S_P[k],S_P[k+1],S_P[k+2]:S_P[T]|\phi_P)}{P(Y_P|\phi_P)}\\
&= \frac{1}{P(Y_P|\phi_P)}\big(P(s_U[k]=i_U,S_P[1]:S_P[k]|\phi_P)\\
&\qquad P(s_n[k+1]=m,S_P[k+1]|s_U[k]=i_U,S_P[1]:S_P[k],\phi_P)\\
&\qquad P(S_P[k+2]:S_P[T]|s_n[k+1]=m,S_P[k+1],s_U[k]=i_U,S_P[1]:S_P[k],\phi_P)\big)\\
&= \frac{1}{P(Y_P|\phi_P)}\big(P(s_U[k]=i_U,S_P[1]:S_P[k]|\phi_P)\\
&\qquad P(s_n[k+1]=m,S_P[k+1]|s_U[k]=i_U,S_P[k],\phi_P)\\
&\qquad P(S_P[k+2]:S_P[T]|s_n[k+1]=m,S_P[k+1],\phi_P)\big)\\
&= \frac{\alpha_{i_U}[k]J_{n_{i,m}}\prod_{l\in\mathcal{N}}J_{l_{i,m_P}}\beta_{n_m}[k+1]}{\sum_{q=1}^{M}\alpha_{l_q}[k]\beta_{l_q}[k]}.
\end{aligned}$$

Combining above two cases for $\xi_{n_{i,m}}[k]$, we get (4.17).

REFERENCES

[1] J. Hu, P. Bhowmick, I. Jang, F. Arvin, and A. Lanzon, "A decentralized cluster formation containment framework for multirobot systems," *IEEE Transactions on Robotics*, vol. 37, no. 6, pp. 1936–1955, 2021.

[2] S. Jo, L. Gao, F. Liu, M. Li, Z. Shen, L. Xu, and Z.-Y. Gao, "Cascading failure with preferential redistribution on bus–subway coupled network," *International Journal of Modern Physics C*, vol. 32, no. 08, p. 2150103, 2021.

[3] U. Nakarmi, "Reliability analysis of power grids and its interdependent infrastructures: An interaction graph-based approach," Ph.D. dissertation, University of South Florida, 2020.

[4] C. C. Aggarwal and T. Abdelzaher, "Social sensing," in *Managing and mining sensor data*. Springer, Boston, MA, 2013, pp. 237–297.

[5] A. R. Hota, J. Godbole, and P. E. Paré, "A closed-loop framework for inference, prediction, and control of SIR epidemics on networks," *IEEE Transactions on Network Science and Engineering*, vol. 8, no. 3, pp. 2262–2278, 2021.

[6] P. Valckenaers, J. Sauter, C. Sierra, and J. A. Rodriguez-Aguilar, "Applications and environments for multi-agent systems," *Autonomous Agents and Multi-Agent Systems*, vol. 14, pp. 61–85, 2007.

[7] K. Li, Q. Liu, and Z. Zeng, "Quantized event-triggered communication based multi-agent system for distributed resource allocation optimization," *Information Sciences*, vol. 577, pp. 336–352, 2021.

[8] K. Muhammad, A. Ullah, J. Lloret, J. D. Ser, and V. H. C. de Albuquerque, "Deep learning for safe autonomous driving: Current challenges and future

directions," *IEEE Transactions on Intelligent Transportation Systems*, vol. 22, no. 7, pp. 4316–4336, 2021.

[9] A. L. Dimeas and N. D. Hatziargyriou, "Multi-agent reinforcement learning for microgrids," in *IEEE PES general meeting*. IEEE, 2010, pp. 1–8.

[10] M. Egorov, "Multi-agent deep reinforcement learning," *CS231n: convolutional neural networks for visual recognition*, pp. 1–8, 2016.

[11] X. Tan, J. Cao, X. Li, and A. Alsaedi, "Leader-following mean square consensus of stochastic multi-agent systems with input delay via event-triggered control," *IET Control Theory & Applications*, vol. 12, no. 2, pp. 299–309, 2018.

[12] Y. Zhou, Y. Wan, S. Roy, C. Taylor, and C. Wanke, "A stochastic modeling and analysis approach to strategic traffic flow management under weather uncertainty," in *Proceedings of AIAA Guidance, Navigation, and Control Conference*, Portland, OR, USA, August 2011, p. 6514.

[13] M. Rahnamay-Naeini, "Designing cascade-resilient interdependent networks by optimum allocation of interdependencies," in *Proceedings of 2016 International Conference on Computing, Networking and Communications (ICNC)*, Kauai, Hawaii, USA, February 2016, pp. 1–7.

[14] C. He, Y. Wan, and F. L. Lewis, "On the identifiability of the influence model for stochastic spatiotemporal spread processes," *IEEE Transactions on Systems, Man, and Cybernetics: Systems*, vol. 51, no. 6, pp. 3876–3888, 2020.

[15] A. K. Jammalamadaka, "Aspects of inference for the influence model and related graphical models," Ph.D. dissertation, Massachusetts Institute of Technology, 2004.

[16] T. K. Choudhury, "Sensing and modeling human networks," Ph.D. dissertation, Massachusetts Institute of Technology, 2004.

[17] W. Dong, "Influence modeling of complex stochastic processes," Master's thesis, Massachusetts Institute of Technology, 2006.

[18] Y.-C. Chen, "Statistical inference with local optima," *Journal of the American Statistical Association*, pp. 1–13, 2022.

[19] X. Wu, D. Wu, and E. Modiano, "An influence model approach to failure cascade prediction in large scale power systems," in *Proceedings of 2020 American Control Conference (ACC)*, Online, July 2020, pp. 4981–4988.

[20] Y. Li, P. Luo, and P. Pin, "Utility-based model for characterizing the evolution of social networks," *IEEE Transactions on Systems, Man, and Cybernetics: Systems*, vol. 50, no. 3, pp. 1083–1094, 2020.

[21] R. Rabovič and P. Čížek, "Estimation of spatial sample selection models: A partial maximum likelihood approach," *Journal of Econometrics*, vol. 232, no. 1, pp. 214–243, 2023.

[22] E. Moradi-Pari, D. Tian, M. Bahramgiri, S. Rajab, and S. Bai, "DSRC versus LTE-V2X: Empirical performance analysis of direct vehicular communication technologies," *IEEE Transactions on Intelligent Transportation Systems*, vol. 24, no. 5, pp. 4889–4903, 2023.

[23] S. Lee, Y. Jung, Y.-H. Park, and S.-W. Kim, "Design of V2X-based vehicular contents centric networks for autonomous driving," *IEEE Transactions on Intelligent Transportation Systems*, vol. 23, no. 8, pp. 13 526–13 537, 2022.

[24] F. Granda, L. Azpilicueta, M. Celaya-Echarri, P. Lopez-Iturri, C. Vargas-Rosales, and F. Falcone, "Spatial V2X traffic density channel characterization for urban environments," *IEEE Transactions on Intelligent Transportation Systems*, vol. 22, no. 5, pp. 2761–2774, 2021.

[25] 3GPP Std., "Study on enhancement of 3GPP support for 5G V2X services (Release 16)," https://www.3gpp.org/ftp//Specs/archive/22_series/22.886/22886-g20.zip, December 2018.

[26] IEEE, "IEEE 802.11-19-1342/r1: 11bd TG Use Cases," https://mentor.ieee.org/802.11/dcn/19/11-19-1342-01-00bd-11bd-use-cases.pptx, July 2019.

[27] B. Coll-Perales, J. Gozalvez, and M. Gruteser, "Sub-6GHz assisted MAC for millimeter wave vehicular communications," *IEEE Communications Magazine*, vol. 57, no. 3, pp. 125–131, 2019.

[28] A. Molina-Galan, B. Coll-Perales, and J. Gozalvez, "C-V2X assisted mmWave V2V scheduling," in *2019 IEEE 2nd Connected and Automated Vehicles Symposium (CAVS)*. IEEE, 2019, pp. 1–5.

[29] C. He, Y. Wan, L. Zhao, H. Lu, and T. Shimizu, "Sub-6 GHz V2X-assisted synchronous millimeter wave scheduler for vehicle-to-vehicle communications," *IEEE Transactions on Vehicular Technology*, vol. 71, no. 11, pp. 11 717–11 728, 2022.

[30] C. He, L. Zhao, Y. Wan, H. Lu, and T. Shimizu, "Sub-6 GHz V2X-assisted mmWave optimal scheduling for vehicular networks," *Vehicular Communications*, vol. 41, p. 100610, 2023.

[31] H.-S. Lee and J.-W. Lee, "QoS and channel-aware distributed link scheduling for D2D communication," in *2016 14th International Symposium on Modeling and Optimization in Mobile, Ad Hoc, and Wireless Networks (WiOpt)*. IEEE, 2016, pp. 1–8.

[32] R. Talak, S. Karaman, and E. Modiano, "Distributed scheduling algorithms for optimizing information freshness in wireless networks," in *2018 IEEE 19th International Workshop on Signal Processing Advances in Wireless Communications (SPAWC)*. IEEE, 2018, pp. 1–5.

[33] L. Xiaoyang, D. Enqing, Q. Fulong, and C. Bo, "Vertex coloring based distributed link scheduling for wireless sensor networks," in *2012 18th Asia-Pacific Conference on Communications (APCC)*. IEEE, 2012, pp. 754–759.

[34] Y. Fu, Y. Hou, Z. Wang, X. Wu, K. Gao, and L. Wang, "Distributed scheduling problems in intelligent manufacturing systems," *Tsinghua Science and Technology*, vol. 26, no. 5, pp. 625–645, 2021.

[35] A. Karimi, K. I. Pedersen, N. H. Mahmood, J. Steiner, and P. Mogensen, "5G centralized multi-cell scheduling for URLLC: Algorithms and system-level performance," *IEEE Access*, vol. 6, pp. 72 253–72 262, 2018.

[36] S. Bayhan and F. Alagoz, "Scheduling in centralized cognitive radio networks for energy efficiency," *IEEE Transactions on Vehicular Technology*, vol. 62, no. 2, pp. 582–595, 2013.

[37] A. Liu, G. Shi, S.-J. Chung, A. Anandkumar, and Y. Yue, "Robust regression for safe exploration in control," in *Proceedings of 2nd Learning for Dynamics & Control Conference (L4DC)*. PMLR, 2020, pp. 608–619.

[38] D. Fridovich-Keil, A. Bajcsy, J. F. Fisac, S. L. Herbert, S. Wang, A. D. Dragan, and C. J. Tomlin, "Confidence-aware motion prediction for real-time collision avoidance1," *The International Journal of Robotics Research*, vol. 39, no. 2-3, pp. 250–265, 2020.

[39] D. D. Fan, A.-a. Agha-mohammadi, and E. A. Theodorou, "Deep learning tubes for tube MPC," *arXiv preprint arXiv:2002.01587*, 2020.

[40] R. Cheng, R. M. Murray, and J. W. Burdick, "Limits of probabilistic safety guarantees when considering human uncertainty," in *Proceedings of 2021 IEEE International Conference on Robotics and Automation (ICRA)*. IEEE, 2021, pp. 3182–3189.

[41] N. Li, Y. Yao, I. Kolmanovsky, E. Atkins, and A. R. Girard, "Game-theoretic modeling of multi-vehicle interactions at uncontrolled intersections," *IEEE Transactions on Intelligent Transportation Systems*, vol. 23, no. 2, pp. 1428–1442, 2020.

[42] B. M. Albaba and Y. Yildiz, "Driver modeling through deep reinforcement learning and behavioral game theory," *IEEE Transactions on Control Systems Technology*, vol. 30, no. 2, pp. 885–892, 2021.

[43] M. Liu, Y. Wan, F. L. Lewis, S. Nageshrao, and D. Filev, "A three-level game-theoretic decision-making framework for autonomous vehicles," *IEEE Transactions on Intelligent Transportation Systems*, vol. 23, no. 11, pp. 20 298–20 308, 2022.

[44] J. C. Harsanyi, "Games with incomplete information played by "Bayesian" players, I–III Part I. The basic model," *Management science*, vol. 14, no. 3, pp. 159–182, 1967.

[45] L. Zhao, C. He, and Y. Wan, "Reduced-order estimation of the uniform completely connected homogeneous influence model (UCC-HIM)," *IEEE Control Systems Letters*, vol. 5, no. 6, pp. 2186–2191, 2021.

[46] L. Zhao, Y. Wan, C. He, and F. L. Lewis, "Structural analysis of the stochastic influence model for identifiability and reduced-order estimation," *submitted to IEEE Transactions on Systems, Man, and Cybernetics: Systems*, 2023.

[47] L. Zhao and Y. Wan, "Identifiability and estimation of partially observed influence models," *IEEE Control Systems Letters*, vol. 6, pp. 3385–3390, 2022.

[48] L. Zhao, C. He, Y. Wan, H. Lu, and T. Shimizu, "Distributed scheduling scheme for Sub-6 GHz V2X-assisted mmWave communication under long highway traffic," *to submit to IEEE Transactions on Intelligent Transportation Systems*, 2023.

[49] L. Zhao, Y. Wan, F. L. Lewis, S. Nageshrao, and H. E. Tseng, "Stochastic hierarchical game (SHG) for multiagent autonomous driving," *to submit to IEEE Intelligent Transportation Systems Magazine*, 2023.

[50] C. He, Z. Zhang, Y. Wan, L. Zhao, H. Lu, and T. Shimizu, "An efficient Sub-6 GHz assisted millimeter wave V2X communication scheduler," *submitted to IEEE Transactions on Vehicular Technology*, 2023.

[51] M. Deniz, L. Zhao, Y. Wan, and F. L. Lewis, "Game-theoretic decision-making and payoff design for UAV collision avoidance in a 3-dimensional airspace," *Submitted to Unmanned Systems*, 2023.

[52] L. Zhao, C. He, and Y. Wan, "Reduced-order estimation of the uniform completely connected homogeneous influence model (UCC-HIM)," *IEEE Control Systems Letters*, vol. 5, no. 6, pp. 2186–2191, 2021.

[53] C. Asavathiratham, "The influence model: A tractable representation for the dynamics of networked markov chains," Ph.D. dissertation, Massachusetts Institute of Technology, 2001.

[54] C. Asavathiratham, S. Roy, B. Lesieutre, and G. Verghese, "The influence model," *IEEE Control Systems Magazine*, vol. 21, no. 6, pp. 52–64, 2001.

[55] Y. Wan, S. Roy, A. Saberi, and B. Lesieutre, "A flexible stochastic automaton-based algorithm for network self-partitioning," *International Journal of Distributed Sensor Networks*, vol. 4, no. 3, pp. 223–246, 2008.

[56] M. Garetto, W. Gong, and D. Towsley, "Modeling malware spreading dynamics," in *Proceedings of IEEE INFOCOM 2003. Twenty-second Annual Joint Conference of the IEEE Computer and Communications Societies (IEEE Cat. No. 03CH37428)*, vol. 3, San Francisco, CA, USA, April 2003, pp. 1869–1879.

[57] C. He and Y. Wan, "Clustering stochastic weather scenarios using influence model-based distance measures," in *Proceedings of AIAA Aviation 2019 Forum*, Dallas, TX, June 2019.

[58] C. He, Y. Wan, and F. L. Lewis, "On the identifiability of the influence model for stochastic spatiotemporal spread processes," *IEEE Transactions on Systems, Man, and Cybernetics: Systems*, pp. 1–13, 2020, doi: 10.1109/TSMC.2019.2946856.

[59] S. Gramatikov, D. Trajanov, L. Kocarev, and A. Grnarov, "Network topology impact on influence spreading," *Novel Algorithms and Techniques in Telecommunications and Networking*, pp. 379–384, 2010.

[60] Y. Wan, S. Roy, and A. Saberi, "Designing spatially heterogeneous strategies for control of virus spread," *IET Systems Biology*, vol. 2, no. 4, pp. 184–201, 2008.

[61] Y. Wan, J. Yan, Z. Lin, V. Sheth, and S. K. Das, "On the structural perspective of computational effectiveness for quantized consensus in layered uav networks," *IEEE Transactions on Control of Network Systems*, vol. 6, no. 1, pp. 276–288, 2018.

[62] F. Allen and D. Gale, "Financial contagion," *Journal of political economy*, vol. 108, no. 1, pp. 1–33, 2000.

[63] O. Sen and S. Sen, "Effects of social network topology and options on norm emergence," in *International Workshop on Coordination, Organizations, Institutions, and Norms in Agent Systems*, Springer, Berlin, Heidelberg, May 2009.

[64] Z. H. Mir and Y.-B. Ko, "A topology management framework for wireless sensor networks via power control," in *IEEE INFOCOM Workshops 2008*, Phoenix, AZ, April 2008.

[65] S. Wuchty, Z. N. Oltvai, and A.-L. Barabási, "Evolutionary conservation of motif constituents in the yeast protein interaction network," *Nature genetics*, vol. 35, no. 2, pp. 176–179, 2003.

[66] J. J. Quinn and A. T. Benjamin, *Proofs That Really Count: The Art of Combinatorial Proof*. The Mathematical Association of America, 2003.

[67] C. Georghiou and A. Philippou, "Harmonic sums and the zeta-function," *Fibonacci Quart*, vol. 21, pp. 29–36, 1983.

[68] F. M. Dekking, C. Kraaikamp, H. P. Lopuhaä, and L. E. Meester, *A Modern Introduction to Probability and Statistics: Understanding why and how*. London: Springer Science & Business Media, 2005.

[69] D.-C. Cercel and S. Trausan-Matu, "Opinion propagation in online social networks: A survey," in *Proceedings of the 4th International Conference on Web Intelligence, Mining and Semantics (WIMS14)*, Thessaloniki, Greece, June 2014.

[70] H. Ma, H. Li, and J. B. Song, "Influence models of cascading failure and frequency oscillation in the power grid," in *Proceedings of 2013 IEEE PES Innovative Smart Grid Technologies Conference (ISGT)*, Washington, D.C., USA, February 2013, pp. 1–6.

[71] D. Kempe, J. Kleinberg, and É. Tardos, "Maximizing the spread of influence through a social network," in *Proceedings of the 9th ACM SIGKDD International Conference on Knowledge Discovery and Data Mining*, Washington, D.C., USA, August 2003, pp. 137–146.

[72] A. S. Pentland, "Automatic mapping and modeling of human networks," *Physica A: Statistical Mechanics and its Applications*, vol. 378, no. 1, pp. 59–67, 2007.

[73] S. Basu, T. Choudhury, B. Clarkson, A. Pentland, *et al.*, "Learning human interactions with the influence model," in *Proceedings of NIPS*2001 Conference*, Vancouver, British Columbia, Canada, December 2001, pp. 1–12.

[74] Y. Yang, A. Huang, and W. Guan, "Statistic properties and cascading failures in a coupled transit network consisting of bus and subway systems," *International Journal of Modern Physics B*, vol. 28, no. 30, p. 1450212, 2014.

[75] C.-J. Heiker and P. Falcone, "Decision modeling in Markovian multi-agent systems," in *2022 IEEE 61st Conference on Decision and Control (CDC)*, 2022, pp. 7235–7240.

[76] P. Van Mieghem, J. Omic, and R. Kooij, "Virus spread in networks," *IEEE/ACM Transactions on Networking*, vol. 17, no. 1, pp. 1–14, 2008.

[77] P. Van Mieghem, "The N-intertwined SIS epidemic network model," *Computing*, vol. 93, no. 2-4, pp. 147–169, 2011.

[78] M. Xue, S. Roy, Y. Wan, and A. Saberi, "Designing asymptotics and transients of linear stochastic automaton networks," in *Proceedings of AIAA Guidance, Navigation, and Control Conference*, Toronto, Ontario, Canada, August 2010, p. 8150.

[79] Y. Wang, A. V. Vasilakos, J. Ma, and N. Xiong, "On studying the impact of uncertainty on behavior diffusion in social networks," *IEEE Transactions on Systems, Man, and Cybernetics: Systems*, vol. 45, no. 2, pp. 185–197, 2015.

[80] D. Silvestre, P. Rosa, J. P. Hespanha, and C. Silvestre, "Stochastic and deterministic state-dependent social networks," *IEEE Transactions on Systems, Man, and Cybernetics: Systems*, vol. 52, no. 2, pp. 911–926, 2022.

[81] Q. He, X. Yan, X. Wang, T. Nan, Z. Chen, X. He, and M. Huang, "Dynamic opinion maximization framework with hybrid method in social networks," *IEEE*

Transactions on Network Science and Engineering, vol. 10, no. 1, pp. 441–451, 2023.

[82] D. W. Andrews, "Stability comparison of estimators," *Econometrica: Journal of the Econometric Society*, pp. 1207–1235, 1986.

[83] A. Santos, V. Matta, and A. H. Sayed, "Local tomography of large networks under the low-observability regime," *IEEE Transactions on Information Theory*, vol. 66, no. 1, pp. 587–613, 2019.

[84] D. Zhang, Z. Ye, and X. Dong, "Co-design of fault detection and consensus control protocol for multi-agent systems under hidden DoS attack," *IEEE Transactions on Circuits and Systems I: Regular Papers*, vol. 68, no. 5, pp. 2158–2170, 2021.

[85] C. A. Gómez Uribe, "Estimation on a partially observed influence model," Ph.D. dissertation, Massachusetts Institute of Technology, 2003.

[86] L. Zhao and Y. Wan, 2022. [Online]. Available: https://www.researchgate.net/publication/360699256_Appendix_for_L-CSS-22-0440

[87] B. Coll-Perales, M. Gruteser, and J. Gozalvez, "Evaluation of IEEE 802.11 ad for mmWave V2V communications," in *2018 IEEE Wireless Communications and Networking Conference Workshops (WCNCW)*. IEEE, 2018, pp. 290–295.

[88] I. Rasheed, F. Hu, Y.-K. Hong, and B. Balasubramanian, "Intelligent vehicle network routing with adaptive 3D beam alignment for mmWave 5G-based V2X communications," *IEEE Transactions on Intelligent Transportation Systems*, vol. 22, no. 5, pp. 2706–2718, 2021.

[89] M. Hadded, P. Muhlethaler, A. Laouiti, R. Zagrouba, and L. A. Saidane, "TDMA-based MAC protocols for vehicular ad hoc networks: A survey, qualitative analysis, and open research issues," *IEEE Communications Surveys & Tutorials*, vol. 17, no. 4, pp. 2461–2492, 2015.

[90] K. Yu, Y. Wang, J. Yu, D. Yu, X. Cheng, and Z. Shan, "Localized and distributed link scheduling algorithms in IoT under Rayleigh fading," *Computer Networks*, vol. 151, pp. 232–244, 2019.

[91] X. Zhang, S. Sarkar, A. Bhuyan, S. K. Kasera, and M. Ji, "A non-cooperative game-based distributed beam scheduling framework for 5G millimeter-wave cellular networks," *IEEE Transactions on Wireless Communications*, vol. 21, no. 1, pp. 489–504, 2021.

[92] B. Naderi and R. Ruiz, "The distributed permutation flowshop scheduling problem," *Computers & operations research*, vol. 37, no. 4, pp. 754–768, 2010.

[93] G. M. Abdalla, M. A. Abu-Rgheff, and S.-M. Senouci, "Space-orthogonal frequency-time medium access control (SOFT MAC) for VANET," in *2009 Global Information Infrastructure Symposium (GIIS)*, 2009, pp. 1–8.

[94] H. A. Omar, W. Zhuang, and L. Li, "VeMAC: A TDMA-based MAC protocol for reliable broadcast in VANETs," *IEEE transactions on mobile computing*, vol. 12, no. 9, pp. 1724–1736, 2012.

[95] W.-d. YANG, L. Pan, H.-s. ZHU, *et al.*, "Adaptive TDMA slot assignment protocol for vehicular ad-hoc networks," *The Journal of China Universities of Posts and Telecommunications*, vol. 20, no. 1, pp. 11–25, 2013.

[96] H. Yu, Z. He, and K. Niu, "STDMA for vehicle-to-vehicle communication in a highway scenario," in *2013 5th IEEE International Symposium on Microwave, Antenna, Propagation and EMC Technologies for Wireless Communications*. IEEE, 2013, pp. 133–138.

[97] D. N. M. Dang, H. N. Dang, V. Nguyen, Z. Htike, and C. S. Hong, "HER-MAC: A hybrid efficient and reliable MAC for vehicular ad hoc networks," in *2014 IEEE 28th International Conference on Advanced Information Networking and Applications*. IEEE, 2014, pp. 186–193.

[98] L. B. Le, E. Modiano, C. Joo, and N. B. Shroff, "Longest-queue-first scheduling under SINR interference model," in *Proceedings of the eleventh ACM international symposium on Mobile ad hoc networking and computing*, 2010, pp. 41–50.

[99] Y. Zhou, X.-Y. Li, M. Liu, X. Mao, S. Tang, and Z. Li, "Throughput optimizing localized link scheduling for multihop wireless networks under physical interference model," *IEEE Transactions on Parallel and Distributed Systems*, vol. 25, no. 10, pp. 2708–2720, 2013.

[100] L. Qu, J. He, and C. Assi, "Distributed link scheduling in wireless networks with interference cancellation capabilities," in *Proceeding of IEEE International Symposium on a World of Wireless, Mobile and Multimedia Networks 2014*. IEEE, 2014, pp. 1–7.

[101] Y. Shoham and K. Leyton-Brown, *Multiagent systems: Algorithmic, game-theoretic, and logical foundations*. Cambridge University Press, 2008.

[102] T. Alpcan, T. Başar, R. Srikant, and E. Altman, "CDMA uplink power control as a noncooperative game," *Wireless Networks*, vol. 8, no. 6, pp. 659–670, 2002.

[103] U. O. Candogan, I. Menache, A. Ozdaglar, and P. A. Parrilo, "Near-optimal power control in wireless networks: A potential game approach," in *2010 Proceedings IEEE INFOCOM*. IEEE, 2010, pp. 1–9.

[104] C. Shi, F. Wang, M. Sellathurai, and J. Zhou, "Non-cooperative game theoretic power allocation strategy for distributed multiple-radar architecture in a spectrum sharing environment," *IEEE Access*, vol. 6, pp. 17 787–17 800, 2018.

[105] F. Palmieri, L. Buonanno, S. Venticinque, R. Aversa, and B. Di Martino, "A distributed scheduling framework based on selfish autonomous agents for federated cloud environments," *Future Generation Computer Systems*, vol. 29, no. 6, pp. 1461–1472, 2013.

[106] C.-F. Wang and X.-Y. Chu, "A new branch and bound method for solving sum of linear ratios problem," *IAENG International Journal of Applied Mathematics*, vol. 47, no. 3, 2017.

[107] X. Ding, X. Liu, and H. Li, "Improved branch and bound global optimization algorithm for a class of sum of linear ratios problems," *IAENG International Journal of Applied Mathematics*, vol. 52, no. 3, 2022.

[108] G. Cohen, "Auxiliary problem principle and decomposition of optimization problems," *Journal of optimization Theory and Applications*, vol. 32, pp. 277–305, 1980.

[109] S. M.-K. Jawad, M. H. Al-Ali, and A. A. Jasim, "Adaptive CSMA scheduling algorithm for queuing delay enhancement and energy optimization," *Ad Hoc Networks*, p. 102908, 2022.

[110] P. Muts, "Decomposition methods for mixed-integer nonlinear programming," Ph.D. dissertation, University of Málaga, 2021.

[111] J. Liu and J. Han, "Spectral Clustering," in *Data clustering*. Chapman and Hall/CRC, 2018, pp. 177–200.

[112] U. Von Luxburg, "A tutorial on spectral clustering," *Statistics and computing*, vol. 17, no. 4, pp. 395–416, 2007.

[113] D. J. Fagnant and K. Kockelman, "Preparing a nation for autonomous vehicles: Opportunities, barriers and policy recommendations," *Transportation Research Part A: Policy and Practice*, vol. 77, pp. 167–181, 2015.

[114] G. Rodrigues de Campos, P. Falcone, R. Hult, H. Wymeersch, and J. Sjöberg, "Traffic coordination at road intersections: Autonomous decision-making algorithms using model-based heuristics," *IEEE Intelligent Transportation Systems Magazine*, vol. 9, no. 1, pp. 8–21, 2017.

[115] G. Li, L. Yang, S. Li, X. Luo, X. Qu, and P. Green, "Human-like decision making of artificial drivers in intelligent transportation systems: An end-to-end driving behavior prediction approach," *IEEE Intelligent Transportation Systems Magazine*, vol. 14, no. 6, pp. 188–205, 2022.

[116] F. Leon and M. Gavrilescu, "A review of tracking, prediction and decision making methods for autonomous driving," *arXiv preprint arXiv:1909.07707*, 2019.

[117] P. Koopman and M. Wagner, "Autonomous vehicle safety: An interdisciplinary challenge," *IEEE Intelligent Transportation Systems Magazine*, vol. 9, no. 1, pp. 90–96, 2017.

[118] S. Brechtel, T. Gindele, and R. Dillmann, "Probabilistic decision-making under uncertainty for autonomous driving using continuous pomdps," in *Proceedings of the 17th IEEE International Conference on Intelligent Transportation Systems (ITSC)*. IEEE, 2014, pp. 392–399.

[119] W. Song, G. Xiong, and H. Chen, "Intention-aware autonomous driving decision-making in an uncontrolled intersection," *Mathematical Problems in Engineering*, vol. 2016, pp. 1–15, 2016.

[120] C. Hubmann, M. Becker, D. Althoff, D. Lenz, and C. Stiller, "Decision making for autonomous driving considering interaction and uncertain prediction of surrounding vehicles," in *Proceedings of 2017 IEEE Intelligent Vehicles Symposium (IV)*. IEEE, 2017, pp. 1671–1678.

[121] Z. Qiao, K. Muelling, J. Dolan, P. Palanisamy, and P. Mudalige, "POMDP and hierarchical options MDP with continuous actions for autonomous driving at intersections," in *Proceedings of the 21st IEEE International Conference on Intelligent Transportation Systems (ITSC)*. IEEE, 2018, pp. 2377–2382.

[122] A. G. Cunningham, E. Galceran, R. M. Eustice, and E. Olson, "MPDM: Multipolicy decision-making in dynamic, uncertain environments for autonomous driving," in *Proceedings of 2015 IEEE International Conference on Robotics and Automation (ICRA)*. IEEE, 2015, pp. 1670–1677.

[123] E. Galceran, A. G. Cunningham, R. M. Eustice, and E. Olson, "Multipolicy decision-making for autonomous driving via changepoint-based behavior prediction: Theory and experiment," *Autonomous Robots*, vol. 41, no. 6, pp. 1367–1382, 2017.

[124] H. Bai, D. Hsu, and W. S. Lee, "Integrated perception and planning in the continuous space: A POMDP approach," *The International Journal of Robotics Research*, vol. 33, no. 9, pp. 1288–1302, 2014.

[125] M. Bouton, "Safe and scalable planning under uncertainty for autonomous driving," Ph.D. dissertation, Stanford University, 2020.

[126] M. Werling, J. Ziegler, S. Kammel, and S. Thrun, "Optimal trajectory generation for dynamic street scenarios in a frenet frame," in *Proceedings of 2010 IEEE International Conference on Robotics and Automation (ICRA)*. IEEE, 2010, pp. 987–993.

[127] F. Damerow and J. Eggert, "Risk-aversive behavior planning under multiple situations with uncertainty," in *Proceedings of the 18th IEEE International Conference on Intelligent Transportation Systems (ITSC)*. IEEE, 2015, pp. 656–663.

[128] P. Trautman, J. Ma, R. M. Murray, and A. Krause, "Robot navigation in dense human crowds: Statistical models and experimental studies of human–robot cooperation," *The International Journal of Robotics Research*, vol. 34, no. 3, pp. 335–356, 2015.

[129] D. Sadigh, S. Sastry, S. A. Seshia, and A. D. Dragan, "Planning for autonomous cars that leverage effects on human actions." in *Proceedings of 2016 Robotics: Science and Systems Conference*, vol. 2. Ann Arbor, MI, USA, 2016, pp. 1–9.

[130] K. Driggs-Campbell, V. Govindarajan, and R. Bajcsy, "Integrating intuitive driver models in autonomous planning for interactive maneuvers," *IEEE Transactions on Intelligent Transportation Systems*, vol. 18, no. 12, pp. 3461–3472, 2017.

[131] H. Sartipizadeh and B. Açıkmeşe, "Approximate convex hull based scenario truncation for chance constrained trajectory optimization," *Automatica*, vol. 112, p. 108702, 2020.

[132] A. Gupta, J. Johnson, L. Fei-Fei, S. Savarese, and A. Alahi, "Social GAN: Socially acceptable trajectories with generative adversarial networks," in *Proceedings of the IEEE Conference on Computer Vision and Pattern Recognition (CVPR)*, 2018, pp. 2255–2264.

[133] A. Sadeghian, V. Kosaraju, A. Sadeghian, N. Hirose, H. Rezatofighi, and S. Savarese, "SoPhie: An attentive GAN for predicting paths compliant to social and physical constraints," in *Proceedings of the IEEE/CVF Conference on Computer Vision and Pattern Recognition (CVPR)*, 2019, pp. 1349–1358.

[134] R. Kelley, A. Tavakkoli, C. King, M. Nicolescu, M. Nicolescu, and G. Bebis, "Understanding human intentions via hidden Markov models in autonomous mobile robots," in *Proceedings of the 3rd ACM/IEEE International Conference on Human-Robot Interaction (HRI)*, 2008, pp. 367–374.

[135] C. L. McGhan, A. Nasir, and E. M. Atkins, "Human intent prediction using Markov decision processes," *Journal of Aerospace Information Systems*, vol. 12, no. 5, pp. 393–397, 2015.

[136] Y. Wan, K. Namuduri, Y. Zhou, and S. Fu, "A smooth-turn mobility model for airborne networks," *IEEE Transactions on Vehicular Technology*, vol. 62, no. 7, pp. 3359–3370, 2013.

[137] J. Xie, Y. Wan, B. Wang, S. Fu, K. Lu, and J. H. Kim, "A comprehensive 3-dimensional random mobility modeling framework for airborne networks," *IEEE Access*, vol. 6, pp. 22 849–22 862, 2018.

[138] F. Bai and A. Helmy, "A survey of mobility models," *Wireless Adhoc Networks. University of Southern California, USA*, vol. 206, p. 147, 2004.

[139] M. Liu, Y. Wan, S. Li, F. L. Lewis, and S. Fu, "Learning and uncertainty-exploited directional antenna control for robust long-distance and broad-band aerial communication," *IEEE Transactions on Vehicular Technology*, vol. 69, no. 1, pp. 593–606, 2019.

[140] T. Li, Y. Wan, M. Liu, and F. L. Lewis, "Estimation of random mobility models using the expectation-maximization method," in *Proceeding of 14th IEEE International Conference on Control and Automation (ICCA)*. IEEE, 2018, pp. 641–646.

[141] J. Bernhard and A. Knoll, "Robust stochastic Bayesian games for behavior space coverage," *arXiv preprint arXiv:2003.11281*, 2020.

[142] M. Garzón and A. Spalanzani, "Game theoretic decision making based on real sensor data for autonomous vehicles' maneuvers in high traffic," in *Proceedings of 2020 IEEE International Conference on Robotics and Automation (ICRA)*. IEEE, 2020, pp. 5378–5384.

[143] F. Camara, N. Bellotto, S. Cosar, F. Weber, D. Nathanael, M. Althoff, J. Wu, J. Ruenz, A. Dietrich, G. Markkula, *et al.*, "Pedestrian models for autonomous driving part II: high-level models of human behavior," *IEEE Transactions on Intelligent Transportation Systems*, vol. 22, no. 9, pp. 5453–5472, 2020.

[144] V. G. Lopez, F. L. Lewis, M. Liu, Y. Wan, S. Nageshrao, and D. Filev, "Game-theoretic lane-changing decision making and payoff learning for autonomous vehicles," *IEEE Transactions on Vehicular Technology*, vol. 71, no. 4, pp. 3609–3620, 2022.

[145] Q. Zhang, R. Langari, H. E. Tseng, D. Filev, S. Szwabowski, and S. Coskun, "A game theoretic model predictive controller with aggressiveness estimation for mandatory lane change," *IEEE Transactions on Intelligent Vehicles*, vol. 5, no. 1, pp. 75–89, 2019.

[146] M. Liu, Y. Wan, F. L. Lewis, S. Nageshrao, H. E. Tseng, and D. Filev, "Hierarchical game-based multi-agent decision-making for autonomous vehicles," *Submitted to IEEE Transactions on Intelligent Vehicles*, 2021.

[147] J. Xie, Y. Wan, Y. Zhou, K. Mills, J. J. Filliben, and Y. Lei, "Effective and scalable uncertainty evaluation for large-scale complex system applications," in *Proceedings of the Winter Simulation Conference (WSC) 2014*. IEEE, 2014, pp. 733–744.

[148] J. Xie, Y. Wan, K. Mills, J. J. Filliben, Y. Lei, and Z. Lin, "M-PCM-OFFD: An effective output statistics estimation method for systems of high dimensional uncertainties subject to low-order parameter interactions," *Mathematics and Computers in Simulation*, vol. 159, pp. 93–118, 2019.

[149] J. C. Harsanyi, "Games with incomplete information played by "Bayesian" players, I–III part II. Bayesian equilibrium points," *Management Science*, vol. 14, no. 5, pp. 320–334, 1968.

[150] Y. Zhou, Y. Wan, S. Roy, C. Taylor, C. Wanke, D. Ramamurthy, and J. Xie, "Multivariate probabilistic collocation method for effective uncertainty evaluation with application to air traffic flow management," *IEEE Transactions on Systems, Man, and Cybernetics: Systems*, vol. 44, no. 10, pp. 1347–1363, 2014.

[151] A. Di Crescenzo, "On random motions with velocities alternating at Erlang-distributed random times," *Advances in Applied Probability*, vol. 33, no. 3, pp. 690–701, 2001.

BIOGRAPHICAL STATEMENT

Lu Zhao received her B.S. degree in geological engineering from Sun Yat-sen University, Guangzhou, China, in 2016. She is currently working toward the Ph.D. degree at the Department of Electrical Engineering, University of Texas at Arlington, Arlington, TX, USA. Her research interests include spatiotemproal stochastic networks, Vehicle-to-Everything (V2X) communications, unmanned aerial vehicle (UAV) traffic management, optimal control, and decision-making for multiagent systems.